ISSN Print: 2518-4245
ISSN Online: 2518-4253
Vol. 63(1), March 2026

PROCEEDINGS
OF THE PAKISTAN ACADEMY OF SCIENCES:
A. Physical and Computational Sciences

PAKISTAN ACADEMY OF SCIENCES
ISLAMABAD, PAKISTAN

Proceedings of the Pakistan Academy of Sciences: Part A
Physical and Computational Sciences

Proceedings of the Pakistan Academy of Sciences A. Physical and Computational Sciences is the official flagship, the peer-reviewed quarterly journal of the Pakistan Academy of Sciences. This open-access journal publishes original research articles and reviews on current advances in the field of Computer Science (all), Materials Science (all), Physics and Astronomy (all), Engineering Sciences (all), Chemistry, Statistics, Mathematics, Geography, Geology in English. Authors are not required to be Fellows or Members of the Pakistan Academy of Sciences or citizens of Pakistan. The journal is covered by Print and Online ISSN, indexed in Scopus, and distributed to scientific organizations, institutes and universities throughout the country, by subscription and on an exchange basis.

Annual Subscription: **Pakistan:** Institutions, Rupees 8000/-; Individuals, Rupees 4000/- (Delivery Charges: Rupees 300/-)
Other Countries: US$ 200.00 (includes air-lifted overseas delivery)

HEC Recognized; Scopus Indexed

Published by **Pakistan Academy of Sciences**, 3 Constitution Avenue, G-5/2, Islamabad, Pakistan
Email: editor@paspk.org; **Tel:** 92-51-920 7140 & 921 5478; **Websites:** www.paspk.org/proceedings/; www.ppaspk.org

Printed at **Graphics Point.,** Office 3-A, Wasal Plaza, Fazal-e-Haq Road Blue Area Islamabad.
Ph: 051-2806257, **E-mail:** graphicspoint16@gmail.com

PROCEEDINGS OF THE
PAKISTAN ACADEMY OF SCIENCES: PART A
Physical and Computational Sciences

CONTENTS

Volume 63, No. 1, March 2026 **Page**

Research Articles

Submission of Manuscripts: Manuscripts may be submitted as an e-mail attachment at editor@paspk.org or submit online at http://ppaspk.org/index.php/PPASA/about/submissions. Authors must consult the ***Instructions for Authors*** at the end of this issue or at the Website: www.paspk.org/proceedings/ or www.ppaspk.org.

Proceedings of the Pakistan Academy of Sciences: A Physical and Computational Sciences 63(1): 1-16 (2026)

ISSN (Print): 2518-4245; ISSN (Online): 2518-4253
http://doi.org/10.53560/PPASA(63-1)709

Pakistan Academy of Sciences

Research Article

Computational Approach to Unveil Mechanisms of Action of Sesquiterpene Glycosides from *Calendula officinalis* against Gastric Cancer

Hung Duc Nguyen*

Faculty of Biology, Thai Nguyen University of Education, Thai Nguyen, Vietnam

Abstract: Gastric cancer remains a major global health burden, and prognosis for advanced disease is frequently limited by late diagnosis and the toxicity of systemic chemotherapy. Mcl-1, an anti-apoptotic Bcl-2 family protein often overexpressed in gastric cancer, contributes to apoptosis evasion and treatment resistance, supporting its relevance as a therapeutic target. In this study, sesquiterpene glycosides from *Calendula officinalis* were evaluated as Mcl-1 (PDB: 6QFQ)-directed ligands using an integrated in silico workflow, with Etoposide as a reference. Docking identified CPD2 as the top-ranked compound (-10.75 kcal/mol), exceeding Etoposide (-9.80 kcal/mol), with a binding mode dominated by nonpolar contacts within the pocket and hydrogen-bond assignment to Arg263 and Leu267. During 100 ns molecular dynamics simulations, both complexes remained stable; CPD2 showed a RMSD values predominantly between 0.11-0.15 nm after equilibration and lower compactness/solvent-exposure trends (Rg 1.42-1.44 nm; SASA 82-88 nm²) relative to the Etoposide complex. MM/GBSA predicted a favorable association for both ligands, yielding comparable ΔTOTAL values (-28.72 ± 4.45 kcal/mol for CPD2; -29.80 ± 10.53 kcal/mol for Etoposide). ADMET prediction indicated high intestinal absorption for CPD2 (94.482%) despite low water solubility (-5.034 log mol/L), and DFT suggested greater electronic pliability for CPD2 (ΔE = 5.2502 eV) than Etoposide (ΔE = 11.1496 eV). Overall, CPD2 emerges as a prioritized computational hit for structure-guided optimization, and subsequent biochemical and cellular validation is expected to clarify its translational potential.

Keywords: Anti-apoptosis, *Calendula officinalis*, Gastric Cancer, In Silico, Mcl-1, Sesquiterpene Glycosides.

1. INTRODUCTION

Cancer remains a significant global health threat, with an estimated 20 million new cases and over 10 million deaths annually. Both incidence and mortality rates are rising due to factors like population aging, lifestyle risk factors, and disparities in healthcare access [1]. Forecasts further anticipate a marked expansion in annual incidence by 2050 (approximately 30.5 to 35 million cases), representing about a 77% increase relative to 2022, mainly attributable to demographic growth, longer life expectancy, and development-associated risks such as tobacco use, alcohol consumption, and obesity [2]. Gastric cancer remains the world's fifth most common cancer and the fifth leading cause of cancer-related deaths globally. Although treatment options have advanced, including surgery, systemic chemotherapy, and molecularly targeted approaches, outcomes for advanced gastric cancer remain unfavorable because many cases are detected late and exhibit rapid dissemination, leaving few curative opportunities, and median survival is commonly below one year [3, 4]. Standard management typically combines chemotherapy with surgery and/or radiotherapy according to disease stage, tumor location, and patient condition [5]. However, cytotoxic chemotherapy frequently damages proliferative normal tissues, causing fatigue, gastrointestinal toxicity, mucositis, and alopecia, and may also induce myelosuppression, neuropathy, appetite loss, and organ toxicities; effects are drug-dependent and are mainly managed with supportive care [6]. This toxicity and tolerability profile supports continued investigation of safer adjunctive or alternative strategies,

Received: January 2026; Revised: February 2026; Accepted: March 2026
* Corresponding Author: Hung Duc Nguyen <hungnd@tnue.edu.vn>

including plant-derived bioactive candidates for gastric cancer management.

Mcl-1 (Myeloid cell leukemia-1) is a key anti-apoptotic protein often overexpressed in gastric cancer, promoting tumor growth, invasion, and resistance to chemotherapy by blocking programmed cell death. Its high expression indicates a worse prognosis for patients. It is associated with advanced stages, making it a significant target for novel therapies, especially when combined with standard treatments to enhance effectiveness [7-9]. Systematic investigation has identified several natural products traditionally used for gastric disorders that exhibit potential Mcl-1-modulating activity in gastric cancer cells. These compounds can induce apoptosis by downregulating the anti-apoptotic protein Mcl-1 or shifting its splicing towards the pro-apoptotic variant [10, 11]. The use of *Calendula officinalis* L. (known as Jin Zhan Ju) in Traditional Chinese Medicine is primarily for topical applications to promote circulation and healthy skin. However, in Western and folk herbal medicine traditions, it is often used internally to treat various gastric diseases such as gastritis, stomach ulcers, and inflammatory bowel conditions [12]. This ethnopharmacological background provides a rationale for focusing on characteristic secondary metabolites of *C. officinalis*, particularly constituents with reported anticancer potential. Sesquiterpene glycosides are natural compounds found in plants, formed by a sesquiterpene linked to one or more sugar units, which confer water solubility. They are known for diverse biological activities, including anti-inflammatory, enzyme inhibition, and anticancer activities. Previous study indicates that sesquiterpene glycosides isolated from *C. officinalis* show significant promise for treating gastric cancer [13]. Despite these observations, the specific target-level basis underlying the reported anticancer effects, especially with respect to apoptosis-regulatory proteins, has not been clearly delineated. Accordingly, the mechanistic link between sesquiterpene glycosides and Mcl-1-mediated apoptotic control remains incompletely defined at the molecular level. To address this gap, a multi-computational approach was implemented to map binding propensity and stability, integrating structure-based docking with time-resolved molecular dynamics, MM/GBSA, in silico ADMET profiling, and DFT calculations. This combined framework enables comparative candidate prioritization and provides a rational basis for subsequent experimental verification and structure-guided lead refinement in gastric cancer drug development.

2. MATERIALS AND METHODS

2.1. Data Collection

These selected sesquiterpene glycosides, including α-Elemol 11-*O*-β-D-fucopyranoside 2′-*O*-angelate ester (CPD1), β-Eudesmol-β-D-fucopyranoside-2’-*O*-angelate (CPD2), officinoside D (CPD3), have molecular formulas of $C_{26}H_{42}O_6$, $C_{26}H_{42}O_6$, $C_{27}H_{44}O_6$, respectively, with molecular weights of 450.2981, 450.2981, 464.3138 *m/z*. Etoposide, possessing a molecular formula of $C_{29}H_{32}O_{13}$ and a molecular weight of 588.1843 *m/z*, was chosen as the positive control (Figure 1).

2.2. Molecular Docking Analysis

Three-dimensional structures of the selected ligands and Etoposide were generated in PDB format using BIOVIA Discovery Studio Visualizer. During ligand preparation, polar hydrogen atoms were added, Gasteiger partial charges were assigned, and torsional degrees of freedom were retained by treating rotatable bonds as flexible. The crystallographic coordinates of the anti-apoptotic protein Mcl-1 (PDB ID: 6QFQ) were retrieved from the RCSB Protein Data Bank [14].

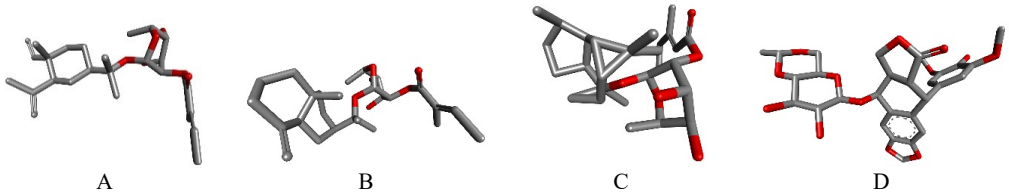

Fig. 1. 3D Structures of selected ligands. (A) CPD1, (B) CPD2, (C) CPD3, (D) Etoposide.

Because Mcl-1 is closely associated with apoptosis resistance in gastric cancer, this target was selected to evaluate the disease relevance of the investigated sesquiterpene glycosides. Docking calculations were performed with AutoDock Tools using a cubic search space defined by 60 grid points along each Cartesian axis (x, y, z) at a spacing of 0.375 Å, with the grid center positioned at x = 3.934 Å, y = -18.343 Å, and z = 18.680 Å to cover the binding region. Conformational exploration and pose prioritization were conducted using the Lamarckian genetic algorithm, enabling identification of energetically favorable binding orientations and consistent interaction patterns. The highest-scoring protein-ligand complex was subsequently examined in Discovery Studio Client 2024, and its interaction profile was assessed in parallel with the docking pose of Etoposide within the same Mcl-1 structure to delineate overlapping or divergent binding characteristics.

2.3. Molecular Dynamics Simulations

Molecular dynamics simulations were conducted to evaluate the time-dependent stability of the docked Mcl-1-ligand complex based on the Mcl-1 crystal structure (PDB ID: 6QFQ). This analysis was performed to further examine the behavior of the prioritized complexes in a gastric cancer-relevant Mcl-1 targeting context. Simulations were executed in GROMACS 2024.4 employing the CHARMM36 force field over a 100 ns trajectory [15]. Protein preprocessing involved reconstruction of missing atoms and residues using Swiss-PdbViewer [16], whereas CHARMM-compatible ligand topology and parameter files were generated via SwissParam [17]. The assembled complex was placed in a triclinic periodic simulation cell, solvated with SPC water, and supplemented with NaCl to achieve 0.15 M ionic strength while ensuring overall electroneutrality. To alleviate steric clashes and unfavorable contacts, steepest-descent energy minimization was applied for 50,000 steps. The equilibration stage consisted of 100 ps under the NVT ensemble at 300 K followed by 100 ps under the NPT ensemble at 1 bar. System stability prior to production was assessed by monitoring temperature, pressure, and potential energy, which reached stable behavior before the 100 ns production run. To ensure stable numerical integration with a 2 fs time step, covalent bonds involving hydrogen atoms were constrained using the LINCS algorithm. The production stage comprised a single 100 ns run for each complex with a 2 fs integration step, and coordinate frames were saved every 10 ps for subsequent analysis. Trajectory-derived descriptors were obtained in Grace, including root mean square deviation (RMSD), root mean square fluctuation (RMSF), radius of gyration (Rg), solvent-accessible surface area (SASA), and number of hydrogen bonds (Hbonds). Conformational agreement among representative structures was additionally assessed in UCSF Chimera (v1.13.3) via coordinate superposition to compare characteristic states across the simulations [18].

2.4. Molecular Mechanics Generalised Born Surface Area (MM/GBSA) Analysis

Binding free-energy calculations for the CPD2-6QFQ and Etoposide-6QFQ complexes were performed using the gmx_MMPBSA workflow in conjunction with the CHARMM36 parameter set. This step was used to refine ligand prioritization against the gastric cancer-relevant target Mcl-1. The polar solvation contribution was computed with a generalized Born implicit-solvent approach, while the non-polar solvation component was estimated from solvent-accessible surface area. Energetic components were extracted from the molecular dynamics trajectories by analyzing 125 evenly distributed snapshots, sampled at 80 ps intervals over an 80 ns evaluation period spanning 20-100 ns. Mean values obtained from this snapshot ensemble enabled a direct comparison of ligand-protein interaction energetics and facilitated interpretation of relative binding propensity and complex persistence within the simulated timeframe [19].

2.5. Assay Protocol for ADMET Prediction

Early evaluation of absorption, distribution, metabolism, excretion, and toxicity (ADMET) properties is essential for identifying prospective pharmacokinetic constraints and safety concerns, thereby guiding compound selection and mitigating late-stage attrition. In the present study, this analysis supported the early selection of compounds with potential suitability for gastric cancer-related drug development. Thus, the pkCSM web platform was used to estimate the ADMET profiles of CPD2 and Etoposide computationally. pkCSM utilizes graph-based molecular signatures to predict descriptors linked to absorption, distribution, metabolism,

excretion, and toxicity, facilitating a systematic comparison of developability-related attributes between the examined compounds [20].

2.6. Quantum Chemistry Computation Using the Density Functional Theory (DFT) Method

Geometric optimization of CPD2 and Etoposide was carried out using the ORCA quantum-chemistry package (v6.1.0). Initial molecular geometries were assembled in Avogadro, and molecular-orbital inspection, along with associated electronic analyses, was performed in IboView (v20211019). Density functional theory computations were executed with the B3LYP exchange-correlation functional and the 6-31G(d,p) basis set to obtain electronic wavefunctions at the optimized minima. This level of theory was selected because it provides a practical balance between computational cost and reliability for geometry optimization and frontier-orbital analysis of small organic molecules. However, because these calculations were performed in the gas phase, solvent effects and dispersion-related contributions were not explicitly accounted for, and the resulting electronic descriptors may overestimate molecular pliability relative to an implicitly solvated aqueous environment. Based on the converged structures, frontier-orbital energies (HOMO and LUMO) were extracted, and the energy gap (ΔE) was determined. Conceptual DFT indices, chemical potential (μ), electronegativity (χ), global hardness (η), softness (σ), and electrophilicity index (ω), were subsequently derived using a Koopmans-type approximation, enabling interpretation of electronic structure features and reactivity trends for the investigated molecules [21-23].

3. RESULTS AND DISCUSSION

3.1. Molecular Docking Analysis

Molecular docking enables *in silico* estimation of preferred ligand orientations within a protein cavity and provides a comparative proxy for binding propensity through scoring functions that approximate noncovalent stabilization. Contemporary structure-based discovery workflows commonly interpret docking outputs by integrating energetic ranking with recurrence of pocket-defining residues and interaction classes (hydrogen bonding, hydrophobic, and van der Waals interactions) [24]. These interaction modes contribute in distinct yet cooperative ways: hydrogen bonding supports directional polar anchoring, whereas hydrophobic and dispersion-driven contacts enhance geometric complementarity and thermodynamic stabilization of protein-ligand assemblies [25].

As summarized in Table 1, CPD2 produced the most favorable docking score (-10.75 kcal/mol), followed by CPD3 (-10.64 kcal/mol) and CPD1 (-10.51 kcal/mol). Because Mcl-1 is implicated in apoptosis resistance in gastric cancer, this favorable docking profile suggests that CPD2 may have potential relevance as a gastric cancer-oriented Mcl-1 modulator. Each of these three candidates exceeded the reference Etoposide (-9.80 kcal/mol) under the same docking workflow, indicating higher

Table 1. The interactions between the docked ligands and the protein 6QFQ.

Docked ligands	Binding energy (kcal/mol)	Hydrogen bond interaction	Van der Waals interaction	Hydrophobic interaction
CPD1	-10.51	Arg263, Leu267	Ala227, Val253, Phe254, Thr266, Leu290	Phe228, Met231, Leu235, Leu246, Val249, Met250, Phe270, Val274, Leu267
CPD2	-10.75	Arg263, Leu267	Phe254, Thr266, Gly271, Val274, Leu290	Phe228, Met231, Leu235, Leu246, Val249, Met250, Val253, Leu267, Phe270
CPD3	-10.64	Met250, Leu267	His224, Val249, Val253, Phe254, Gly271	Ala227, Phe228, Met231, Leu235, Leu246, Val274, Leu290, Ile294
Etoposide	-9.80	Arg263, Thr266, Leu267	Leu235, Val249, Val253, Phe254, Gly262, Gly271, Val274, Ile294	His224, Ala227, Phe228, Met231, Leu246, Met250, Arg263, Thr266, Phe270, Leu290

predicted affinity within the scoring function used. Because docking scores represent an approximate ranking derived from the balance of modeled non-covalent terms, subsequent validation with dynamic sampling and more rigorous free-energy estimation remains advisable when advancing to mechanistic interpretation [26]. CPD2 engaged a compact interaction constellation dominated by hydrophobic and aromatic residues (Phe228, Met231, Val249, Met250, Val253, Ile267, Phe270), supplemented by Arg263 and Gly271 as annotated active-site participants. Hydrogen-bond contacts were assigned to Arg263 and Leu267, suggesting polar anchoring at the Arg263 side chain together with backbone-mediated polar complementarity in the vicinity of residue 267. Van der Waals contributions were reported for Phe254, Thr266, Gly271, Val274, and Leu290, consistent with close-range packing at the cavity periphery. The hydrophobic interaction list for CPD2 (Phe228, Met231, Leu235, Leu246, Val249, Met250, Val253, Leu267, Phe270) indicates extensive nonpolar burial, which is commonly associated with stabilization of ligand poses through desolvation and dispersion complementarity in aqueous environments (Figure 2A) [27, 28].

Relative to CPD2, CPD1 displayed a closely related contact pattern but incorporated Ala227 among the annotated active-site residues (Ala227, Phe228, Met231, Val249, Met250, Val253, Arg263, Ile267, Phe270). Hydrogen bonds were likewise assigned to Arg263 and Leu267, implying a conserved polar-recognition element shared with CPD2. The van der Waals interaction set for CPD1 (Ala227, Val253, Phe254, Thr266, Leu290) and the hydrophobic set (Phe228, Met231, Leu235, Leu246, Val249, Met250, Phe270, Val274, Leu267) support an interaction model in which tight packing against Phe228/Phe270 and multiple aliphatic side chains dominates, while Arg263 contributes a recurrent directional component [29].

CPD3 differed by recruiting His224 as an additional pocket contact (His224, Ala227, Phe228, Met231, Val249, Met250, Val253, Ile267, Gly271), and its hydrogen-bond annotations shifted to Met250 and Leu267 rather than Arg263. This pattern is consistent with an alternative polar-anchoring scheme centered on Met250 (likely via backbone participation, given the limited hydrogen-bonding capacity of the Met side chain) while maintaining

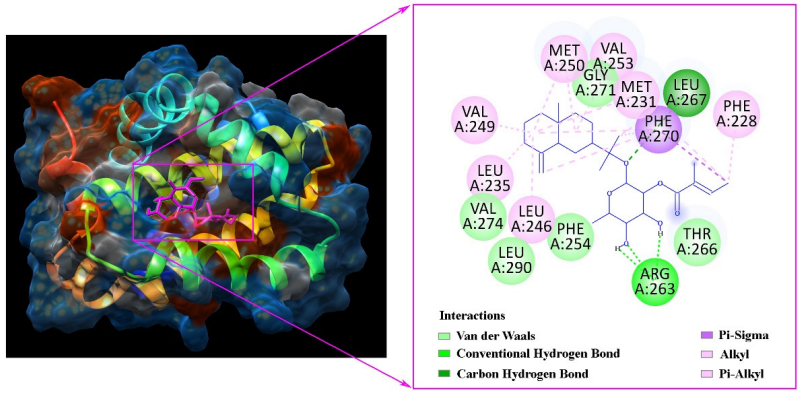

A

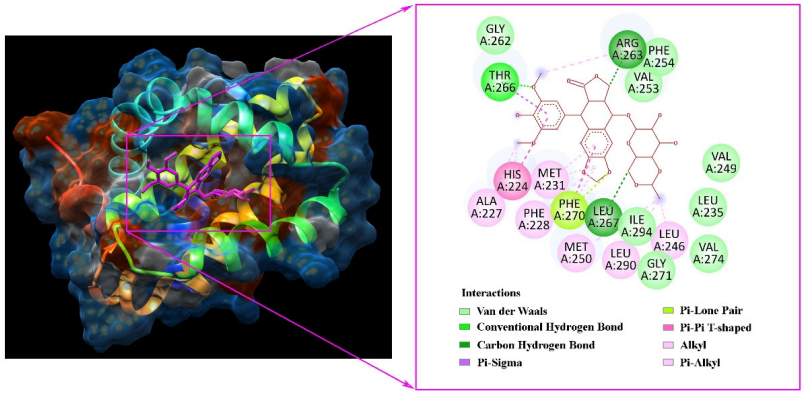

B

Fig. 2. Molecular docking model and 2D interaction diagram of CPD2 (A) and Etoposide (B) with 6QFQ protein.

residue-267 involvement. CPD3 also exhibited van der Waals interactions with His224, Val249, Val253, Phe254, and Gly271, and hydrophobic contacts extending toward Ile294 (Ala227, Phe228, Met231, Leu235, Leu246, Val274, Leu290, Ile294), implying a slightly reoriented pose that samples an adjacent nonpolar subregion of the binding cavity. Etoposide occupied an overlapping core region with broader residue coverage (His224, Ala227, Phe228, Met231, Val249, Met250, Val253, Gly262, Arg263, Ile267, Phe270, Gly271). Hydrogen bonds were assigned to Arg263, Thr266, and Leu267, indicating a triad of polar contacts that includes Thr266, a residue also present in the van der Waals or active-site lists of the CPD series. The van der Waals set for Etoposide (Leu235, Val249, Val253, Phe254, Gly262, Gly271, Val274, Ile294). Hydrophobic interactions (His224, Ala227, Phe228, Met231, Leu246, Met250, Arg263, Thr266, Phe270, Leu290) suggest simultaneous utilization of both aromatic/hydrophobic packing and multiple polar-capable residues, albeit with a less favorable docking score than CPD1-CPD3 (Figure 2B).

Across all four ligands, repeated engagement of Phe228, Met231, Val249, Met250, Val253, Leu267, and Phe270 supports the presence of a conserved recognition nucleus dominated by aromatic and aliphatic side chains, a physicochemical context in which dispersion and hydrophobic effects frequently contribute substantially to pose stabilization [30]. Differences in annotated hydrogen-bond partners imply ligand-dependent anchoring preferences that may alter residence within local minima of the docking energy landscape and could affect stability once receptor and solvent flexibility are represented explicitly. For this reason, pose refinement using interactions and follow-on molecular dynamics, with endpoint or more rigorous free-energy methods, can improve confidence beyond docking rank-order alone.

3.2. Molecular Dynamics Simulations

Molecular dynamics (MD) simulations are an established computational approach for resolving time-dependent atomic motions in molecular systems. By integrating the equations of motion under defined force fields and solvent conditions, MD yields trajectories that capture conformational fluctuations and interaction patterns at the atomic level. This capability supports mechanistic interrogation of phenomena that remain challenging to access experimentally, including protein folding pathways, ligand recognition and retention, allosteric rearrangements, and structure-property relationships in materials. Consequently, MD has become a core component of modern workflows in drug discovery, molecular chemistry, and materials engineering [31]. A 100 ns molecular dynamics protocol was carried out for the CPD2-6QFQ and Etoposide-6QFQ systems, and trajectory-derived conformational ensembles were examined through backbone RMSD, residue RMSF, radius of gyration (Rg), solvent-accessible surface area (SASA), and hydrogen-bond monitoring to characterize structural deviation, compactness, surface exposure, and polar-contact persistence [32]. The CPD2-6QFQ complex exhibited total and potential energies of -220,699 kJ/mol and -274,708 kJ/mol, respectively, whereas the corresponding values for Etoposide-6QFQ were -220,400 kJ/mol and -274,358 kJ/mol. Temperature regulation maintained the simulations at 300 K.

The time-resolved structural descriptors differentiate the dynamical signatures of the CPD2-6QFQ and Etoposide-6QFQ complexes over the 100 ns trajectory. In the backbone RMSD profiles, CPD2-6QFQ shows an early relaxation phase followed by a comparatively narrow fluctuation envelope, with most frames distributed around 0.11-0.15 nm and without a pronounced long-term drift (Figure 3A). This stable dynamic behavior is consistent with the prioritization of CPD2 for further investigation against the gastric cancer-relevant target Mcl-1. By contrast, the Etoposide-6QFQ trace stabilizes at a higher RMSD level and displays broader variability, frequently occupying 0.16-0.22 nm, with intermittent excursions toward 0.24-0.27 nm during the early segment and again in the late trajectory. Such persistent separation between RMSD bands is commonly interpreted as a higher-amplitude conformational response of the protein-ligand assembly rather than purely stochastic thermal noise, particularly when sustained over tens of nanoseconds [33].

For residue-wise flexibility, the analysis is restricted to Asp172-Val321, which contains the principal recognition corridor reported by docking (including His224, Ala227, Phe228, Met231, Val249-Val253, Arg263, Thr266, Leu267, Phe270, and Val274). Within this segment, both complexes

exhibit low-amplitude fluctuations, remaining largely below 0.10 nm across most positions (Figure 3B). RMSF represents the standard deviation of positional fluctuations around an average structure after optional fitting, and low RMSF values are generally consistent with retention of local secondary-structure order. A modest upward shift of the Etoposide trace relative to CPD2 is apparent across much of this interval, suggesting slightly increased local mobility of the groove region when Etoposide is bound, even though the most prominent RMSF maxima in the full-length profile occur outside the Asp172-Val321 window. This pattern supports a model in which CPD2 stabilizes the binding groove segment more effectively, whereas Etoposide is associated with a somewhat more compliant local environment.

Compactness and solvent exposure metrics exhibit coherent trends with RMSD/RMSF. The radius of gyration (Rg) for CPD2-6QFQ remains lower overall and more uniform, with most values clustered around 1.42-1.44 nm after initial equilibration (Figure 3C). Etoposide-6QFQ shows a higher central tendency and broader excursions, occupying 1.44-1.48 nm for extended intervals and briefly sampling still more expanded conformations early in the run. In parallel, SASA values for CPD2-6QFQ concentrate primarily around 82-88 nm², while Etoposide-6QFQ remains shifted upward (commonly 88-95 nm²) and more variable (Figure 3D). Elevated Rg together with persistently higher SASA is consistent with increased solvent exposure and a less compact protein ensemble, which can reflect cavity breathing motions or partial loosening of tertiary packing in response to ligand accommodation.

The hydrogen-bond time series reveals a mechanistic distinction in the mode of stabilizing interaction. Etoposide-6QFQ sustains a denser hydrogen-bonding pattern, particularly within the first 20 ns, where 1-3 hydrogen bonds dominate with occasional peaks reaching 4 (Figure 3E). Beyond

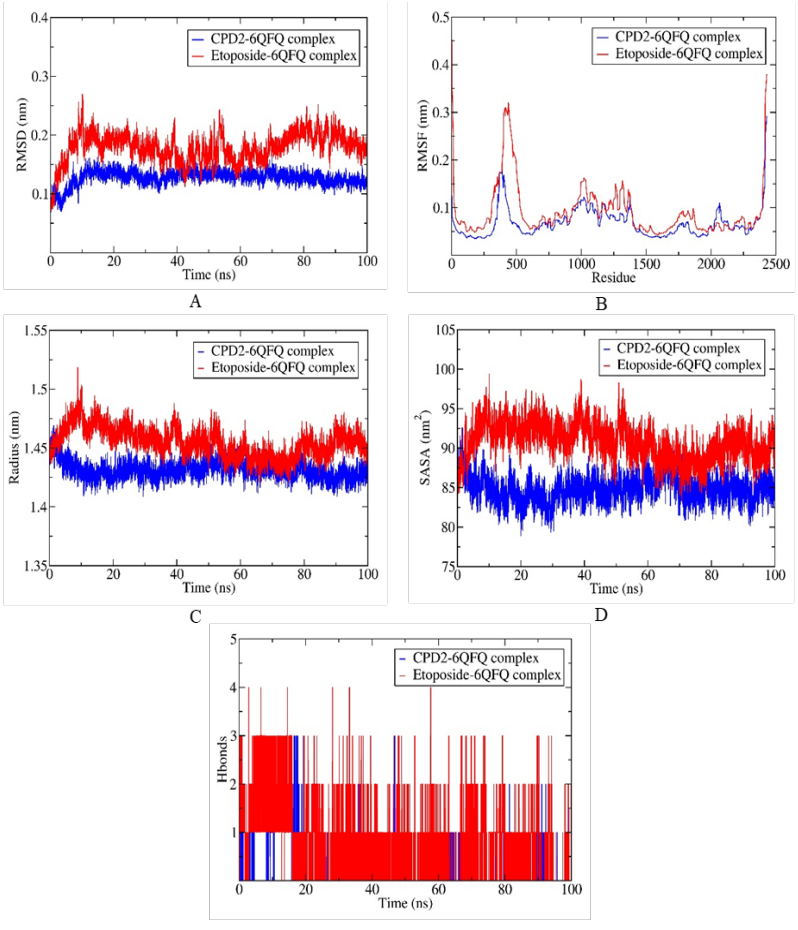

Fig. 3. Results of MD simulation for the bindings of CPD2 (blue) and Etoposide (red) with 6QFQ protein. (A) RMSD, (B) RMSF, (C) Rg, (D) SASA, (E) Hbonds.

this period, the Etoposide complex continues to display recurrent hydrogen-bond events (typically 0-1, punctuated by frequent short-lived rises to 2-3 and occasional spikes). In contrast, CPD2-6QFQ presents sparse hydrogen bonding for most of the trajectory, with prolonged intervals at zero and only intermittent episodes reaching 1; higher counts appear mainly as short bursts (including transient peaks up to 3) rather than a sustained network. High-occupancy hydrogen bonding is often associated with increased interaction specificity. It can support pose retention, yet the current comparison indicates that hydrogen-bond abundance alone does not necessarily correlate with reduced global backbone deviation, underscoring that nonpolar packing, dispersion stabilization, and collective protein motions may dominate the net dynamical response. Despite its lower hydrogen-bond persistence, CPD2 maintained lower RMSD, Rg, and SASA values throughout the simulation, indicating that its stability was not dependent on a dense hydrogen-bond network. Instead, the CPD2-6QFQ complex appears to be stabilized predominantly by hydrophobic enclosure and van der Waals complementarity, consistent with the docking interaction pattern.

Taken together, the combined metrics indicate that CPD2-6QFQ adopts a more compact and conformationally restrained ensemble (lower RMSD, lower Rg, reduced SASA) despite limited hydrogen-bond persistence, consistent with stabilization driven predominantly by hydrophobic enclosure and close-range packing. Etoposide-6QFQ, while exhibiting more frequent hydrogen-bond formation, shows larger-amplitude structural fluctuations and higher solvent exposure, suggesting greater conformational plasticity of the protein in the bound state. Within contemporary simulation-based screening pipelines, such a profile supports prioritization of CPD2 for subsequent energetic refinement while retaining Etoposide as a comparative reference due to its distinct polar-contact signature.

3.3. Free Binding Energy (MM/GBSA) Analysis

MM/GBSA is an end-state free-energy scheme that combines molecular-mechanics interaction terms (van der Waals and Coulombic electrostatics) with an implicit-solvent treatment in which the polar solvation contribution is approximated by a generalized Born (GB) model. In contrast, the nonpolar term is often associated with solvent-accessible surface area (SASA). In routine applications, configurational entropy is frequently excluded because of cost and methodological variability; consequently, MM/GBSA is typically interpreted as a comparative ranking metric whose outcomes depend on sampling quality and model choices such as dielectric settings and solvation parametrization [34, 35].

As reported in Table 2, both CPD2-6QFQ and Etoposide-6QFQ display favorable mean total binding free energies (ΔTOTAL), equal to -28.72 ± 4.45 kcal/mol and -29.80 ± 10.53 kcal/mol, respectively. Given the role of Mcl-1 in gastric cancer cell survival, these energetics support the relevance of CPD2 as a computationally promising ligand in this disease setting. The slightly more negative mean for Etoposide suggests a marginally stronger association within the same MM/GBSA protocol; however, the substantially larger dispersion for Etoposide across components (notably ΔVDWAALS and ΔEEL) indicates greater energetic heterogeneity among sampled configurations, which can arise from broader pose

Table 2. Free energy of binding obtained using MMGBSA calculations.

Energy component	Average (kcal/mol)		Standard deviation	
	CPD2-6QFQ	Etoposide-6QFQ	CPD2-6QFQ	Etoposide-6QFQ
ΔVDWAΔALS	-34.96	-41.35	4.29	9.50
ΔEEL	-2.39	-20.21	4.87	9.38
ΔEGB	12.82	37.27	4.90	8.14
ΔESURF	-4.19	-5.50	0.54	1.02
ΔGGAS	-37.35	-61.57	5.50	13.89
ΔGSOLV	8.63	31.77	4.93	7.97
ΔTOTAL	**-28.72**	**-29.80**	**4.45**	**10.53**

microstate diversity or larger amplitude fluctuations of interfacial contacts.

Energy decomposition indicates distinct driving forces. For CPD2-6QFQ, the gas-phase term is moderately favorable (ΔGGAS = -37.35 ± 5.50 kcal/mol) and is dominated by dispersion stabilization (ΔVDWAALS = -34.96 ± 4.29 kcal/mol), whereas Coulombic electrostatics contribute only weakly (ΔEEL = -2.39 ± 4.87 kcal/mol). This interaction gain is counterbalanced by a comparatively small net solvation penalty (ΔGSOLV = 8.63 ± 4.93 kcal/mol), arising primarily from the polar desolvation contribution (ΔEGB = 12.82 ± 4.90 kcal/mol) and partially compensated by a favorable nonpolar surface term (ΔESURF = -4.19 ± 0.54 kcal/mol). Such a profile is consistent with a binding mode that relies mainly on close-range packing and hydrophobic/van der Waals complementarity, while incurring a limited polar desolvation cost.

In contrast, Etoposide-6QFQ exhibits substantially stronger gas-phase stabilization (ΔGGAS = -61.57 ± 13.89 kcal/mol), reflecting both enhanced van der Waals attraction (ΔVDWAALS = -41.35 ± 9.50 kcal/mol) and markedly favorable electrostatics (ΔEEL = -20.21 ± 9.38 kcal/mol). These gains are opposed by a much larger solvation penalty (ΔGSOLV = 31.77 ± 7.97 kcal/mol), dominated by the GB polar component (ΔEGB = 37.27 ± 8.14 kcal/mol) with a modest compensatory nonpolar term (ΔESURF = -5.50 ± 1.02 kcal/mol). The near-cancellation between stronger vacuum interactions and amplified polar desolvation rationalizes why ΔTOTAL remains close to that of CPD2 despite the more attractive ΔGGAS. This energetic balance is frequently observed for ligands with pronounced electrostatic engagement, where favorable Coulombic contacts often coincide with increased desolvation costs in implicit-solvent end-state formalisms [36].

Overall, the MM/GBSA results indicate that both ligands are predicted to bind favorably, with Etoposide showing a slightly more negative mean ΔTOTAL but substantially higher variability. At the same time, CPD2 presents a more compact energetic distribution and a binding signature primarily governed by dispersion with a minor desolvation penalty. Given the known sensitivity of end-state estimates to sampling and parameterization, the close ΔTOTAL values (within the observed standard deviations) support a conservative interpretation in which CPD2 and Etoposide exhibit broadly comparable MM/GBSA binding tendencies under the present setup, and additional validation through extended sampling and/or entropy-aware refinements would improve confidence in fine rank distinctions.

3.4. ADMET Prediction Analysis

In silico ADMET screening is commonly used as an early developability filter because it summarizes absorption, distribution, metabolism, excretion, and safety-relevant liabilities before resource-intensive experimental campaigns. Such predictions are most reliable for comparative triage within a consistent workflow and should be interpreted alongside assay confirmation, given model dependence on training data, chemical domain, and endpoint definitions [37]. Table 3 summarizes the in silico ADMET outputs for CPD2 and Etoposide, providing a comparative overview of predicted absorption, distribution, metabolism, excretion, and toxicity parameters used to support early developability assessment.

- **Absorption:** The absorption panel differentiates CPD2 and Etoposide primarily through solubility-permeability balance. CPD2 shows lower predicted aqueous solubility (-5.034 log mol/L) than Etoposide (-3.487 log mol/L), suggesting a larger dissolution constraint for CPD2 despite favorable membrane transport metrics. In parallel, CPD2 shows higher predicted Caco-2 permeability (1.144 vs 0.403 log Papp) and higher predicted human intestinal absorption (94.482% vs 75.614%), consistent with a stronger epithelial transport propensity upon solubilization. Caco-2 permeability is widely used as a surrogate of intestinal transcellular permeation, although assay and model variability can influence absolute interpretation [38]. Skin permeability predictions are more negative for CPD2 (-3.327 log Kp) than for Etoposide (-2.735 log Kp), indicating lower modeled transdermal permeation for CPD2 under the same estimator. Both compounds are classified as P-glycoprotein (P-gp) substrates and as P-gp I/II inhibitors, a combination that may complicate exposure prediction because efflux liability and transporter inhibition can modulate net absorption and drug-drug interaction risk depending on co-administered substrates and inhibitors.

Table 3. Predicted ADMET properties of CPD2 and Etoposide.

ADMET properties	Unit	CPD2	Etoposide
Water Solubility	(Log mol/L)	-5.034	-3.487
Caco2 permeability	(Log Papp in 10-6 cm/s)	1.144	0.403
Intestinal absorption (Human)	(% Absorbed)	94.482	75.614
Skin permeability	(Log Kp)	-3.327	-2.735
P-glycoprotein substrate	Yes/No	Yes	Yes
P-glycoprotein I inhibitor	Yes/No	Yes	Yes
P-glycoprotein II inhibitor	Yes/No	Yes	Yes
VDss	(Log L/kg)	-0.301	-0.218
Fraction unbound (human)	(Fu)	0.05	0.038
BBB permeability	(Log BB)	-0.018	-1.567
CNS permeability	(Log PS)	-2.529	-4.115
CYP2D6 substrate	Yes/No	No	No
CYP3A4 substrate	Yes/No	Yes	Yes
CYP1A2 inhibitor	Yes/No	No	No
CYP2C19 inhibitor	Yes/No	No	No
CYP2C9 inhibitor	Yes/No	No	No
CYP2D6 inhibitor	Yes/No	No	No
CYP3A4 inhibitor	Yes/No	No	No
Total clearance	(Log ml/min/kg)	0.96	-0.068
Renal OCT2 substrate	Yes/No	Yes	No
AMES toxicity	Yes/No	No	No
Max. tolerated dose (human)	(Log mg/kg/day)	-0.21	0.171
hERG I inhibitor	Yes/No	No	No
hERG II inhibitor	Yes/No	No	No
Oral rat acute toxicity (LD50)	(mol/kg)	2.637	3.25
Oral rat chronic toxicity (LOAEL)	(Log mg/kg_bw/day)	2.36	2.429
Hepatotoxicity	Yes/No	No	No
Skin sensation	Yes/No	No	No
Tetrahymena pyriformis toxicity	(Log ug/L)	0.31	0.285
Minnow toxicity	(Log mM)	0.644	2.217

- **Distribution:** Distribution descriptors indicate broadly similar systemic disposition with notable divergence in CNS-related indices. VDss values are comparably low (-0.301 log L/kg for CPD2; -0.218 log L/kg for Etoposide), while the predicted unbound fraction is slightly higher for CPD2 (Fu = 0.05) than for Etoposide (Fu = 0.038), implying a modestly larger free circulating pool for CPD2. CNS exposure surrogates separate the compounds: CPD2 shows higher predicted BBB permeability (logBB = -0.018) than Etoposide (logBB = -1.567), and likewise higher predicted CNS permeability (logPS = -2.529 vs -4.115). Contemporary BBB modeling emphasizes that logBB/logPS indices primarily support comparative ranking rather than definitive brain exposure prediction, especially when transporter effects (e.g., P-gp at the BBB) are plausible [39].

- **Metabolism:** The metabolic liability panel indicates convergent biotransformation routing. Both CPD2 and Etoposide are predicted to be CYP3A4 substrates and non-substrates for CYP2D6, suggesting a predominant dependence on CYP3A-mediated oxidative metabolism rather than CYP2D6 turnover. No inhibition alerts are reported for CYP1A2, CYP2C19, CYP2C9, CYP2D6, or CYP3A4 for either compound, which reduces, without eliminating, concerns about CYP-mediated perpetrator drug-drug interactions in this prediction

set. Because CYP3A4 contributes substantially to clinical drug clearance, substrate classification remains relevant for victim interaction potential in the presence of potent CYP3A inhibitors or inducers [40].

- **Excretion:** Clearance predictions diverge markedly: CPD2 shows a higher predicted total clearance (0.96 log mL/min/kg) than Etoposide (-0.068 log mL/min/kg), consistent with faster modeled systemic elimination for CPD2 within the same framework. Renal OCT2 substrate classification is positive for CPD2 and negative for Etoposide, implicating a potential role of cation-transport pathways for CPD2 renal handling and transporter-mediated variability. OCT2 (often in functional interplay with MATE transporters) is recognized as an essential determinant of renal secretion and transporter-based interactions for susceptible substrates [41].

- **Toxicity:** Both compounds are predicted as AMES-negative, indicating no modeled bacterial mutagenicity signal, and both are classified as non-inhibitors for hERG I and hERG II in the provided output, which is generally interpreted as a lower predicted risk for hERG-associated cardiotoxicity within the limitations of in silico classifiers. Modern computational toxicology highlights that mutagenicity and hERG endpoints benefit from confirmation using orthogonal experimental assays because false negatives remain possible outside model applicability domains [42]. Additional toxicity-related outputs indicate no predicted hepatotoxicity or skin sensitization for either ligand. The maximum tolerated dose (human) is lower for CPD2 (-0.21 log mg/kg/day) than for Etoposide (0.171 log mg/kg/day). Acute oral rat LD50 is 2.637 mol/kg (CPD2) versus 3.25 mol/kg (Etoposide), while chronic oral rat LOAEL values are similar (2.36 vs 2.429 log mg/kg_bw/day). Aquatic toxicity proxies differ by endpoint: *T. pyriformis* toxicity is 0.31 (CPD2) versus 0.285 log µg/L (Etoposide), and minnow toxicity is 0.644 (CPD2) versus 2.217 log mM (Etoposide), indicating non-uniform environmental toxicity trends across organisms and units [43].

Overall, CPD2 combines high predicted intestinal absorption and higher modeled epithelial permeability with substantially poorer predicted solubility, indicating that formulation or solubility optimization could be a limiting consideration if empirical solubility confirms the trend. From a gastric cancer drug-development perspective, this profile suggests that CPD2 has encouraging absorption-related properties, although solubility may require further optimization. Etoposide presents comparatively better solubility but lower predicted intestinal absorption and permeability indices. Both ligands share P-gp substrate and inhibitor classifications, which may influence oral exposure and interaction risk in transporter-sensitive contexts. Distribution predictions indicate markedly reduced CNS exposure for Etoposide relative to CPD2 (logBB/logPS), while metabolism predictions suggest shared CYP3A4 substrate dependence with no predicted CYP inhibition flags. Clearance and renal transporter outputs further separate the profiles, with CPD2 showing higher predicted clearance and a positive OCT2-substrate classification, consistent with a potentially greater contribution of renal transporter processes to variability.

3.5. Quantum Chemistry Computation Using the DFT Method

DFT-derived frontier orbital energies and global conceptual-DFT descriptors were used to contextualize the electronic response characteristics of CPD2 relative to Etoposide (Table 4). In the frontier-orbital framework, a higher (less negative) HOMO energy is commonly associated with increased electron-donating propensity, whereas a lower LUMO energy is often linked to greater electron-accepting capability; the HOMO-LUMO separation (ΔE) is frequently interpreted as an index of electronic adaptability, where smaller gaps suggest easier polarization and charge redistribution under perturbation [44]. Table 4 presents the DFT-derived frontier orbital energies (EHOMO, ELUMO, and ΔE) together with key conceptual-DFT reactivity descriptors (μ, χ, η, σ, and ω) for CPD2 and Etoposide to support a comparative assessment of their electronic structure and global reactivity profiles.

CPD2 exhibits EHOMO = -3.1299 eV, substantially higher than that of Etoposide (-8.3206 eV), supporting a comparatively stronger donor character for CPD2 under the same computational protocol. In the acceptor channel, CPD2 also exhibits a lower ELUMO (2.1203 eV) than

Table 4. Quantum descriptors of CPD2 and Etoposide.

Molecule	EHOMO (eV)	ELUMO (eV)	ΔE (eV)	μ (eV)	χ (eV)	η (eV)	σ (eV^{-1})	ω (eV)
CPD2	-3.1299	2.1203	5.2502	-0.5048	0.5048	2.6251	0.3809	0.0485
Etoposide	-8.3206	2.8290	11.1496	-2.7458	2.7458	5.5748	0.1794	0.6762

EHOMO (eV): highest occupied molecular orbitals; **ELUMO (eV)**: lowest unoccupied molecular orbitals; **ΔE (eV)**: energy gap; **μ (eV)**: chemical potential; **χ (eV)**: electronegativity; **η (eV)**: hardness; **σ (eV^{-1})**: softness; **ω (eV)**: electrophilicity index.

Etoposide (2.8290 eV), indicating a more accessible accepting orbital. Consistent with these trends, CPD2 shows a markedly smaller ΔE (5.2502 eV) than Etoposide (11.1496 eV), suggesting that CPD2 is electronically more pliable, while Etoposide is characterized by a more rigid electronic structure with higher kinetic stability in the conceptual-DFT sense (Figure 4A, B) [45].

Global descriptors reinforce this separation. The chemical potential is less harmful for CPD2 (μ = -0.5048 eV) than for Etoposide (μ = -2.7458 eV), while electronegativity follows the inverse relation (χ = 0.5048 eV for CPD2; 2.7458 eV for Etoposide), indicating a stronger electron-attracting tendency for Etoposide. Hardness-softness behavior is consistent with the gap ordering: CPD2 exhibits lower hardness (η = 2.6251 eV) and higher softness (σ = 0.3809 eV^{-1}), whereas Etoposide shows higher hardness (η = 5.5748 eV) and lower softness (σ = 0.1794 eV^{-1}), implying greater resistance to electron-density deformation for Etoposide.

The electrophilicity index further differentiates charge-acceptance propensity at the global level. CPD2 presents a low ω value (0.0485 eV), while Etoposide displays a notably higher ω (0.6762 eV). Using the conceptual-DFT definition ($\omega = \mu^2/2\eta$) and commonly cited interpretive scales, both values fall within the marginal electrophile range, yet Etoposide retains a substantially stronger electrophilic signature than CPD2. This electronic profile is compatible with an interaction model in which CPD2 is more polarizable and donation-prone, whereas Etoposide expresses comparatively stronger electron-withdrawing character despite its larger orbital gap and higher hardness [46, 47]. These conceptual-DFT trends should be interpreted with caution because the calculations were performed in the gas phase; therefore, the apparent electronic pliability of CPD2 may be somewhat overestimated relative to a solvated environment. However, the smaller HOMO-LUMO gap and higher softness of CPD2 still suggest greater electronic adaptability, which may facilitate more efficient adjustment to

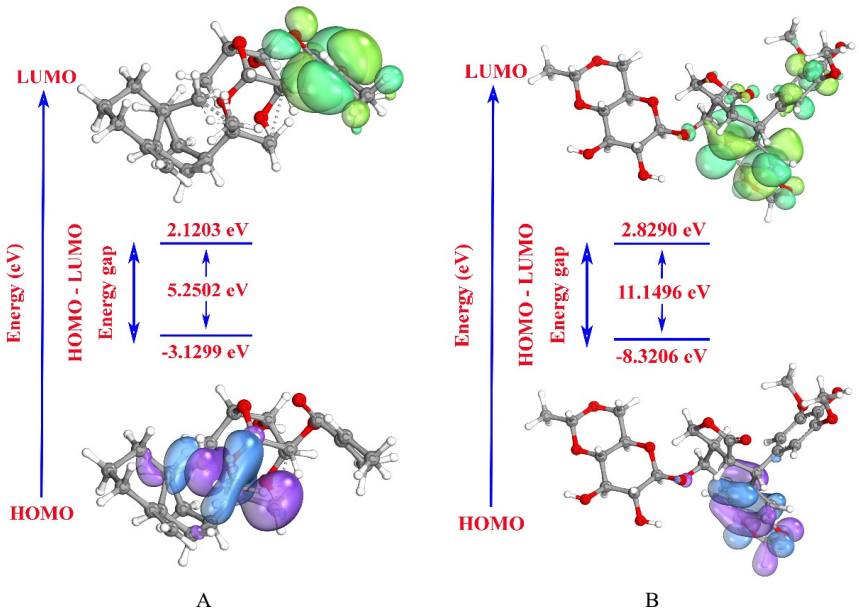

Figure 4. HOMO and LUMO surface diagrams of (A) CPD2 and (B) Etoposide.

the steric and electrostatic features of the Mcl-1 binding groove, consistent with the lower RMSD, Rg, and SASA values observed during MD simulations. This electronic adaptability may be advantageous for sustaining productive interactions with Mcl-1, thereby further supporting CPD2 as a promising computational hit for subsequent anti-gastric-cancer investigation.

4. CONCLUSIONS

Computational modelling assessed CPD2 as an Mcl-1 (6QFQ)-oriented candidate, using Etoposide as the reference ligand. Docking ranked CPD2 as the strongest binder among the tested sesquiterpene glycosides (-10.75 kcal/mol), exceeding Etoposide (-9.80 kcal/mol), with key contacts centered on Phe228, Met231, Val249, Met250, Val253, Leu267, and Phe270 and hydrogen-bond assignment to Arg263 and Leu267. Over 100 ns of molecular dynamics, the CPD2-6QFQ complex maintained a tighter conformational envelope, reflected in lower RMSD clustering (0.11-0.15 nm) and reduced, more stable Rg (1.42-1.44 nm) and SASA (82-88 nm²). In contrast, Etoposide showed higher deviation and solvent exposure but more frequent hydrogen-bond events. MM/GBSA supported favorable association for both ligands, with closely comparable totals (ΔTOTAL = -28.72 ± 4.45 kcal/mol for CPD2; -29.80 ± 10.53 kcal/mol for Etoposide); CPD2 was driven primarily by van der Waals stabilization (ΔVDWAALS = -34.96 ± 4.29 kcal/mol) with a modest solvation penalty (ΔGSOLV = 8.63 ± 4.93 kcal/mol). At the same time, Etoposide combined stronger gas-phase terms with a larger polar desolvation cost (ΔEGB = 37.27 ± 8.14 kcal/mol). ADMET prediction indicated high intestinal absorption for CPD2 (94.482%) despite low solubility (-5.034 log mol/L), and DFT suggested predicted higher electronic polarizability for CPD2 (EHOMO = -3.1299 eV; ΔE = 5.2502 eV; ω = 0.0485 eV) relative to Etoposide (EHOMO = -8.3206 eV; ΔE = 11.1496 eV; ω = 0.6762 eV). Overall, convergence across docking, molecular dynamics, MM/GBSA, ADMET estimation, and DFT descriptors supports CPD2 as the leading in silico candidate, warranting lead-optimization efforts and experimental confirmation.

Taken together, these findings support CPD2 as a prioritized in silico hit for gastric cancer research through potential modulation of the anti-apoptotic protein Mcl-1. Nevertheless, in silico outputs represent prioritization evidence rather than biological proof, and experimental confirmation remains necessary to establish quantitative binding and functional impact. The present work did not incorporate in vitro or in vivo assays, limiting translational interpretation of predicted affinity, stability, and pharmacokinetic liabilities. Future studies should therefore implement biochemical binding measurements, gastric cancer cell-based assays, cellular models relevant to Mcl-1-dependent phenotypes, and pharmacokinetic testing to clarify exposure constraints suggested by the solubility-permeability balance and transporter-related predictions. Additional refinement via extended sampling and entropy-aware free-energy methods may further resolve the close energetic differences observed between CPD2 and the reference ligand.

5. ETHICAL STATEMENT

This work does not include any studies involving human or animal subjects.

6. CONFLICT OF INTEREST

The author declares no conflict of interest.

7. FUNDING

No funding was received to conduct this research.

8. AUTHORSHIP CONTRIBUTION STATEMENT

Hung Duc Nguyen: The author was solely responsible for the conception of the study, interpretation of the results, and preparation of the manuscript. All data were generated in-house, and no paper mill was used. All results were interpreted solely by the author; Grammarly and Google Translate were used for English language refinement.

9. REFERENCES

1. F. Bray, M. Laversanne, H. Sung, J. Ferlay, R.L. Siegel, I. Soerjomataram, and A. Jemal. Global cancer statistics 2022: GLOBOCAN estimates of incidence and mortality worldwide for 36 cancers in 185 countries. *CA: A Cancer Journal for Clinicians* 74(3): 229-263 (2024). DOI: 10.3322/caac.21834
2. Q. Luo and D.P. Smith. Global cancer burden: progress, projections, and challenges. *The Lancet* 406(10512): 1536-1537 (2025). DOI: 10.1016/S0140-6736(25)01570-3
3. T.I. Mamun, S. Younus, and M.H. Rahman.

Gastric cancer-epidemiology, modifiable and non-modifiable risk factors, challenges and opportunities: An updated review. *Cancer Treatment and Research Communications* 41: 100845 (2024). DOI: 10.1016/j.ctarc.2024.100845

4. H. Kumagai, S. Baba, H. Nikai, R. Fujisawa, M. Shimooki, and A. Sasaki. Stage IV gastric cancer with microsatellite instability-high achieving long-term survival by gastrectomy after nivolumab as third-line therapy: A case report and literature review. *Surgical Case Reports* 10(1): 221 (2024). DOI: 10.1186/s40792-024-02022-5
5. Y. Semenova, A. Kerimkulov, T. Uskenbayev, D. Zharlyganova, O. Shatkovskaya, T. Sarina, A. Manatova, G. Yessenbayeva, and T. Adylkhanov. Chemotherapy options for locally advanced gastric cancer: A review. *Cancers* 17(5): 809 (2025). DOI: 10.3390/cancers17050809
6. H.I. Akbarali, K.H. Muchhala, D.K. Jessup, and S. Cheatham. Chemotherapy induced gastrointestinal toxicities. In: Strategies to mitigate the toxicity of cancer therapeutics. D. A. Gewirtz and P. B. Fisher (Eds.). *Academic Press, Boston, USA* pp. 131-166 (2022). DOI: 10.1016/bs.acr.2022.02.007
7. H. Akagi, H. Higuchi, H. Sumimoto, T. Igarashi, A. Kabashima, H. Mizuguchi, M. Izumiya, G. Sakai, M. Adachi, S. Funakoshi, S. Nakamura, Y. Hamamoto, T. Kanai, H. Takaishi, Y. Kawakami, and T. Hibi. Suppression of myeloid cell leukemia-1 (Mcl-1) enhances chemotherapy-associated apoptosis in gastric cancer cells. *Gastric Cancer* 16(1): 100-110 (2012). DOI: 10.1007/s10120-012-0153-6
8. L.P. Zhang, Y.M. Wei, M.J. Luo, S.Y. Ren, X.W. Zhan, C. Wang, Z.F. Li, R.M. Zhu, S. Yan, Y. Cheng, J.L. Xu, X.J. Yang, K.L. Du, J.Q. Wang, G. Zhang, D.X. Du, R. Gao, D.B. Zhao, and J.N. Gong. Both direct and indirect suppression of MCL1 synergizes with BCLXL inhibition in preclinical models of gastric cancer. *Cell Death & Disease* 16(1): 170 (2025). DOI: 10.1038/s41419-025-07481-8
9. W. Likui, L. Qun, Z. Wanqing, S. Haifeng, L. Fangqiu, and L. Xiaojun. Prognostic role of myeloid cell leukemia-1 protein (Mcl-1) expression in human gastric cancer. *Journal of Surgical Oncology* 100(5): 396-400 (2009). DOI: 10.1002/jso.21344
10. F. Muller, C. Cerella, F. Radogna, M. Dicato, and M. Diederich. Effects of natural products on Mcl-1 expression and function. *Current Medicinal Chemistry* 22(30): 3447-3461 (2015). DOI: 10.2174/0929867322666150716115435
11. S.Y. Kang, D. Hwang, S. Shin, J. Park, M. Kim, M.D.H. Rahman, M.A. Rahman, S.G. Ko, and B. Kim. Potential of bioactive food components against gastric cancer: insights into molecular mechanism and therapeutic targets. *Cancers* 13(18): 4502 (2021). DOI: 10.3390/cancers13184502
12. Y. Jasoria, M. Agrawal, S. Kumar, H. Chaudhary, K.K. Sahu, M. Singhal, S. Arora, P. Chandolia, S. Saha, K. Singh, S. Mahour, W. Akram, and D. Jain. In-vivo evaluation of neuroprotective effect of Chinese plant *Calendula officinalis* Linn. flower extract against aluminium chloride-induced alzheimer's in wistar rats. *Pharmacological Research - Modern Chinese Medicine* 12: 100458 (2024). DOI: 10.1016/j.prmcm.2024.100458
13. M. D'Ambrosio, A. Ciocarlan, E. Colombo, A. Guerriero, C. Pizza, E. Sangiovanni, and M. Dell'Agli. Structure and cytotoxic activity of sesquiterpene glycoside esters from *Calendula officinalis* L.: Studies on the conformation of viridiflorol. *Phytochemistry* 117: 1-9 (2015). DOI: 10.1016/j.phytochem.2015.05.005
14. J.B. Murray, J. Davidson, I. Chen, B. Davis, P. Dokurno, C.J. Graham, R. Harris, A. Jordan, N. Matassova, C. Pedder, and S. Ray. Establishing drug discovery and identification of hit series for the anti-apoptotic proteins, Bcl-2 and Mcl-1. *ACS Omega* 4(5): 8892-8906 (2019). DOI:10.1021/acsomega.9b00611
15. D.V.D. Spoel, E. Lindahl, B. Hess, G. Groenhof, A.E. Mark, and H.J.C. Berendsen. GROMACS: Fast, flexible, and free. *Journal of Computational Chemistry* 26(16): 1701-1718 (2005). DOI: 10.1002/jcc.20291
16. N. Guex and M.C. Peitsch. SWISS-MODEL and the Swiss-Pdb Viewer: An environment for comparative protein modeling. *ELECTROPHORESIS* 18(15): 2714-2723 (1997). DOI: 10.1002/elps.1150181505
17. V. Zoete, M.A. Cuendet, A. Grosdidier, and O. Michielin. SwissParam: A fast force field generation tool for small organic molecules. *Journal of Computational Chemistry* 32(11): 2359-2368 (2011). DOI: 10.1002/jcc.21816
18. E.F. Pettersen, T.D. Goddard, C.C. Huang, G.S. Couch, D.M. Greenblatt, E.C. Meng, and T.E. Ferrin. UCSF Chimera-A visualization system for exploratory research and analysis. *Journal of Computational Chemistry* 25(13): 1605-1612 (2004). DOI: 10.1002/jcc.20084
19. H.D. Nguyen. Unveiling the anti-apoptotic mechanism of magnolialide as a colorectal cancer inhibitor via molecular modeling, ADMET, and MMGBSA analysis. *Physical Chemistry Research* 13(4): 783-796 (2025). DOI: 10.22036/

pcr.2025.535946.2708

20. D.E. Pires, T.L. Blundell, and D.B. Ascher. pkCSM: Predicting small-molecule pharmacokinetic and toxicity properties using graph-based signatures. *Journal of Medicinal Chemistry* 58(9): 4066-4072 (2015). DOI: 10.1021/acs.jmedchem.5b00104
21. F. Neese. Software update: The ORCA program system-version 6.0. *WIREs Computational Molecular Science* 15(2): e70019 (2025). DOI: 10.1002/wcms.70019
22. G. Knizia and J.E. Klein. Electron flow in reaction mechanisms-revealed from first principles. *Angewandte Chemie International Edition* 54(18): 5518-5522 (2015). DOI: 10.1002/anie.201410637
23. M.D. Hanwell, D.E. Curtis, D.C. Lonie, T. Vandermeersch, E. Zurek, and G.R. Hutchison. Avogadro: an advanced semantic chemical editor, visualization, and analysis platform. *Journal of Cheminformatics* 4(1): 17 (2012). DOI: 10.1186/1758-2946-4-17
24. A. Tiwari and S. Singh. Computational approaches in drug designing. In: Bioinformatics. D.B. Singh and R.K. Pathak (Eds.). *Academic Press, Boston, USA* pp. 207-217 (2022). DOI: 10.1016/B978-0-323-89775-4.00010-9
25. G.G. Ferenczy and M. Kellermayer. Contribution of hydrophobic interactions to protein mechanical stability. *Computational and Structural Biotechnology Journal* 20: 1946-1956 (2022). DOI: 10.1016/j.csbj.2022.04.025
26. L. Wang, Y. Chen, M. Zhang, J. Liu, H. Li, M. Liu, S. Wu, Y. Zhang, W. Li, and B. Wang. Chemical dissection of selective myeloid leukemia-1 inhibitors: How they were found and evolved. *European Journal of Medicinal Chemistry* 283: 117168 (2025). DOI: 10.1016/j.ejmech.2024.117168
27. F. Molani and A.E. Cho. Accurate protein-ligand binding free energy estimation using QM/MM on multi-conformers predicted from classical mining minima. *Communications Chemistry* 7(1): 247 (2024). DOI: 10.1038/s42004-024-01328-7
28. Q. Sun. The hydrophobic effects: Our current understanding. *Molecules* 27(20): 7009 (2022). DOI: 10.3390/molecules27207009
29. M.F. Adasme, K.L. Linnemann, S.N. Bolz, F. Kaiser, S. Salentin, V.J. Haupt, and M. Schroeder. PLIP 2021: Expanding the scope of the protein–ligand interaction profiler to DNA and RNA. *Nucleic Acids Research* 49(W1): W530-W534 (2021). DOI: 10.1093/nar/gkab294
30. M. Bello and C. Bandala. Evaluating the ability of end-point methods to predict the binding affinity tendency of protein kinase inhibitors. *RSC Advances* 13(36): 25118-25128 (2023). DOI: 10.1039/D3RA04916G
31. H. Uludağ and T. Tang, How can molecular dynamics simulations assist with gene medicines? *Biomaterials and Biosystems* 2: 100014 (2021). DOI: 10.1016/j.bbiosy.2021.100014
32. Z. Jin and Z. Wei. Molecular simulation for food protein–ligand interactions: A comprehensive review on principles, current applications, and emerging trends. *Comprehensive Reviews in Food Science and Food Safety* 23(1): e13280 (2024). DOI: 10.1111/1541-4337.13280
33. I.J. dos S. Nascimento, J.N.S. Gomes, J. de O. Viana, Y.M.S. de M. e Silva, E.G. Barbosa, and R.O. de Moura. The power of molecular dynamics simulations and their applications to discover cysteine protease inhibitors. *Mini Reviews in Medicinal Chemistry* 24(11): 1125-1146 (2024). DOI: 10.2174/1389557523666230901152257
34. S. Wang, X. Sun, W. Cui, and S. Yuan. MM/PB(GB)SA benchmarks on soluble proteins and membrane proteins. *Frontiers in Pharmacology* 13: 1018351 (2022). DOI: 10.3389/fphar.2022.1018351
35. E. Akkus, O. Tayfuroglu, M. Yildiz, and A. Kocak. Revisiting MMPBSA by adoption of MC-based surface area/volume, ani-ml potentials, and two-valued interior dielectric constant. *The Journal of Physical Chemistry B* 127(20): 4415-4429 (2023). DOI: 10.1021/acs.jpcb.3c00834
36. M. Taylor and J. Ho. MM/GBSA prediction of relative binding affinities of carbonic anhydrase inhibitors: effect of atomic charges and comparison with Autodock4Zn. *Journal of Computer-Aided Molecular Design* 37(4): 167-182 (2023). DOI: 10.1007/s10822-023-00499-0
37. R. Ancuceanu, B.E. Lascu, D. Drăgănescu, and M. Dinu. In silico ADME methods used in the evaluation of natural products. *Pharmaceutics* 17(8): 1002 (2025). DOI: 10.3390/pharmaceutics17081002
38. C.L. Pires and M.J. Moreno. Improving the accuracy of permeability data to gain predictive power: assessing sources of variability in assays using cell monolayers. *Membranes* 14(7): 157 (2024). DOI: 10.3390/membranes14070157
39. E.T.C. Huang, J.S. Yang, K.Y.K. Liao, W.C.W. Tseng, C.K. Lee, M. Gill, C. Compas, S. See, and F.J. Tsai. Predicting blood–brain barrier permeability of molecules with a large language model and machine learning. *Scientific Reports* 14(1): 15844 (2024). DOI: 10.1038/s41598-024-66897-y
40. Y. Zhang, Z. Wang, Y. Wang, W. Jin, Z. Zhang, L.

Jin, J. Qian, and L. Zheng. CYP3A4 and CYP3A5: the crucial roles in clinical drug metabolism and the significant implications of genetic polymorphisms. *PeerJ* 12: e18636 (2024). DOI: 10.7717/peerj.18636

41. S. Asano, A. Galetin, Y. Tomita, K.M. Giacomini, X. Chu, X. Yang, T. Nakamura, H. Kusuhara, and Y. Sugiyama, Predicting OCT2/MATEs-mediated drug interactions in healthy volunteers and patients with chronic kidney disease: insights from extended clearance concept, endogenous biomarkers, and in vitro inhibition studies (perspectives from the international transpor. *Clinical Pharmacology & Therapeutics* 118(5): 994-1014 (2025). DOI: 10.1002/cpt.3727
42. G. Falcón-Cano, A. Morales-Helguera, H. Lambert, M.Á. Cabrera-Pérez, and C. Molina. hERG toxicity prediction in early drug discovery using extreme gradient boosting and isometric stratified ensemble mapping. *Scientific Reports* 15(1): 15585 (2025). DOI: 10.1038/s41598-025-99766-3
43. N. Cerisier, E. Truong, T. Watanabe, T. Oshiro, T. Takahashi, S. Ito, and O. Taboureau. Computational prediction of mutagenicity through comprehensive cell painting analysis. *Mutagenesis* 40(4): 560-574 (2025). DOI: 10.1093/mutage/geaf014
44. P. Geerlings. From density functional theory to conceptual density functional theory and biosystems. *Pharmaceuticals* 15(9): 1112 (2022). DOI: 10.3390/ph15091112
45. M. Franco-Pérez, F. Heidar-Zadeh, P.W. Ayers, F. De Proft, A. Vela, J.L. Gázquez, and P. Geerlings. Temperature and external fields in conceptual density functional theory. *Chemical Science* 15(48): 20090-20121 (2024). DOI: 10.1039/D4SC04181J
46. S.R. Pilli, T. Banerjee, and K. Mohanty. HOMO–LUMO energy interactions between endocrine disrupting chemicals and ionic liquids using the density functional theory: Evaluation and comparison. *Journal of Molecular Liquids* 207: 112-124 (2015). DOI: 10.1016/j.molliq.2015.03.019
47. P. Pérez, L.R. Domingo, A. Aizman, and R. Contreras. The electrophilicity index in organic chemistry. In: Theoretical aspects of chemical reactivity. Chapter 19. A. Toro-Labbé (Ed.). *Elsevier, Amsterdam, Netherlands* pp. 139-201 (2007) DOI: 10.1016/S1380-7323(07)80010-0

Proceedings of the Pakistan Academy of Sciences: A Physical and Computational Sciences 63(1): 17-32 (2026)

ISSN (Print): 2518-4245; ISSN (Online): 2518-4253
http://doi.org/10.53560/PPASA(63-1)710

Pakistan Academy of Sciences

Research Article

Development and Characterization of Epoxy Composites Reinforced with Banana Peel Powder and Jute Fiber

Moumita Basak, Nanjiba Ahnaf, Moumita Tasnim Meem, Usayed Khan, and Pabitro Prosad Mondal*

Department of Materials Science & Engineering, Rajshahi University of Engineering & Technology, Rajshahi-6204, Bangladesh

Abstract: Eco-friendly and sustainable composites materials have become a topic of great interest in the development of structural materials. Epoxy-based materials have been widely used for their inherent properties. However, thermal instability and the non-biodegradability are the main drawbacks of epoxy. This study incorporates natural fillers into the epoxy matrix with an aim to make them partially biodegradable while enhancing their mechanical and thermal properties. Banana peel powder-epoxy composites and jute fiber-epoxy composites of varying concentrations as well as a hybrid composite comprising of their best single filler loadings were fabricated using solution casting method. The optimum loadings for banana peel powder composites and jute fiber composites were determined to be 20 wt.% and 5 wt.% respectively as the maximum tensile strength of 27 MPa and 21.64 MPa and maximum flexural strength of 43.66 MPa and 42.06 MPa were observed respectively. The hybrid composite displayed both a higher tensile strength of 30.32 MPa and flexural strength of 44.5 MPa. The hardness was increased by increasing filler content up to a certain amount. The hybrid composite, however, displayed the lowest hardness value of 59.78 even compared to blank epoxy (68.11) making it more resilient and less likely to fail catastrophically. The hybrid composite also maintained an intermediary thermal stability among the samples. Water absorption of the hybrid composite was likewise intermediate but exhibited greater deterioration in soil.

Keywords: Epoxy Composite, Agro-Waste Filler, Hybrid Natural Reinforcement, Jute Fiber, Banana Peel Powder, Hardness.

1. INTRODUCTION

Biodegradable composites are a class of materials developed through innovative and ecologically conscious techniques of materials engineering that integrate sustainability, environmental responsibility, and technical performance. The potential of these composites made up of two or more materials with at least one biodegradable component, to break down into innocuous components while maintaining their mechanical, thermal, and functional qualities has drawn interest from a variety of industries [1]. The accumulation of plastic waste and environmental deterioration can be addressed with the use of these biodegradable composites. Currently, just 9% of plastic garbage is recycled, and 12 billion metric tonnes are predicted to wind up in landfills or marine areas by 2050. This is because the production of plastic waste is expected to quadruple over the next 20 years, posing a serious environmental threat [2-4]. Epoxy polymers, accounting for 7.1% of the world's plastic production in 2021, are crucial for creating fiber-reinforced polymers. These versatile synthetic polymers, known for their adhesive, mechanical, and electrical properties, are widely used in various industries. They distinguish themselves from conventional thermosetting polymers due to their unique attributes [5].

The biodegradability of epoxy resin is a significant issue as they can remain in the environment for extended periods if not handled properly [6]. As non-biodegradable epoxy-based

Received: August 2025; Revised: February 2026; Accepted: March 2026
* Corresponding Author: Pabitro Prosad Mondal <pabitroprosad2014@gmail.com>

composites worsen the problem of plastic waste; biodegradable composites are needed to address this issue [7]. Epoxy resins are often modified with fillers and additives like carbon nanotubes, plasticizers, reactive oligomeric compounds, low molecular weight polymers, and nanoparticles to enhance composite performance. Fibers, organic or inorganic, are crucial reinforcing elements in various applications [8]. Factors like fiber surface properties, length, modulus of elasticity, and material composition are essential for increasing tensile capacity [9]. The remarkable qualities of steel, glass, propylene, and carbon fibers made them the focus of research. However, these synthetic fibers have disadvantages such as increased stiffness, environmental impact, scarcity, and high costs. There are others who argue for natural fibers because they are inexpensive, easily accessible, environmentally friendly, and can occasionally lessen stiffness in certain composite applications [10].

As of today, many studies have utilized several kinds of reinforcements within the epoxy matrix to produce composites with comparable if not better mechanical, thermal and degradation characteristics. Ranjan *et al.* [11] created biodegradable epoxy composites using rice straw fibers, both treated and untreated as reinforcement. It was observed that while both type of fibers had increased strength than blank epoxy, the composite with rice straws treated with NaOH yielded the maximum strength. Treated and untreated kenaf fibers were also introduced in epoxy matrices, where the composite laminate with NaOH alkali treated kenaf fiber yielded superior thermal stability and less degradation, suitable for aerospace and automobile applications [12]. Similarly, epoxy-based composite with chemically treated luffa fiber showed better suitability for medium load structural applications as opposed to using untreated fibers [13]. Raghav *et al.* [14] extracted cellulose nanofibers from red coconut peduncle waste to reinforce epoxy sheets, producing composites with enhanced mechanical and thermal properties. Similarly, Yusuf *et al.* [15] extracted cellulose nanofibers albeit from a different source of oil palm produced epoxy-based composites with significantly improved mechanical properties and marginal decrement of thermal parameters. Several studies have utilized more than one reinforcement to produce hybrid epoxy-based composites. Shariff *et al.* [16] reinforced epoxy matrix with boron nitride or alumina with *Millettia pinnata* leaf powder and glass sheets. The observed increase of mechanical properties through this study opened the door for potential industrial applications of epoxy-based hybrid composites. Zeleke *et al.* [17] utilized sisal and glass fiber to create an epoxy hybrid composite that showed better mechanical strength than when only one of the reinforcements was introduced into the matrix. Arpitha *et al.* [18] incorporated sugarcane bagasse along with alumina micro fillers within an epoxy matrix which resulted in an increase in physical, thermal as well as mechanical properties. Ashok *et al.* [19] incorporated raw jute fibers and banana fibers in several weight ratios within epoxy and concluded that a 1:1 ratio of jute-banana fiber resulted in an improved mechanical and thermal properties with significant reduction in water absorption. Another study conducted utilized banana fiber and glass fiber as reinforcements in epoxy-based hybrid composites that were deemed suitable for lightweight structural and automobile applications [20]. Moreover, a separate study found hybrid composites composed of hybridized banana, jute, glass, and carbon fiber in epoxy resin matrix yielded lightweight materials with enhanced mechanical properties that are suitable for high-speed vehicles [21]. Corncob bio-waste and boron nitride particles were also introduced into epoxy matrices to produced hybrid composites with 2 to 3 time more tensile strength, suitable for lightweight applications [22]. Natural fiber-reinforced epoxy composites made from jute and powdered banana peels show promise in achieving a balance between biodegradability, sustainability, and performance [23].

Basalt, sisal, coconut, bagasse, hemp, jute, and banana peel have all been shown to improve the compressive and tensile strength of composite materials [24]. By incorporating these chopped natural fiber reinforcements, the composite's ability to absorb energy is increased, resulting in the transformation of brittle materials into more ductile ones. Furthermore, the application of continuous fiber reinforcement has resulted in the creation of a new class of building materials with enhanced ductility and tensile strength [2]. As reinforcing agents, natural fibers fill in the gaps in the matrix and transfer stress into it. Furthermore, the development of microcracks in composite materials is successfully prevented [25]. The natural plant-based fiber that is jute, also called the "Golden Fiber", is produced from the stems of the

Corchorus plant, which is grown readily in tropical places like Bangladesh and India with little fertilizer or pesticides [26, 27]. Biodegradable polymers and composites made of jute have been made possible by advancements in response to consumer demand for environmentally friendly products [28]. The remarkable tensile strength of jute fiber is one of its noteworthy features. Owing to its well-known durability, it can be used in a variety of contexts, such as construction, packaging, and textiles. It is especially useful when making durable sacks and bags to package agricultural goods. The peel of a banana has many uses and advantages, ranging from use in cooking to sustainable practices. In order to improve qualities of a polymer or resin for a variety of applications, dried and processed banana peels are mixed with a matrix material to make composite materials. Unripe banana peels have more fiber than ripe bananas do. When added to the matrix, the fiber can improve the material's overall performance, strength, durability which becomes more resilient to stress and deformation [1]. Because these peels naturally decompose over time, they lower pollution levels and promote a circular economy. Moreover, their affordability and abundance make this composite a cost-effective option in comparison to other synthetic substitutes [29].

The research aims to create biodegradable composites using jute fibers and banana peel powder, addressing the growing demand for environmentally friendly alternatives to traditional composites. It explores the use of natural fiber-reinforced epoxy composites, balancing engineering needs with environmental considerations, and contributes to the evolving field of materials science and engineering, where performance and sustainability can coexist. Although various studies have been conducted on the individual reinforcement of banana peel powder or jute fiber inside an epoxy matrix, research on a hybrid composite including both fillers simultaneously, focusing not only on the enhancement of strength but also increasing durability through reduction of hardness remain unexplored. The purpose of this work is to first optimise the loading of banana peel powder and jute fiber powder into epoxy-based composites. Next, a hybrid composite with the ideal loading of both fillers would be fabricated, and its properties would be compared to those of plain epoxy and the individual composites.

2. MATERIALS AND METHODS

2.1. Materials

Raw unripe bananas and raw jute collected from the local store were used for this study. For the matrix and hardener, Bisphenol A Diglycidyl Ether (BADGE) and diethylene triamine were used respectively. To make the mold, glass and aluminum foil were utilized while using petroleum Vaseline as the releasing agent.

2.2. Methodology

The process of making banana peel powder is given in Figure 1. Firstly, the peels were carefully removed from the bananas and thoroughly washed with distilled water to remove any dust or impurities. Subsequently, the banana peels were cut into small pieces and placed in an oven to dry for 24 hours at 60 °C. After the drying process, the peels were ground into a fine powder using a grinder. The resulting powder was sifted through a 1 mm sieve net multiple times to get the desired banana peel powder with average particle size less than or equal 1 mm. The process is analogous to previous similar studies [30, 31].

Figure 2 shows the making process of jute fiber. First, long jute fibers were separated from each other, cut into 6-inch lengths and thoroughly washed with distilled water. Then the jute fibers were treated with 1% NaOH solution, leaving them to soak within the solution for 1 hour, to ensure all fibers were fully submerged [32]. After that the fibers were removed from the solution and washed multiple times with distilled water to eliminate any remaining NaOH. The treated jute fibers were then placed in an oven and dried for 8 hours at 70 °C. Once dried, the jute fibers were meticulously separated and cut into approximately 10 mm lengths and the jute fibers were ready for use as reinforcement in epoxy composites [10, 32].

A glass measuring 20 inches in length, 16 inches in width, and 0.118 inches in thickness was used as the mold base. A transparent Rexene cloth was wiped with acetone and then affixed to the glass using Scotch tape. Four glass pieces, each 6 inches in length, 1 inch in width, and 0.236 inches in thickness, were selected and covered with aluminum foil. These wrapped glass pieces were

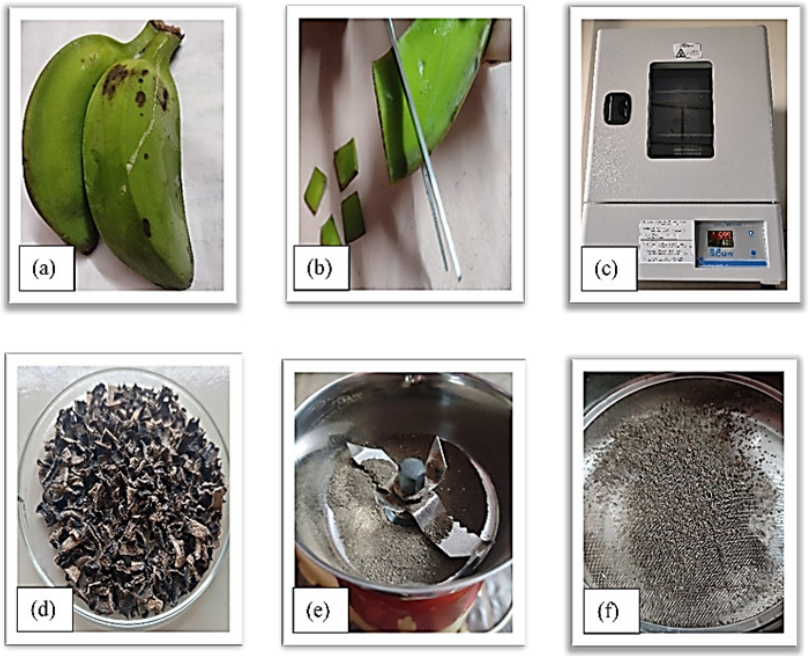

Fig. 1. Making banana peel powder, (a) Raw unripe banana, (b) Cutting banana peel, (c) Drying in oven, (d) Dried banana peel, (e) Grinding of banana peel, and (f) Sieving of powder.

Fig. 2. Jute fiber treatment, (a) Jute fiber cut into 6 inches, (b) Washing jute, (c) Weighing NaOH, (d) Jute soaked in NaOH, (e) Drying in oven, and (f) Cut into 10mm.

securely fastened together in a rectangular shape on top of the base glass using scotch tape to create the mold. A small amount of petroleum Vaseline was applied to the mold as a releasing agent [33].

To prepare the blank epoxy, a ratio of 3:1 epoxy and hardener were carefully measured, placed in a plastic cup and thoroughly mixed for 5 minutes using a popsicle stick. The epoxy-hardener mixture was subsequently poured into the glass mold. To release initial bubbles within the epoxy, the filled mold was lightly tapped on the table. All remaining bubbles were carefully removed by blowing through a straw. After bubble removal,

the mold was left to cure for 48 hours. Once the curing process was completed, the solid epoxy was carefully removed from the mold [34].

For the preparation of banana peel powder-based epoxy composites the measured hardener and epoxy were mixed as mentioned before and 20 wt.% banana peel powder was added and mixed for an additional 10-15 minutes. Any bubbles that formed were carefully removed by blowing through a straw. Subsequently, the entire mixture was poured into a mold and cured for 48 hours. Once fully cured, the composite was removed from the mold. Similarly, composites with 25 wt.% and 30 wt.% banana peel powder were prepared following the same procedure.

Again, three different weight percentages of 5 wt.%, 6.5 wt.%, and 8 wt.% of jute fibers were added into the epoxy to prepare the composites. The epoxy-herdener mixture was prepared and half of the mixture was poured into the mold. Then the measured jute fibers (5 wt.%) were evenly distributed onto the epoxy layer and the remaining mixture was poured on top. The rest of the procedure was done as mentioned before. Similarly, jute fiber-epoxy composites with 6.5 wt.% and 8 wt.% jute content were prepared.

To fabricate the hybrid composite, combining banana peel powder and jute fibers, the filler contents were selected based on the best individual results observed from the banana peel powder-epoxy and jute fiber- epoxy composites. Based on the mechanical tests, the optimum compositions were determined to be 20 wt.% banana peel powder and 5 wt.% jute fiber. Initially, a mixture of epoxy, hardener and banana peel powder was prepared following the same procedure to produce banana peel powder- epoxy composites. Then half of the mixture was poured into the mold and the measured jute fibers were evenly distributed onto the composite mixture layer. The remaining mixture was poured into the mold, and the rest of the procedure was performed as mentioned as before. Figure 3 shows the fabricated mold, blank epoxy, epoxy-banana peel powder composite, epoxy-jute fiber composite and hybrid composite samples.

2.3. Characterization

2.3.1. Mechanical tests

To assess the mechanical properties of the composites, tensile test, flexural test, and Shore D hardness test were carried out. The flexural strength was measured using a universal testing machine (UTM, model: Instron) under a three-point loading condition according to ASTM D790 standard [35]. Tensile tests were also performed on the same UTM according to ASTM D3039 standard [36], with the samples securely held between the machine's grips, and the load was applied at a cross-sectional head speed of 5 mm/min. These tests were conducted on

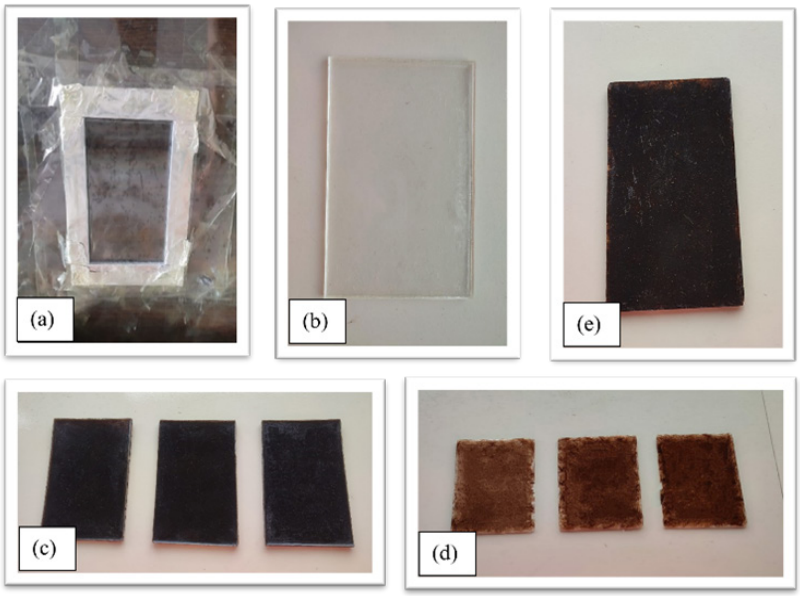

Fig. 3. (a) Mold making, (b) Blank epoxy, (c) Epoxy-banana peel powder composite, (d) Epoxy-jute fiber composite, and (e) Hybrid composite.

eight samples. Hardness was measured according to ASTM D2240 standard [37] using a Digital Shore D Durometer with a 10-second ball indentation time. To minimize errors, this test was repeated three times for each of the eight samples with the dimensions of 1 × 1 × 0.2 inches, and the average values were recorded. All tests were carried out at room temperature.

2.3.2. Thermal analysis

The thermal property of the composites was measured using TGA machine (Pyris STA 8000) maintaining a heating rate of 20 °C/min, reaching a maximum temperature of 750 °C. This test was conducted for four samples of blank epoxy composite, 20 wt.% banana peel-epoxy composite, 5 wt.% jute fiber-epoxy composite, and hybrid composite containing 20 wt.% banana peel powder and 5 wt.% jute fibers under air atmosphere where a flow rate of 200mL/min was maintained.

2.3.3. Water absorption test

Water absorption was assessed by quantifying the weight increase of composite specimens while immersing in water at ambient temperature, following the standard procedure outlined in ASTM D570 [38]. The water absorption test was conducted on four samples that were mentioned in the TGA test. For this evaluation, freshly cut samples of appropriate dimensions (1 × 1 inch) with a thickness of 0.2 inch were used as well as the corners of each sample were made to be curved for ensuring uniform water diffusion. The process involved measuring the initial weight of the samples using a precision weight balance machine. These samples were then submerged in a water bath maintained at an ambient temperature for 24 hours. After that the samples were carefully removed, dried using absorbent paper to eliminate the excess surface moisture, and reweighted. The weight gain of each sample, expressed as an increase in weight percentage, was calculated using Equation (1).

$$\text{Increase in wt.\%} = \frac{\text{Wet weight} - \text{Sample weight}}{\text{Sample weight}} \times 100 \quad (1)$$

2.3.4. Soil burial test

The biodegradability of epoxy composite samples was observed through a simple soil burial test, simulating the natural biodegradation of this composite. This test was conducted according to [39] with some minor modifications for the four samples mentioned in TGA test. Four 1000 ml beakers with equal diameters were taken and filled with grey-colored soil from the garden. The pH of the soil was maintained at 7-7.5. The soil in the beakers was properly blended, and epoxy composites of uniform rectangular dimensions were placed in the middle of each beaker at a depth of 2 inches. Before being placed in the soil, the initial weight of each composite was measured with the help of a weight balance. The beakers were numbered separately for each sample. High relative humidity was maintained in the soil by regularly sprinkling water. The test was performed at an ambient temperature. The samples were first removed after 7 days, gently washed with water to remove adhered soil from their surfaces and weighed using a weight balance. Weight loss was calculated by employing Equation (2).

$$\text{Loss of wt.\%} = \frac{\text{Initail weight} - \text{Final weight}}{\text{Initial weight}} \times 100 \quad (2)$$

In the same way, the samples were subjected to the test process for 14 days and 21 days, and weight loss was calculated. Weight loss of the sample concerning time was recorded as a measure of their biodegradation.

3. RESULTS AND DISCUSSION

3.1. Tensile Test

Tensile properties of prepared composite material are exhibited in Figure 4. The filler contents were determined through trial and error as well as comparative analysis with similar studies [30, 40]. The prepared epoxy-banana peel powder composites (20, 25, and 30 wt.%) along with the epoxy-jute fiber composites (5, 6.5, and 8 wt.%) were initially subjected to tensile testing to optimize their loading into epoxy- based composites. The graph revealed that the tensile strength of the composites decreased with the increase of fiber. The highest tensile strength of epoxy-banana peel powder composites was achieved at 20 wt.% reinforcement at 27 MPa. The tensile strength was reduced further to 24.27 MPa with a 25 wt.% addition of banana peel powder, and it was lowest at 18.41 MPa with

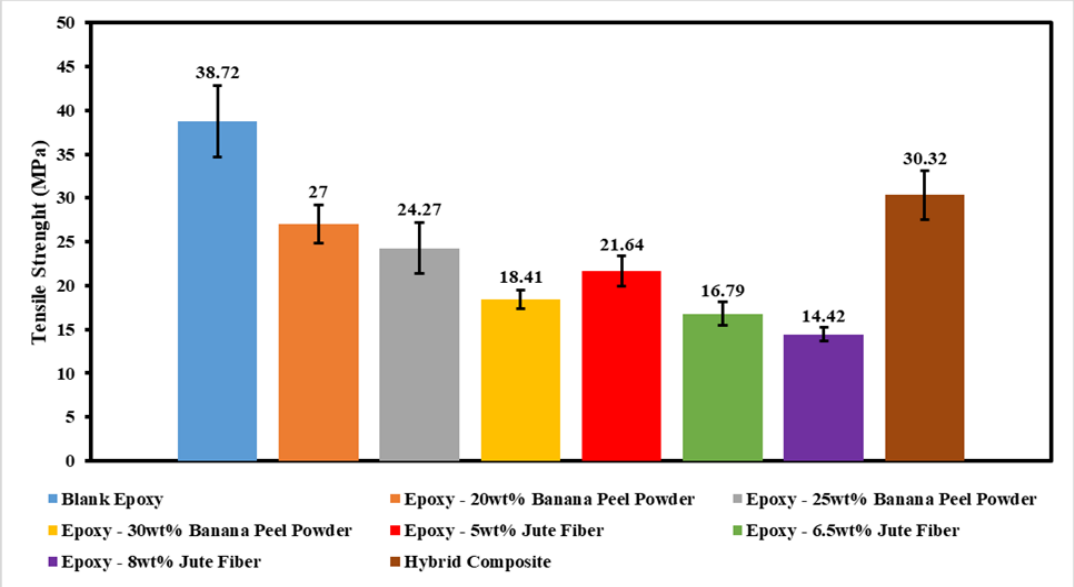

Fig. 4. Tensile strength of epoxy and epoxy-based composites.

a 30 wt.% addition of banana peel powder. The findings are in accordance to similar systems [30].

Similarly, for jute fiber-reinforced epoxy composites, the highest tensile strength was at 5 wt.% addition of jute fiber at 21.64 MPa, which reduced further to 16.79 MPa with 6.5 wt.% addition of jute fiber, the lowest being 14.42 MPa with reinforcement of 8 wt.% jute fiber. After reinforcing with banana peel powder and jute fiber, the optimum value of tensile strength was obtained at 20 wt.% for the banana peel powder-reinforced epoxy composites and at 5 wt.% for the jute fiber-reinforced epoxy composites. The hybrid composite containing both 20 wt.% for the banana peel powder and 5 wt.% for the jute fiber had a higher tensile strength of 30.32 MPa. Similar studies show the hybrid composites having superior tensile properties than single filler-based composites [41, 42]. However, it was found that the maximum tensile strength was obtained in the blank epoxy.

The tensile strength of a composite decreases with increasing fiber loading due to factors such as fiber clustering, poor adhesion between the fibers and the matrix, fiber misalignment, and reduced matrix contribution. Firstly, as fiber loading increases, fibers may begin to cluster or agglomerate, creating stress concentration points within the composite, potentially leading to premature failure. Secondly, inadequate adhesion between the fibers and the matrix can occur at high fiber loadings, weakening the matrix's ability to efficiently transfer stress to the fibers. Thirdly, maintaining a well-aligned fiber structure becomes challenging at high fiber loadings, and misaligned fibers cannot effectively contribute to load-bearing, resulting in reduced strength. Finally, when the fiber content is very high, the matrix material's contribution to load-bearing decreases significantly as the matrix becomes a smaller proportion of the composite. If the matrix itself is weak, this can further decrease the overall tensile strength [43, 44].

In the case of the hybrid composite, the higher tensile strength can be due to several factors. The presence of both the banana peel powder as well as jute fiber prevented the movement and deformation of the polymer chains. The reduction of voids, and therefore, a better adhesion between the matrix and fillers resulted in an improved load transfer of the fillers into the matrix [45, 46]. Moreover, the jute fibers improve the strength and toughness of the composite when cracks and subsequently, debonding between the filler-matrix interface occur, they keep the upper and lower part of the crack joined together due to the phenomenon known as "fiber bridging" [46, 47].

3.2. Flexural Test

Figure 5 illustrates the flexural strength of banana peel powder and jute fiber reinforced epoxy

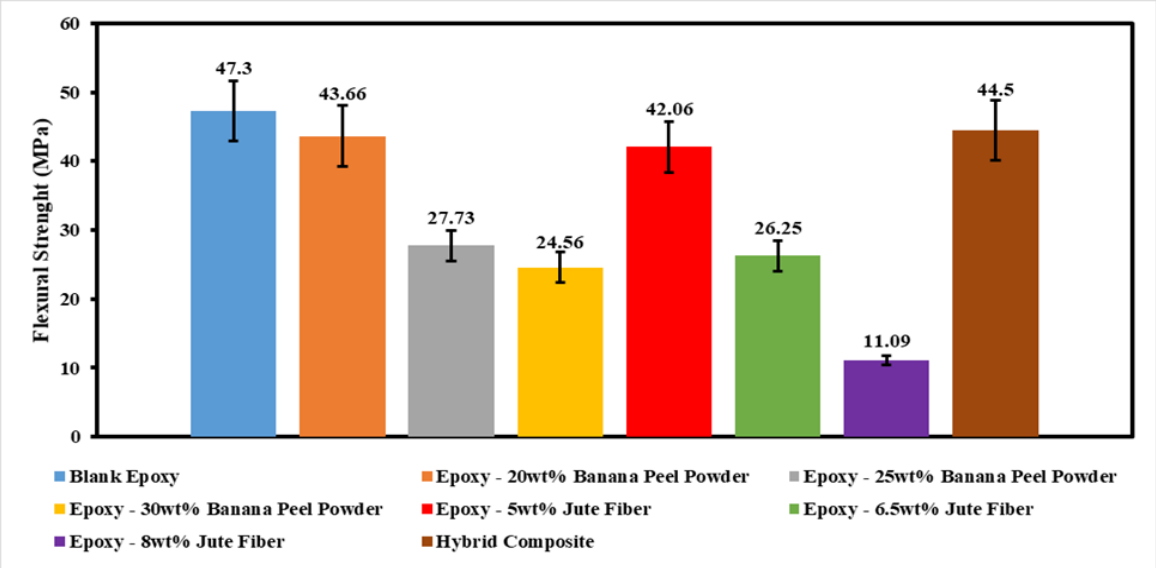

Fig. 5. Flexural strength of epoxy and epoxy-based composites.

composites at various fiber loadings compared to blank epoxy. The prepared epoxy-banana peel powder composites (20, 25, and 30 wt.%) as well as the epoxy-jute fiber composites (5, 6.5, and 8 wt.%) were initially subjected to flexural testing only to optimize their loading into the epoxy-based composites. Similar to the tensile strength, the flexural strength of the composites also showed a decline with the increase of fiber content.

The maximum flexural strength of epoxy-banana peel powder composites was achieved at 20 wt.% reinforcement at 43.66 MPa. The flexural strength was reduced further to 27.73 MPa with a 25 wt.% addition of banana peel powder, and it was lowest at 24.56 MPa with a 30 wt.% addition of banana peel powder. Similarly, for jute fiber-reinforced epoxy composites, the highest flexural strength was at 5 wt.% addition of jute fiber at 42.06 MPa, which reduced further to 26.25 MPa with 6.5 wt.% addition of jute fiber, the lowest being 11.09 MPa with reinforcement of 8 wt.% jute fiber. Hence, the optimum value of tensile strength was obtained at 20 wt.% for the banana peel powder-reinforced epoxy composites and at 5 wt.% for the jute fiber-reinforced epoxy composites. The hybrid composite containing both 20 wt.% for the banana peel powder and 5 wt.% for the jute fiber had a small increase in flexural strength to 44.5 MPa, which is greater than any of the single filler-based composites; this is in accordance to similar studies [41].

However, again it was found that the maximum flexural strength was obtained in the blank epoxy composite due to the strong adhesion between epoxy and hardener. With fiber loading adhesion between epoxy and hardener will be less. So, tensile strength and flexural strength both are decreased with fiber loading. At higher fiber content, a weak interface was created due to the increase in fiber-to-fiber interactions, the fibers not being perfectly aligned with matrix, voids, and dispersion problems [48].

The increased flexural strength of the hybrid composite may be the result of the same causes that increased the tensile strength. The polymer chains were stopped from moving and deforming by the presence of both jute fiber and banana peel powder. Stress transmission from the matrix to the fillers was enhanced as a result of the decrease in voids and increased adhesion between the matrix and fillers [45, 46]. Additionally, the jute fibers strengthen and toughen the composite through “fiber bridging” [46, 47].

3.3. Hardness Test

Figure 6 shows the hardness of banana peel powder and jute fiber reinforced epoxy composites at various fiber loadings compared to blank epoxy. It can be observed that the hardness increased up to a certain percentage with fiber loading for both banana peel powder and jute fiber reinforced epoxy composites, then began to decrease. Incorporation

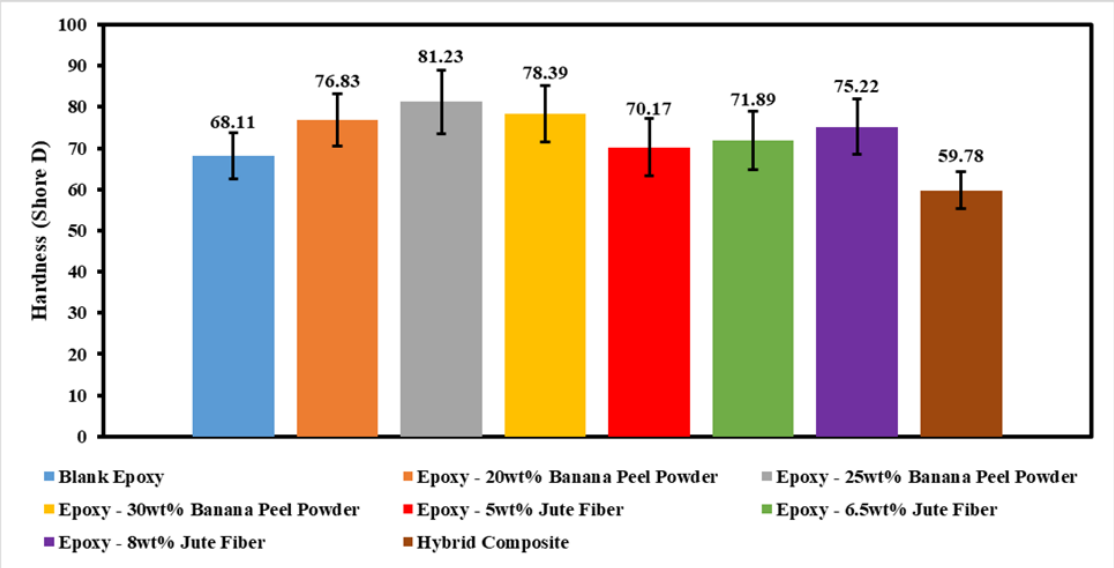

Fig. 6. Hardness of epoxy and epoxy-based composites.

of fiber into the matrix reduced the flexibility of the matrix resulting in more rigid composites. The addition of 20 wt.% banana peel powder and 5 wt.% jute fiber individually resulted in increased hardness values from 68.1 for blank epoxy to 76.83 and 70.17 respectively.

Due to the increase of stiffness of respective composite, the hardness of the composites showed a slight increasing trend with an increase in the fiber content as higher hardness values were observed for both 25 wt.% banana peel powder and 6.5 wt.% with 81.23 and 71.89 respectively. Better dispersion of the filler into the matrix with minimization of voids between the matrix and the filler also enhanced hardness. So, with fiber loading increased, average hardness also slightly increased [43]. However, as excessive fiber loading may lead to agglomeration or alignment issues, the effectiveness of reinforcement was reduced. Additionally, it could be due to a change in the material's overall structural integrity or other factors affecting its mechanical properties [49]. Hence, the hardness value for the 30 wt.% banana peel powder reinforced epoxy composite was reduced to 78.39. However, for 8.5 wt.% jute fiber reinforcement, the hardness value still increased to 75.22, indicating a better dispersion of the fibers within the matrix with minimization of voids.

The hardness value for the hybrid (20 wt.% banana peel powder + 5 wt.% jute fiber) composite was found to be 59.78. Since the tensile and flexural strengths of the hybrid composite increased compared to those of the banana-epoxy and jute-epoxy composites, the hardness was expected to decrease as strong and ductile fibers can enhance tensile strength but may simultaneously reduce the composite's hardness due to their increased susceptibility to localized deformation. Similar studies correlate the decrease of hardness to increased porosity and water absorption of the natural fibers which causes deterioration of the surface integrity and reduces the rigidity of the matrix [50]. Moreover, the weak interfacial wetting with increased fiber loadings has a softening effect on the composites as alluded in other similar systems [51]. The reduced hardness of the hybrid polymer composite enhances its toughness and decreases the probability of catastrophic failure, aligning with prior research on epoxy composites containing natural and particulate fillers [52].

3.4. Thermal Analysis

Thermal study was observed through TGA curves which indicate the weight loss of the composites in relation to rising temperature. For blank epoxy, a two step degradation is observed with the the onset thermal degradation beginning at around 275 °C as can be observed from Figure 7(a). This could be attributed to the depolymerization of the macromolecular network of epoxy resin while the latter could be due to further degradation of the

carbon residue through oxidation at around 375 °C to 445 °C. The composites on the other hand showed one-step degradation curves as the fillers protected the epoxy resin from oxidation [53]. An initial weight loss can be observed before reaching the onset degradation temperature due to evaporation of moisture from the surface after which, the main weight loss could be attributed to the degradation and volatilization of the fillers and matrix. These findings are in accordance with similar studies [53, 54].

At lower temperatures, the composites experienced greater weight loss than the blank epoxy. The weight loss at 300 °C for blank epoxy was 7.12% while the weight loss for the composites were 13.56%, 21.22% and 31.22% for 20 wt.% BPP reinforced epoxy, hybrid epoxy and 5 wt.% jute fiber reinforced epoxy respectively. However at higher temperatures, the blank epoxy faced significantly more weight loss, leaving less char residue. At 500 °C, the weight loss for blank epoxy was 85.19% while the weight loss for the composites were 71.83%, 72.96% and 73.78% for 20 wt.% BPP reinforced epoxy, hybrid epoxy and 5 wt.% jute fiber reinforced epoxy respectively.

From the DTG curve, it can be observed that epoxy-based composites had lower onset as well as maximum degradation temperatures compared to blank epoxy as shown in Figure 7(b). However, while the blank epoxy exhibited a secondary degradation period between 375 °C to 445 °C due to oxidation, the composites showed no reactions. Table 1 compares the onset degradation and maximum degradation temperatures of the selected samples.

From the Figure 7 it is evident that the reinforcement in the epoxy composites initially experienced a greater weight loss but demonstrated more resistance to degradation at higher temperatures compared to the epoxy blank composite. Notably, the hybrid composite comprising 20 wt.% banana peel powder and 5 wt.% jute fiber displays a distinct weight loss curve that falls between the curves of the individual composites containing 20 wt.% banana peel powder and 5 wt.% jute fibers. This behavior can be attributed to the presence of treated jute fibers within the hybrid composite, which results in less degradation [55].

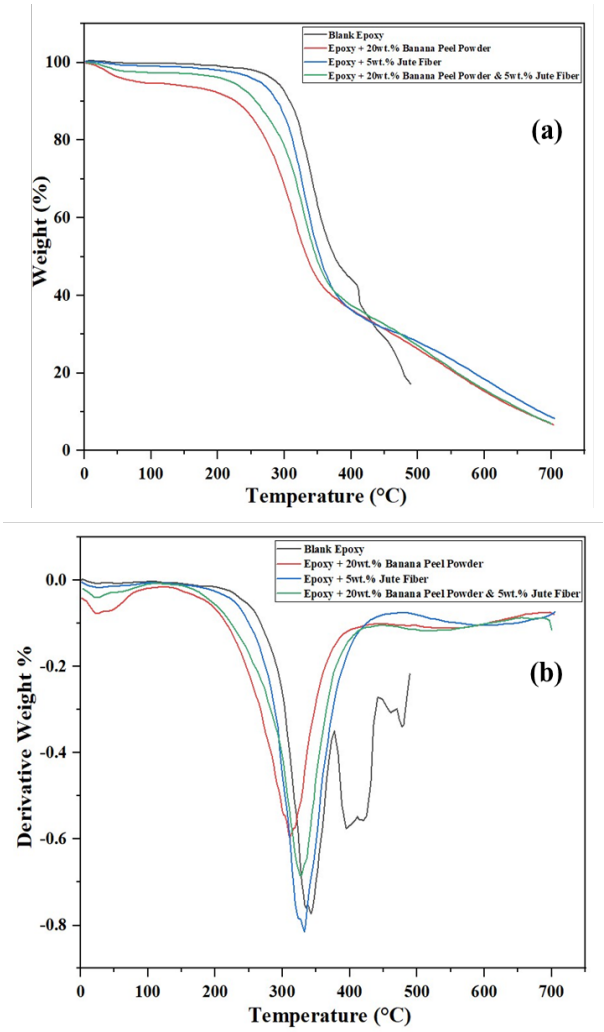

Fig. 7. Thermal analysis results of epoxy and epoxy-based composites (a) TGA and (b) DTG.

Table 1. Degradation temperatures of epoxy and epoxy-based composites.

Sample	Onset degradation temperature (°C)	Maximum degradation temperature (°C)
Blank Epoxy	275.42	342.34
20 wt.% BPP Reinforced Epoxy	200.22	311.04
5 wt.% Jute Fiber reinforced Epoxy	240.68	332.55
Hybrid Epoxy	225.54	326.94

3.5. Water Absorption Test

Biodegradable composites are designed to break down when exposed to environmental conditions, including moisture. Water absorption is a crucial step in the degradation process of biodegradable materials. As water penetrates the composite, it can initiate hydrolysis that breaks down the polymer chains leading to eventual degradation. The rate at which water is absorbed can vary depending on factors such as the type of biodegradable polymer and the composite's structure. Faster water absorption can lead to quicker biodegradation, which may be desirable in specific applications [56, 57].

The water absorption behavior of all four specimens was determined in terms of weight increase for composite specimen immersed in water at room temperature for 24 hours [58]. From Figure 8, it can be observed that the water absorption of the blank epoxy composite is nearly zero as the matrix material is hydrophobic, which restricts the interaction of the water molecules [34].

On the other hand, both the 20 wt.% banana peel powder-reinforced composite and the 5 wt.% jute fiber reinforced composite have higher water absorption compared to the blank epoxy composite, as the fillers are hygroscopic in nature, meaning they have a natural affinity to absorb moisture from the environment. This hygroscopic behavior can lead to increased water absorption in the composite. This is in accordance to similar studies [59]. However, the 20 wt.% banana peel powder-reinforced composite had the highest water absorption as the banana peel powder was non- treated while the jute fiber was treated [56]. Moreover, the water absorption of the hybrid composite was intermediate of the banana peel powder reinforced composite the jute fiber reinforced composite [34].

3.6. Soil Burial Test

Soil burial degradation tests were carried out by sandwiching the polymer films between two layers of commercial soil to simulate soil degradation after their use lifetime. Figure 9 illustrates the increasing weight loss values of different composites with time. This test was conducted to assess the biodegradability of the composite under both ideal and practical environmental conditions. While the presence of jute fiber and banana peel powder in the matrix may contribute significantly to the biodegradation of these composites, it's important to note that epoxy resin itself is not biodegradable. While the weight of the blank epoxy sample remained nearly unchanged throughout the burial period, the proportion of weight loss in the other test samples increased with time [60]. The increased weight loss with increasing filler content is consistent with similar systems [61].

Initially, the weight loss of the composites occurred at a gradual rate. However, after 7 days, a rapid weight loss was observed in the samples. This increased weight loss was likely due to various factors, including the presence of soil particles, moisture, and humidity in the environment [62]. The chemical components, such as cellulose, hemicellulose, and lignin, present in natural fibers,

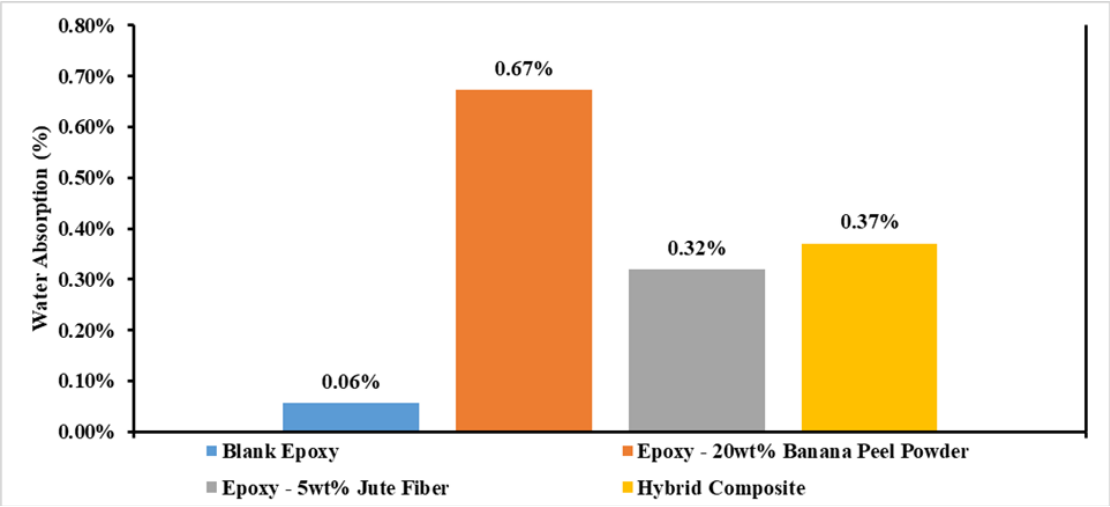

Fig. 8. Water absorption test of epoxy and epoxy-based composites.

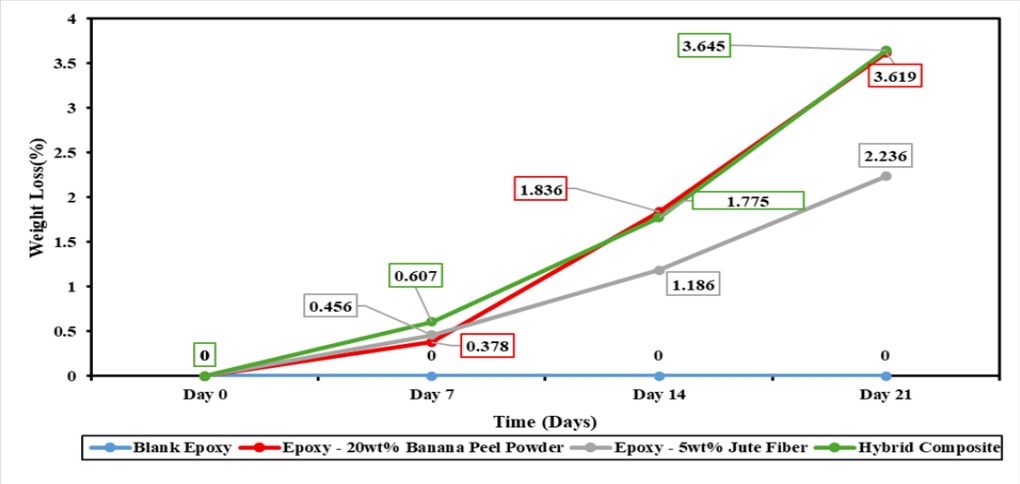

Fig. 9. Soil degradation of epoxy and epoxy-based composites.

promoted microbial activity in the composites during the soil burial test, ultimately resulting in their weight loss. Additionally, the hydrophilic nature of both banana peel powder and jute fiber may have played a significant role. The hydrophilic nature of these components tends to absorb moisture, causing them to swell within the polymer matrix. This swelling can lead to the formation of microcracks within the composite material. These microcracks provide pathways for external factors, such as moisture and microbes, to penetrate and interact with the composite. As these microcracks develop and expand, they create conditions that are conducive to the degradation process. Microbes and other factors can access the polymer matrix more readily through these openings, which can accelerate the degradation process. Importantly, while the formation of microcracks may enhance the rate of degradation, it does not fundamentally alter the overall mechanism of composite degradation [63].

In comparison to other composites, the biodegradability of the hybrid (20 wt.% banana peel powder and 5 wt.% jute fiber) epoxy composite is higher, and there is no degradation observed in the blank epoxy. Therefore, after its useful lifetime, disposing of the hybrid composite will result in relatively rapid degradation, with a somewhat reduced environmental impact.

4. CONCLUSIONS

This study aimed to create epoxy composites using banana peel powder and alkali-treated jute fiber. Different weight percentages of reinforcements were used; (20 wt.%, 25 wt.%, and 30 wt.% banana peel powder) and (5 wt.%, 6.5 wt.%, and 8 wt.% treated jute fiber). The tensile and flexural strength of the composites decreased due to fiber clustering, poor adhesion, fiber misalignment, and reduced matrix contribution. It was found that the highest tensile and flexural strength of the composites were achieved with 20 wt.% banana peel powder (27 MPa and 43.66 MPa) and 5 wt.% jute fiber (21.64 MPa and 42.06 MPa). These optimum loadings (20 wt.% banana and 5 wt.% jute) were incorporated into the epoxy matrix to produce a hybrid composite that displayed superior mechanical properties than the single-filler composites, with tensile and flexural strength of 30.32 MPa and 44.5 MPa. Moreover, the hybrid composite had a hardness value of 59.78 due to increased porosity and water absorption of the natural fibers, which is significantly less than the other composites and even the blank epoxy. Hence, it exhibited greater non-brittleness, resilience, and reduced risk of failure. The thermal analysis showed that the composites initially experienced greater weight loss compared to blank epoxy but demonstrated more resistance to degradation at higher temperatures as the fillers protected the epoxy resin from oxidation. The hybrid composite displayed a weight loss curve between the individual composite curves, indicating that the treatment of jute fiber resulted in less degradation compared to untreated banana peel powder. Similar trends were also observed in water absorption and soil burial tests. Therefore, the hybrid composite balances thermal stability and partial biodegradability while maintaining optimal mechanical properties, which could be a promising eco-friendly alternative to

pure epoxy thermosets in structural applications such as automotive, construction and packaging.

5. FUNDING

The authors received no financial support for the research authorship and/or publication of this article.

6. DATA AVAILABILITY

The datasets used and/or analysed during the current study are available from the corresponding authors.

7. CONFLICT OF INTEREST

The authors declare no conflict of interest.

8. ETHICAL STATEMENT

This work does not include any studies involving human or animal subjects.

9. DECLARATION

We confirm that the results in this manuscript are original and it has not been published elsewhere nor is it under consideration by another journal. All authors have approved the manuscript and agree that in case the article is accepted for publication, its copyright will be assigned to the *Pakistan Academy of Sciences*. Authors have obtained permission to reproduce, where needed, copyrighted material from other sources and ensured that no copyrights have been infringed upon.

10. REFERENCES

1. K. Papadopoulou, P.A. Klonos, A. Kyritsis, O. Mašek, C. Wurzer, K. Tsachouridis, A.D. Anastasiou, and D.N. Bikiaris. Synthesis and Study of Fully Biodegradable Composites Based on Poly (butylene succinate) and Biochar. *Polymers* 15(4): 1049 (2023). https://doi.org/10.3390/polym15041049
2. X. Zhou, S.H. Ghaffar, W. Dong, O. Oladiran, and M. Fan. Fracture and impact properties of short discrete jute fibre-reinforced cementitious composites. *Materials and Design* 49: 35-47 (2013). https://doi.org/10.1016/J.MATDES.2013.01.029
3. M.G. Kibria, N.I. Masuk, R. Safayet, H.Q. Nguyen, and M. Mourshed. Plastic Waste: Challenges and Opportunities to Mitigate Pollution and Effective Management. *International Journal of Environmental Research* 17: 20 (2023). https://doi.org/10.1007/s41742-023-00507-z
4. United Nations Development Programme. Zero Plastic: Study of Plastic Waste in the Republic of Moldova. *UNDP Moldova*, (2023). https://www.undp.org/moldova/publications/study-plastic-waste-republic-moldova
5. T.D. Ngo. Introduction to Composite Materials (Chapter 1). In: Composite and Nanocomposite Materials - From Knowledge to Industrial Applications. T.D. Ngo (Ed.). *IntechOpen* pp. 1-27 (2020). https://doi.org/10.5772/intechopen.91285
6. A.P. Singh. Strength and permeability characteristics of steel fibre reinforced concrete. *International Journal of Civil and Environmental Engineering* 7(10): 733-738 (2013). https://www.semanticscholar.org/paper/Strength-and-Permeability-Characteristics-of-Steel-Singh/31af2139d7a91afaa63bc3a929ffff5ede93d326
7. G. Ramakrishna and T. Sundararajan. Impact strength of a few natural fibre reinforced cement mortar slabs: A comparative study. *Cement and Concrete Composites* 27: 547-553 (2005). https://doi.org/10.1016/j.cemconcomp.2004.09.006
8. T.A. Branca, V. Colla, D. Algermissen, H. Granbom, U. Martini, A. Morillon, R. Pietruck, and S. Rosendahl. Reuse and Recycling of By-Products in the Steel Sector: Recent Achievements Paving the Way to Circular Economy and Industrial Symbiosis in Europe. *Metals* 10(3): 345 (2020). https://doi.org/10.3390/met10030345
9. F.A. Silva, B. Mobasher, and R.D.T. Filho. Cracking mechanisms in durable sisal fiber reinforced cement composites. *Cement and Concrete Composites* 31(10): 721-730 (2009). https://doi.org/10.1016/J.CEMCONCOMP.2009.07.004
10. J. Ahmad, M.M. Arbili, A. Majdi, F. Althoey, A.F. Deifalla, and C. Rahmawati. Performance of concrete reinforced with jute fibers (natural fibers): A review. *Journal of Engineered Fiber Fabrics* 17: 1-17 (2022). https://doi.org/10.1177/15589250221121871
11. C. Ranjan, Z. Ahmed, S.R. Kumar, A. Kumar, A. Kumar, and K. Kumar. Fabrication and strength analysis of rice straw fibers reinforced epoxy biodegradable composite. *Materials Today: Proceedings* 46: 331-335 (2021). https://doi.org/10.1016/J.MATPR.2020.08.299
12. N.D. Muralidharan, J. Subramanian, S.K. Rajamanickam, and V. Gopalan. An experimental investigation of flame retardancy and thermal stability of treated and untreated kenaf fiber reinforced epoxy composites. *Journal of Polymer Engineering* 43(10): 865-874 (2023). https://doi.

org/doi:10.1515/polyeng-2023-0128

13. B.N. Sharath, T.G.Y. Gowda, P. Madhu, C.B.P. Kumar, N. Jain, A. Verma, M.R. Sanjay, and S. Siengchin. Fabrication of raw and chemically treated biodegradable Luffa aegyptica fruit fibre-based hybrid epoxy composite: a mechanical and morphological investigation. *Biomass Conversion and Biorefinery* 15: 8473-8486 (2025). https://doi.org/10.1007/s13399-024-05570-w
14. G.R. Raghav, R.A. Kumar, N.K. Jawaharlal, C. Vignesh, F. Sahayaraj Arockiasamy, and E. Syafri. Effect of Cellulose Nanofibers from Red Coconut Peduncle Waste as Reinforcement in Epoxy Composite Sheets. *Cellulose Chemistry and Technology* 57(7-8): 855-866 (2023). https://doi.org/10.35812/cellulosechemtechnol.2023.57.75
15. J. Yusuf, S.M. Sapuan, U. Rashid, R. A. Ilyas, and M.R. Hassan. Thermal, mechanical, and morphological properties of oil palm cellulose nanofibril reinforced green epoxy nanocomposites. *International Journal of Biological Macromolecules* 278(3): 134421 (2024). https://doi.org/10.1016/J.IJBIOMAC.2024.134421
16. M.M. Shariff, G.R. Arpitha, N. Jain, U. Shankar, A. Verma, and N.D. Shivakumar. A comparative study on the effect of reinforcing boron nitride/alumina in epoxy-based hybrid composite with Millettia pinnata leaf powder and glass sheets: Experimental fabrication, mechanical and micro-structural characterization. *Hybrid Advances* 4: 100095 (2023). https://doi.org/10.1016/J.HYBADV.2023.100095
17. A. Zeleke and H.S. Gebremedhen. Characterization of Sisal-Glass Fiber Reinforced Epoxy Hybrid Composite. *8th EAI International Conference, ICAST 2020, Proceedings, Part II, (October 2nd - 4th, 2020), Bahir Dar, Ethiopia* (2021). http://dx.doi.org/10.1007/978-3-030-80618-7_23
18. G.R. Arpitha, H. Mohit, P. Madhu, and A. Verma. Effect of sugarcane bagasse and alumina reinforcements on physical, mechanical, and thermal characteristics of epoxy composites using artificial neural networks and response surface methodology. *Biomass Conversion and Biorefinery* 14(11): 12539-12557 (2024). https://doi.org/10.1007/s13399-023-03886-7
19. K.R. Ashok, K.A. Ramesh, S. Durairaj, and R.C. Sakthi. Morphological and mechanical evaluation of epoxy hybrid composites reinforced with banana and jute cellulose. *Journal of Mechanical Science and Technology* 40: 455-461 (2026). https://doi.org/10.1007/s12206-025-1237-7
20. G.R. Arpitha, N. Jain, and A. Verma. Banana biofiber and glass fiber reinforced hybrid composite for lightweight structural applications: mechanical, thermal, and microstructural characterization. *Biomass Conversion and Biorefinery* 14(11): 12589-12598 (2024). https://doi.org/10.1007/s13399-023-04300-y
21. M.A. Based. Extraction of banana fiber and characterization analysis of hybrid (banana, jute, carbon and glass) reinforced composite materials. *Results in Materials* 28: 100803 (2025). https://doi.org/10.1016/j.rinma.2025.100803
22. G.R. Arpitha, N. Jain, A. Verma, and M. Madhusudhan. Corncob bio-waste and boron nitride particles reinforced epoxy-based composites for lightweight applications: fabrication and characterization. *Biomass Conversion and Biorefinery* 14(11): 12531-12538 (2024). https://doi.org/10.1007/s13399-022-03717-1
23. P. Agrawal, A.K. Kundu, D. Purohit, P. Sahu, N. Gautam, A. Sharma, and V. Patil. A review paper of composite materials: advantages and applications. *International Journal of Advances in Engineering and Management* 4: 369 (2022). https://doi.org/10.35629/5252-0411369370
24. H. Jamshaid, R.K. Mishra, A. Raza, U. Hussain, M.L. Rahman, S. Nazari, V. Chandan, M. Muller, and R. Choteborsky. Natural cellulosic fiber reinforced concrete: influence of fiber type and loading percentage on mechanical and water absorption performance. *Materials* 5(3): 874 (2022). https://doi.org/10.3390/ma15030874
25. M.S. Islam and S.J. Ahmed. Influence of jute fiber on concrete properties. *Construction and Building Materials* 189: 768-776 (2018). https://doi.org/10.1016/J.CONBUILDMAT.2018.09.048
26. M.R. Islam, M.M. Kamal, M.R. Kabir, M.M. Hasan, A.R. Haque, and S.M.K. Hasan. Phenolic compounds and antioxidants activity of banana peel extracts: Testing and optimization of enzyme-assisted conditions. *Measurement: Food* 10: 100085 (2023). https://doi.org/10.1016/J.MEAFOO.2023.100085
27. K.Z.M.A. Motaleb, A. Ahad, G. Laureckiene, and R. Milasius. Innovative Banana Fiber Nonwoven Reinforced Polymer Composites: Pre- and Post-Treatment Effects on Physical and Mechanical Properties. *Polymers* 13(21): 3744 (2021). https://doi.org/10.3390/polym13213744
28. J. Zhang, H. Dong, L. Tong, L. Meng, Y. Chen, and G. Yue. Investigation of curing kinetics of sodium carboxymethyl cellulose/epoxy resin system by differential scanning calorimetry. *Thermochimica Acta* 549: 63-68 (2012). https://doi.org/10.1016/J.

TCA.2012.09.015

29. G.A. Sabirova, R.R. Safin, N.R. Galyavetdinov, and A.R. Shaikhutdinova. Research of biodegradable wood completed composite materials based on polylactide. *Journal of Physics: Conference Series* 1399(4): 044117 (2019). https://doi.org/10.1088/1742-6596/1399/4/044117
30. A.L. Naidu, D. Raghuveer, and P. Suman. Studies on characterization and mechanical behavior of banana peel reinforced epoxy composites. *International Journal of Scientific & Engineering Research* 4(6): 844-851 (2013). https://www.researchgate.net/publication/344151239_Studies_on_Characterization_and_Mechanical_Behavior_of_Banana_peel_Reinforced_Epoxy_Composites
31. A. Kumar, S. Kumar, D. Kumar, V.K. Mahakur, and S. Bhowmik. Utilization of banana peel as bio-filler to develop bio-composite materials and characterize their physical, mechanical, thermal, and tribological characteristics. *Polymer Bulletin* 81: 16175-16196 (2024). https://doi.org/10.1007/s00289-024-05464-x
32. X. Liu. Surface modification and micromechanical properties of jute fiber mat reinforced polypropylene composites. *Express Polymer Letters* 1: 299-307 (2007). https://doi.org/10.3144/expresspolymlett.2007.43
33. M. Kumar, A. Sachdeva, S. Singh, and A.P. Singh. Prediction of Mechanical Properties and Morphological Characterization of the Reinforced Hybrid Natural Fiber Polymer Composites using the Bidirectional Sisal Fiber and Woven Jute. *International Journal of Mechanical Engineering* 5(5): 27-31 (2018). https://doi.org/10.14445/23488360/IJME-V5I5P105
34. M. Boopalan, M. Niranjanaa, and M.J. Umapathy. Study on the mechanical properties and thermal properties of jute and banana fiber reinforced epoxy hybrid composites. *Composites Part B: Engineering* 51: 54-57 (2013). https://doi.org/10.1016/J.COMPOSITESB.2013.02.033
35. Test methods for flexural properties of unreinforced and reinforced plastics and electrical insulating materials *ASTM International, West Conshohocken, PA* (2017). https://doi.org/10.1520/D0790-17
36. Standard test method for tensile properties of polymer matrix composite materials. *ASTM International, West Conshohocken, PA* (2014). DOI: 10.1520/D3039_D3039M-08
37. Test method for rubber property-durometer hardness. *ASTM International, West Conshohocken, PA* (2015). DOI: 10.1520/D2240-15R21
38. Test method for water absorption of plastics. *ASTM International, West Conshohocken, PA* (2022). https://doi.org/10.1520/D0570-22
39. R. Kumar, M. Yakubu, and R. Anandjiwala. Biodegradation of flax fiber reinforced poly lactic acid. *Express Polymer Letters* 4(7): 423-430 (2010). https://doi.org/10.3144/expresspolymlett.2010.53
40. M.K. Gupta, R.K. Srivastava, and H. Bisaria. Potential of jute fibre reinforced polymer composites: a review. *International Journal of Fiber and Textile Research* 5: 30-38 (2015). https://www.researchgate.net/publication/282073854_Potential_of_Jute_Fibre_Reinforced_Polymer_Composites_A_review
41. B. Sandeep, H.N. Divakar, and K.S. Keerthiprasad. Coupling strength and synergy: exploring the mechanical properties of epoxy hybrid composites with s-glass and basalt fibers. *Scholars International Journal of Chemistry and Material Sciences* 7: 45-59 (2024). DOI: 10.36348/sijcms.2024.v07i05.001
42. N. Saba and M. Jawaid. Epoxy resin based hybrid polymer composites. *Hybrid Polymer Composite Materials: Properties and Characterisation* pp. 57-82 (2017). https://doi.org/10.1016/B978-0-08-100787-7.00003-2
43. M.R. Rahman, M.M. Huque, M.N. Islam, and M. Hasan. Improvement of physico-mechanical properties of jute fiber reinforced polypropylene composites by post-treatment. *Composites Part A: Applied Science and Manufacturing* 39(11): 1739-1747 (2008). https://doi.org/10.1016/J.COMPOSITESA.2008.08.002
44. M. Haque, N. Islam, M. Huque, M. Hasan, S. Islam, and S. Islam. Coir Fiber Reinforced Polypropylene Composites: Physical and Mechanical Properties. *Advanced Composite Materials* 19(1): 91-106 (2010). https://doi.org/10.1163/092430409X12530067339325
45. T. Yokozeki, Y. Iwahori, and S. Ishiwata. Matrix cracking behaviors in carbon fiber/epoxy laminates filled with cup-stacked carbon nanotubes (CSCNTs). *Composites Part A: Applied Science and Manufacturing* 38: 917-924 (2007). https://doi.org/10.1016/j.compositesa.2006.07.005
46. S. Dehrooyeh, M. Vaseghi, M. Sohrabian, and M. Sameezadeh. Glass fiber/Carbon nanotube/Epoxy hybrid composites: Achieving superior mechanical properties. *Mechanics of Materials* 161: 104025 (2021). https://doi.org/10.1016/j.mechmat.2021.104025
47. K.G. Dassios. A review of the pull-out mechanism in the fracture of brittle-matrix-fibre-

reinforced composites. *Advanced Composites Letters* 16(1): 17-24 (2007). https://doi.org/10.1177/096369350701600102

48. M. Davindrabrabu, P.S. Januar, B. Dandi, M.R. Mohd Ruzaimi, and T. Cionita. Effect of fibre loading on the flexural properties of natural fibre reinforced polymer composites. *Applied Mechanics and Materials* 695: 85-88 (2014). https://doi.org/10.4028/www.scientific.net/AMM.695.85
49. S. Siddika, F. Mansura, and M. Hasan. Physico-mechanical properties of jute-coir fiber reinforced hybrid polypropylene composites. *International Journal of Chemical, Molecular, Nuclear, Materials and Metallurgical Engineering* 7(1): 60-64 (2013). https://doi.org/10.5281/zenodo.1328564
50. H.M. Khdier, W.M. Salih, A.H. Ali, and K.A.F. Husham. Comparative study between properties of composite polymer blend reinforced within two kinds of natural fibers. *Journal of Materials Science: Materials in Engineering* 21: 10 (2026). https://doi.org/10.1186/s40712-025-00368-8
51. B. Neher, M.M.R. Bhuiyan, H. Kabir, M.R. Qadir and M.A. Gafur, and F. Ahmed. Study of mechanical and physical properties of palm fiber reinforced acrylonitrile butadiene styrene composite. *Materials Sciences and Applications* 5(1): 39-45 (2014). https://doi.org/10.4236/msa.2014.51006
52. S.C.D. Sharma, P.B. Nishan, M.M. Islam, and A.M. Hossain. Study of Mechanical Properties of Glass Fiber Reinforced Epoxy Composites using Chemically Modified Carbon Nanoparticles as Nano-Fillers. *International Journal of Engineering Research & Technology* 14(12): 18053145 (2025). https://doi.org/10.5281/zenodo.18053145
53. M. Cui, L. Zhang, P. Lou, X. Zhang, X. Han, Z. Zhang, and Z. Shuhua. Study on thermal degradation mechanism of heat-resistant epoxy resin modified with carboranes. *Polymer Degradation and Stability* 176: 109143 (2020). https://doi.org/10.1016/j.polymdegradstab.2020.109143
54. M.K. Lila, G.K. Saini, M. Kannan, and I. Singh. Effect of fiber type on thermal and mechanical behavior of epoxy based composites. *Fibers and Polymers* 18: 806-810 (2017). https://doi.org/10.1007/s12221-017-1147-0
55. S.R. Islam, A. Alassod, M.K. Patoary, T. Naveed, M.A. Ali, and J. Jiang. Study on thermal, thermo-mechanical, and flexural properties of jute fiber surface modification and its reinforced composite. *American Association of Textile Chemists and Colorists Journal of Research* 8(5): 11-17 (2021). https://doi.org/10.14504/ajr.8.5.2
56. S. Sanjeevi, V. Shanmugam, S. Kumar, V. Ganesan, G. Sas, D.J. Johnson, M. Shanmugam, A. Ayyanar, K. Naresh, R.E. Neisiany, and O. Das. Effects of water absorption on the mechanical properties of hybrid natural fibre/phenol formaldehyde composites. *Scientific Reports* 11(1): 13385 (2021). https://doi.org/10.1038/s41598-021-92457-9
57. T. Väisänen, O. Das, and L. Tomppo. A review on new bio-based constituents for natural fiber-polymer composites. *Journal of Cleaner Production* 149: 582-596 (2017). https://doi.org/10.1016/J.JCLEPRO.2017.02.132
58. B. Dan-asabe. Thermo-mechanical characterization of banana particulate reinforced PVC composite as piping material. *Journal of King Saud University - Engineering Sciences* 30(4): 296-304 (2018). https://doi.org/10.1016/j.jksues.2016.11.001
59. O.O. Daramola and O.S. Akintayo. Water absorption characteristics of Epoxy matrix composites reinforced with green silica particles. *Leonardo Electronic Journal of Practices and Technologies* 32: 215-232 (2018). https://www.academia.edu/74417933/Water_absorption_characteristics_of_Epoxy_matrix_composites_reinforced_with_green_silica_particles
60. A. Mahmud, C. Dev, M.T. Meem, M.A. Gafur, and M.A. Hoque. Preparation and mechanical properties of green epoxy/chitosan/silver nanocomposite. *Green Materials* 10(3): 110-118 (2021). https://doi.org/10.1680/jgrma.21.00020
61. S. Dixit. Degradation analysis of lignocellulosic fillers infused coir epoxy composites in different environmental conditions. *International Journal of Lignocellulosic Products* 1(2): 160-179 (2014). https://doi.org/10.22069/ijlp.2014.2073
62. M. Milošević, A. Krkobabić, M. Radoičić, Z. Šaponjić, T. Radetić, and M. Radetić. Biodegradation of cotton and cotton/polyester fabrics impregnated with Ag/TiO2 nanoparticles in soil. *Carbohydrate Polymers* 158: 77-84 (2017). https://doi.org/10.1016/j.carbpol.2016.12.006
63. H. Wang, D. Wei, A. Zheng, and H. Xiao. Soil burial biodegradation of antimicrobial biodegradable PBAT films. *Polymer Degradation and Stability* 116: 14-22 (2015). https://doi.org/10.1016/J.POLYMDEGRADSTAB.2015.03.007

Proceedings of the Pakistan Academy of Sciences: A Physical and Computational Sciences 63(1): 33-45 (2026)

ISSN (Print): 2518-4245; ISSN (Online): 2518-4253
http://doi.org/10.53560/PPASA(63-1)707

Pakistan Academy of Sciences

Research Article

Spatiotemporal Trends of Snow Cover under Climate Change Using Landsat Imagery: A Case Study of the Astore Region, Western Himalaya, Pakistan

Bahadar Khan[1], Abdur Raziq[1]*, Izhar Ullah[2], and Yasir Hanif[1]

[1]Department of Geography, Islamia College Peshawar, Pakistan
[2]Department of Agricultural and Applied Economics, The University of Agriculture, Peshawar, Pakistan

Abstract: The Upper Indus Basin is a significant freshwater resource for Pakistan's irrigation system, with approximately half of its annual water resources are produced from glacier and snow nourished basin within the Himalaya, Karakorum, and Hindu Kush (HKH) region. The basin is increasingly vulnerable to climate change, making it important to study and assess the spatiotemporal changes of snow cover area (SCA) and their relationships with climatic factors for actual water resource management. This study is focused on the sub-basin of Upper Indus Basin Astore region, using Landsat imagery from 1998 to 2023 to calculate SCA during the summer season through the indices of the Normalized Difference Snow Index. Climatic variables, with precipitation and temperature were downloaded from NASA's Prediction of worldwide energy resources (POWER) dataset. Results illustrate a significant decline in SCA at a rate of -4.92 km^2 per year, which is associated with increasing mean annual temperature and decreasing precipitation. These findings confirm that increasing temperature and reduced precipitation are contributing to the reduction of snow cover in Astore. This study highlights the significance of regional scale studies to know the consequence of climate change on change in snow cover within the Upper Indus Basin.

Keywords: Snow Cover Area, Climate Change, Normalized Difference Snow Index, Landsat Imagery, Astore Basin, Precipitation, Temperature.

1. INTRODUCTION

The Astore Basin, a snow-fed sub-basin of the Upper Indus Basin located in the western Himalayas, was selected as the focus of this study. The freshwater ecosystem of the earth is mostly located in mountainous regions, where glaciers have a substantial impact on the worldwide flow of streams and rivers [1, 2]. During drought periods, snow covered mountain regions act as continuous water sources and serve as a lifesaving buffer [3]. The Himalayas, Karakoram, and Hindukush (HKH) are among the highest mountain ranges where glaciers melt significantly and influence regional water supplies [2, 4, 5]. The HKH region comprises the most extensive mountainous areas, spanning many countries including Pakistan, Afghanistan, China, India, Nepal, Bhutan, and Myanmar. These areas are renowned as the 'Third Pole' or 'Water Tower of Asia' due to their substantial freshwater reserves. A significant portion of the major river systems in these countries originate in the HKH region, and are sustained by glacier and snowmelt [6, 7]. Consequently, this area sustains the livelihoods of inhabitants in dowstream areas by providing vital water resources, which are crucial for drinking, agricultural production, power generation, and industrial development [8-11].

Nevertheless, as a consequence of climate change, snow covered and glacier regions are facing significant threats and are undergoing continual transformation [12]. Pakistan is mostly agrarian nation that heavily relies on Indus River

Received: January 2026; Revised: February 2026; Accepted: March 2026
* Corresponding Author: Abdur Raziq <drraziq@icp.edu.pk>

system [13]. The main source of water in this river originates from glacier and snow melt [14, 15]. Snow-covered mountains remain largely unaffected by direct human activities, they are susceptible to climatic variability. Climate change is causing rising temperatures, shorter snowfall durations, and altered snowfall patterns. These factors influence river flow throughout summer and help to cause the snow cover to melt sooner [16-18], ultimately leading to water-shortage and other related natural disasters [19]. Temperature directly affects snowmelt development, whereas precipitation especially in solid form is the key source of snow accumulation [20]. Current studies underscore that the relationship between temperature, precipitation and snow cover area is unstable and intensifying under climate change. With increasing temperature foremost to previous spring melt and decreased snow perseverance in numerous mountain regions [21-22]. Despite advancements, a substantial research gap continuous in developing strong, spatially clear outlines that methodologically integrate Normalized Difference Snow Index (NDSI) obtained Snow Cover Area (SCA) with temporally corresponding temperature and precipitation data to improve the considerate of seasonal snowpack changing aspect and its sensitivity to climatic variables. Some existing analysis remain on description and coarse-resolution climatic datasets that inconsistency the spatial information of satellite-based SCA.

In this study snow cover area generally shows a decline, however some studies [23-25] reported a rising trend in SCA due to increase in winter precipitation and reduced summer temperatures. Subsequent research anticipated that the HKH region would experience increased precipitation from 1901 to 2099; however, temperature trends show strong interannual variability. According to other studies [26, 27], there would be a notable rising trend in precipitation in Gilgit-Baltistan throughout the midcentury (2021-2060). In the Northwest Himalayan area, Negi and Kanda [28] also noted a rising tendency in SCA due to a slowing rate of warming. These variations in climate thus suggest variations in SCA. Therefore, it's important to keep an eye on how the snow cover is changing. Nonetheless, a sizable portion of the HKH region is vulnerable, and there is little information available on the geographic variability of SCA overall. The high altitude and challenging terrain of the SCA made mapping extremely challenging in the past [29, 30]. Since the 1960s, various geospatial techniques have been developed to facilitate snow cover mapping [31]. Khan *et al*. [32] studied snow characteristic in Astore sub-basin using MODIS satellite data, showing robust seasonal spread and spatial changes in snow water correspondent, snow depth, and SCA, with winter snow cover area up to 94% and summer as noted low as 20%. Snowmelt was affected by local basin and metrological factors. Ali *et al*. [33] projected future hydrological responses using CMIP6 models, showing that rising temperatures and variable precipitation could alter streamflow and reduce snowmelt contributions, despite some scenarios indicating increased precipitation. Regionally, Dar and Sarif [34] reported negative glacier mass balance and glacial area loss in the Kashmir Himalayas and UIB, though some Karakoram glaciers show slower loss (Karakoram anomaly). Almagioni *et al*. [35] identify complex, spatially diverse trends over Karakoram, Western Himalaya, and Kunlun Mountain ranges, with change in snow season during connected with temperature and precipitation changes. Hydrological response and snow cover change in Astore are formed by connection among climate, topography, and atmospheric forcing, highlighting the need for combined climate modeling, remote sensing and hydrological assessment.

Currently, geospatial communities use a variety of indices and techniques for SCA mapping, as well as image-classification methods. These indices including normalized difference debris index (NDDI), normalized difference principal component index (NDPSCI), normalized difference water index (NDWI), normalized difference snow thermal index (NDSTI) and normalized difference snow index (NDSI). In this study, NDSI is used for monitoring as it produces good results in mountain terrain and is one of the most famous indices for SCA calculation. Present SCA analysis based on NDSI frequently lack integration with main regulatory climatic variables, temperature and precipitation, restricting the ability to assess the contributing factors behind observed snow cover patterns, trends and anomalies, especially in data-scare mountain regions.

The main purpose of this study is to determine the snow-covered area in Astore with application of normalized difference snow index (NDSI) from 1998-2023. Temperature and precipitation, two

climatic parameters, were analyzed in relation to SCA. Understanding the SCA's relationship to temperature and rainfall was crucial for those who depend on glaciers in mountainous and low-lying locations. The past study elaborated the glacier cover in Astore, Hunza and Gilgit [36]. The western Himalaya region shows exceptional patterns of topographic complexity, erosion, and exposure [37]. The Astore basin, located in the western Himalayas, is a snow-fed system characterized by low- to mid-elevation glaciers and predominantly north-facing slopes. Due to its relatively low elevation, Astore is mostly reliant on precipitation particularly in winter season. These fundamental characteristics give Astore its unique geographic settings. Accordingly, the objectives of this study are to: (1) Monitor the spatial and temporal fluctuation of SCA in the Astore region, and (2) analyze the relationship between climatic variables and SCA to assess climate-change impacts on snow cover dynamics.

2. MATERIALS AND METHODS

2.1. Study Area

The study area is located between 34° 16′-37° 06 N latitude and 72° 03′-77° 44′ E longitude, defining the boundary between greater Himalaya and Karakorum ranges [38]. The Indus River starts from the Tibetan Plateau, flow through northern Pakistan, and provide water to the Tarbela Dam [39, 40]. For this study, the Astore region was selected, which lies in the dangerous western Himalayas of northern Pakistan. Farhan *et al*. [39] described that annual mean temperature in Astore range from -2.9°C to 9.9 °C, however annual precipitation changes between 500 mm and 870 mm. Significant precipitation expected (75%) during the spring and winter season due to westerly distribution, although the residual 25% occurs during the summer and autumn seasons, mainly "affected by local jet streams" and the south Asian monsoon. Both winter rainfall and solid precipitation driven by westerlies meaningfully effect the discharge of the Astore River [41]. Figure 1 shows that Astore is bounded to the North by Gilgit, South by Khyber Pakhtunkhwa, and Neelum valley, East by Skurdu, and West by Diamer district with total cover area about 5200 km^2 [42].

2.2. Methods

This study used a temporal satellite imagery spanning from 1998 to 2023. "Satellite data (Collection 2 level-2) were downloaded from USGS website." Only images with less than 10% cloud coverage were selected to confirm precision and accuracy. All downloaded images underwent standard preprocessing process as delineated in preceding literature [43]. To continue consistency with previous studies and to enable accurate assessment, atmospheric correction was omitted intentionally; this method is mainly valid in high

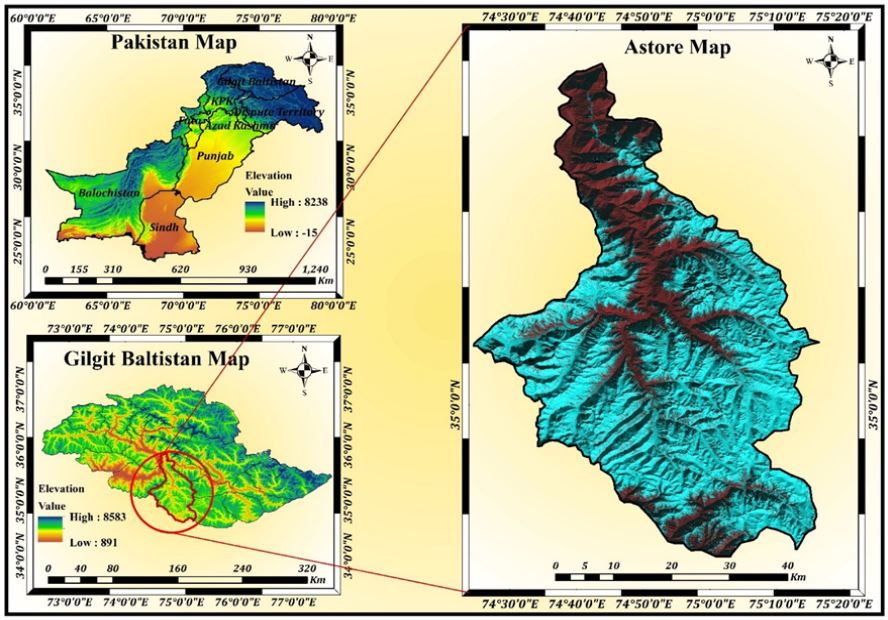

Fig. 1. Geographical location of study area.

altitude mountainous region where atmospheric effect is minimum and do not meaningfully effect snow detection [44-46]. The dataset comprised imagery from different generation of Landsat satellite particularly, Landsat 4-5 TM, Landsat 7 ETM+, and Landsat OLI/TIRS. "All satellite images used had a spatial resolution of 30 m. and were analyzed mainly for the summer season. The NDSI was employed to find and define snow covered areas. This index takes benefit of snow spectral signature, especially its robust reflectance in the visible band (green) and low reflectance in the shortwave infrared (SWIR) band. The NDSI is calculated using below formula, as defined by Hall *et al*. [47]:

$$NDSI = \frac{GREEN-SWIR}{GREEN+SWIR} \quad (1)$$

NDSI value ranges from -1 to +1, with values above 0 representing the presence of snow. A most common threshold of NDSI ≥ 0.4 was used to categorized snow pixels in the satellite imagery, as suggested in various literature studies [48-51]. The optimal threshold should be determined based on the study area, atmospheric and sensor description to minimize misclassification. For the calculation: Landsat 5 TM and 7 ETM+ used band 2 (Green with spectral range 0.52-0.60 µm) and Band 5 (SWIR with spectral range 1.55-1.75 µm). For Landsat 8 OLI used band 3 (Green with spectral range 0.53-0.59 µm) and band 6 (SWIR spectral range 1.57-1.65 µm). Once the NDSI was calculated, the snow cover area (SCA) was extracted by reclassifying the NDSI values into two classes, for instance 1 for snow covered area and 0 for snow free areas. This classification was performed using the reclassify tool. Following classification, the entire snow-covered area within the study area was computed. "This was computed using the filed calculator tool" which allowed for efficient conversion of pixel based into area measurements. Resultantly, the SCA was calculated on an annual basis (for summer season) by totaling up the classified snow pixels, allowing for the evaluation of temporal changes in snow distribution over the 25 years of study period. In addition to satellite imagery, climatic data on precipitation and temperature were acquired from NASA website perdition of worldwide energy resources database (https://www.earthdata.nasa.gov/data/projects/power) for the time period (1998-2023). These data were particularly extracted for the study area to examine the connection between climatic factors and variation in SCA. The correlation between annual snow cover level and corresponding climate variables such as rainfall and temperature were analyzed to evaluate the impact of climate change on snow dynamics in the region. Figure 2 shows the overall methodology of the study area.

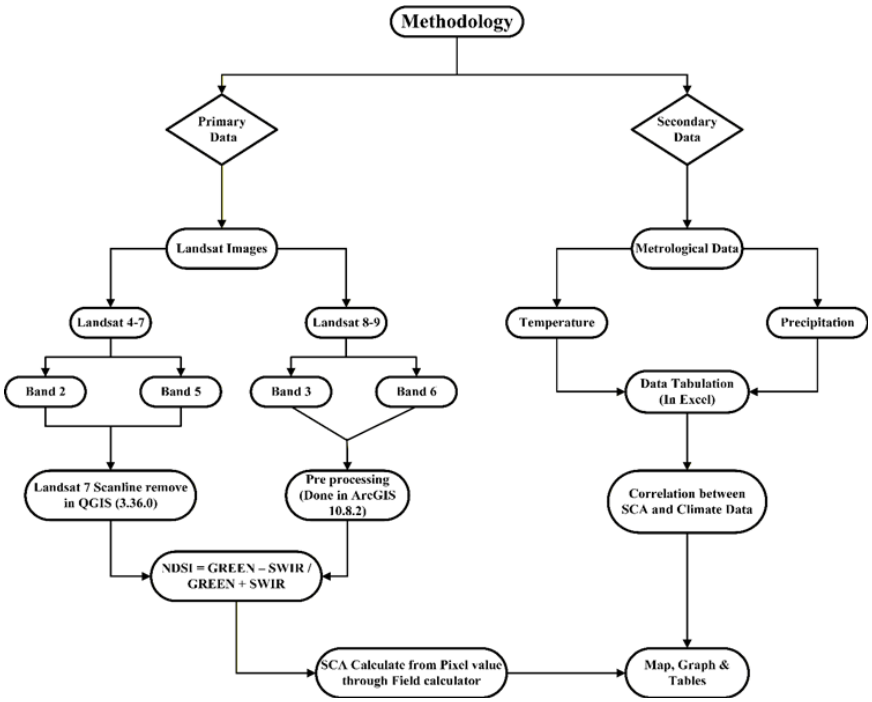

Fig. 2. Layout of the research methodology.

2.3. Landsat Data

Landsat data are easily available, annual Landsat imagery for the study region was freely acquired from USGS website for the period 1998 to 2019 [51]. Rastner *et al.* [52] explained that Landsat delivers extensive time series data with multispectral and spatial resolution, which is especially useful for snow cover area. Every Landsat satellite completes a full orbit cycle particularly every sixteen days. In this research, data from Landsat 5 Thematic Mapper ™, Landsat 7 ETM+, and Landsat 8 OLI were used. The detailed parameters of the satellite sensors are provided in Table 1.

2.4. Predication of Worldwide Energy Resources (POWER) Database (Rainfall and Temperature)

Climate data, with temperature and precipitation, were used to examine change in snow covered area (SCA) in the Astore region. For this drive, climatic data for the study period from 1998 to 2023 were downloaded from NASA Powered portal data. The effect of climate changes on SCA was examined using this dataset. Table 2 illustrated in detailed parameters of the climatic data.

3. RESULTS

The yearly snow cover area (SCA) of Astore was computed applying Landsat data from 1998 to 2023 in ArcGIS 10.8.2. This study shows significant changes in the Astore region due to variation in temperature and precipitation [33, 53]. In July 1998, the SCA of Astore was 6.32%, whereas in July 2008, it reduced to 2.27%. The significant discharge of the Astore River indicates distinguished variations within the regional snow cover. [54] noted, annual and seasonal changes in snow cover considerably effect the flow of the Astore River. Our results show a declining trend in SCA in Astore at a rate of -4.92% per year, determined by changing precipitation and temperature dynamics. In contrast, rise in SCA have been detected in Karakoram and western Himalaya regions [33]. The Upper Indus Basin (UIB) depend heavily on water from snow cover and glacier melt. With the detected decrease in snow cover, the Astore River is probable to be importantly impacted. Warmer summer and low precipitation (increasing summer temperatures and declining precipitation tendencies) accelerate snowmelt in the mountains, potentially leading to water scarcity in the Astore River and rising the risk of glacier lake outburst (GLOFs). Figure 3

Table 1. Detail parameters of Landsat data.

Data type	Date	Spatial resolution (m)	Cloud cover (%)	Path	Row
Landsat 4-5 (TM)	July-1998	30	25	149	035
Landsat 7 (ETM)	July -2003	30	30	149	035
Landsat 7 (ETM)	July- 2008	30	1	149	035
Landsat 7 (ETM)	July -2013	30	1	149	035
Landsat 8 (OLI/TIRS)	Aug -2018	30	2	149	035
Landsat 8 (OLI/TIRS)	Aug -2023	30	4	149	035

Table 2. Detail parameters of climate data.

Date	Minimum temp.	Maximum temp.	Means temp.	Precipitation (mm)
Jul-1998	19.06	26.80	18.93	12.6
Jul-2003	17.88	22.91	20.39	28
Jul-2008	17.15	22.04	19.59	25.1
Jul-2013	15.15	21.32	18.23	35.8
Aug-2018	17.66	22.86	20.26	37.3
Aug-2023	16.79	21.88	19.34	15

illustrates the annual SCA, while Figure 4 presents a graphical description of Astore SCA.

Figure 4 shows a time series analysis of annual temperature, precipitation, and SCA from 1998 to 2023 at five-year gaps. The data show a clear rising trend in precipitation, increasing from 12.6 mm in 1998 to 37.3 mm in 2018 previously decreasing to 15 mm in 2023. This overall positive however weak linear connection is counted by the regression equation y = 0.2891x -555.65 (R^2 = 0.0692). In, comparison, mean annual temperature showed minimal inconsistency across the study period, with values shifting narrowly between 18.2 °C and 20.4 °C, subsequent in a near- flat trend line defined by y = 0.0017x + 16.01 (R^2 = 0.0004). SCA confirmed the most distinct and clear trend, considered by a long-term decline as defined by the equation y = -28.237x + 57501, which consider for a reasonable amount of the change (R^2 = 0.4829). The interannual changeability in snow cover, connecting successive increase and decrease, therefore, overlaid upon a substantial negative secular trend.

The linear data displayed in Figure 4 (1998-2023) share different and statistically diverse trends for three main climatic variables, temperature, precipitation and snow cover area (SCA). A relative analysis highlights the complex topography of mountain or high-latitude ecosystem responses to climatic changes, where SCA acts as a serious integrators' variable with a more sensitive and

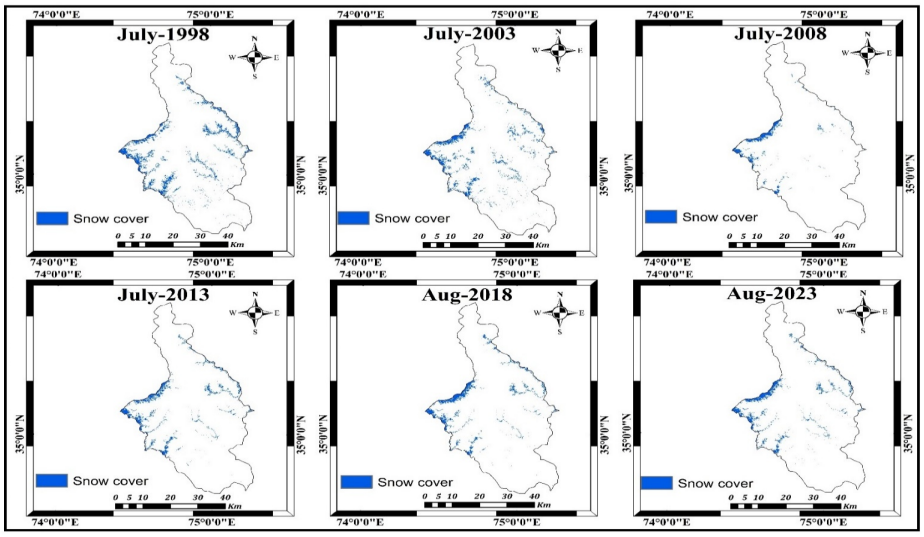

Fig. 3. Annual snow cover of Astore for the period (1998-2023).

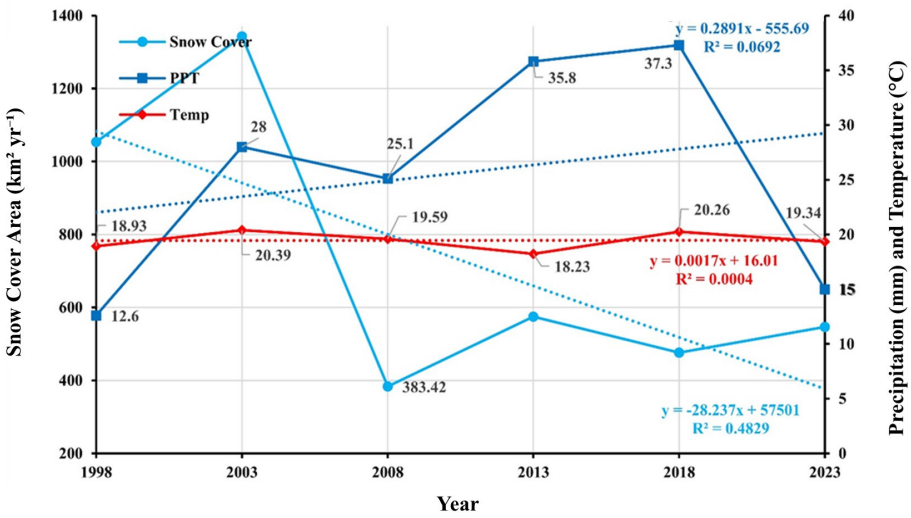

Fig. 4. SCA annual rainfall and temperature of Astore.

distinct trend than the primary climatic variables in this dataset. The main climatic drivers including precipitation, temperature displayed remarkable weak linear trends over the 25-year period in the study area. The precipitation trend, while showing a clear increase (y = 0.2891-555.69), is considered by high interannual instability, as proved by the peak of 37.3 mm in 2018 and following sharp decline to 15.0 in 2023. The very low coefficient of determination (R^2 = 0.0692) confirms that this mountain slope describes less than 7% of the variance in the data, signifying that precipitation is influence by stochastic, short-term changeability rather than a strong, deterministic trend. In contracts, mean annual temperature shows negligible variation no linear warming or cooling trend visible at this temporal and interval. The differentiate between those two weak trends (temperature stable and precipitation slightly increasing) is a serious starting point for analyzing the climatic response.

In sharp difference to the vague climatic sign, the snow cover area (SCA) shows a robust, coherent negative decline trend. The regression equation (y= -28.237x + 57501) shows a considerable rate of decline, which is endorse by the strongest statistical connection in the dataset (R^2 = 0.4829). This reveals that almost 50% of the changes in SCA can be described by the linear way of time, a convincing sign of determined loss. The narrative report "increase, decrease, again increase, again decreased and decreasing trend" precisely define the interannual changes overlaid upon this leading negative route. These year-to-year changes are likely assigned to the instable precipitation patterns that is high snow years in 2013 and 2018 consistent to high precipitation), but the basic secular decline is unique.

The Mann–Kendall test indicates a weak and statistically non-significant decreasing tendency in snow-covered area during 1998-2023. Sen's slope estimator suggests an average decline of approximately 20.3 km² per year. Mean precipitation exhibits a weak increasing tendency, whereas land surface temperature shows no consistent monotonic trend in Table 3. Pearson correlation analysis reveals weak and statistically insignificant relationships between snow cover and both precipitation and temperature, indicating that snow-cover variability is likely influenced by multiple interacting climatic and topographic factors rather than individual climatic variables alone is illustrated in Table 4.

3.1. Climatic Variable and Snow Cover

To improve our considerate of snow cover dynamics, the SCA results were linked with other climate variable, such as precipitation and mean annual temperature. The analysis covered the period from 1998 to 2023. This study linked climatic data to notice changes in SCA and to evaluate the effect of climate variation toward snow cover. By calculating the precipitation and mean annual temperature for Astore, we found that the mean annual temperature is rising while precipitation is declining. Moazzam *et al.* [27] stated a positive trend in summer precipitation, they also observed increasing temperature trend. In this study, we detected an increase in mean temperature follow by a decreasing trend in precipitation, which accelerates snowmelt.

4. DISCUSSION

During this analysis, we evaluated variations in snow cover area in Astore region utilize Landsat data for

Table 3. Showing Mann–Kendall test analysis.

Variable	Z (MK)	Trend direction	Sen's slope (Q)
Snow cover area	−0.75	Decreasing	−20.27 km² yr^{-1}
Mean precipitation (PPT)	0.75	Increasing	+0.62 mm yr^{-1}
Mean LST	0	No clear trend	−0.009 °C yr^{-1}

Table 4. Pearson analysis showing comparison of SCA, LST and PPT.

Relationship	Pearson r	p value	Strength
Snow cover vs PPT	−0.26	0.61	Weak negative
Snow cover vs LST	0.23	0.65	Weak positive

the period 1998-2023. It is confirmed that higher accuracy in shaded and mountainous region [55-57], the NDSI was used to extract snow cover in this study. The study findings confirm a clear declining trend in the SCA of Astore over the study period. The observed decline in SCA negatively affects glacier mass balance, determined by increasing mean temperature and decreasing precipitation in the region [58, 59]. This negative SCA trend prevent glaciers and contribute negatively to the glacier mass balance in the western Himalayas occur earlier recorded and comparing with Global glacial trend. This regional anomaly is links to local climatic trends of increasing temperature and decreasing precipitation trends [36, 39, 60]. The location of Astore in the western Himalayas, with a climate more identical to the southern Karakoram due to westerlies effect, results in varied climatic drivers [40]. A significant decline is snow cover area has been observed, especially at lower and mid elevations. The previous studies demonstrate a strong and persistent long-term warming trend throughout the Gilgit- Baltistan region including Astore [61-63]. While a significant increases in mean and extreme temperatures, especially since the late of 20th century. Although precipitation trends show different variation and complexity, growing evidence of change in precipitation patterns. Previous studies reveal an overall increase in total rainfall convoyed by a decline in snowfall, representing a change from solid to liquid precipitation, especially during winter and spring [64-66].

The results of previous studies [67, 68] show decreasing trend in SCA for the Astore region which aligned and support our results. This negative snow cover area trend stops glaciers and pay negatively to the glacier mass balance in the western Himalayas occur previously recorded and comparing with the global glacier trend. This regional anomaly is matches to local climatic trends of increasing temperature and decreasing precipitation trends [27, 38].

These results match with the previous literature studies relating a declining inclination of snow cover in the area [40, 69]. This changing aspect of snow cover area in the central Karakorum and western Himalayas are mainly governed by patterns of climatic changes, in Astore rising mean annual temperatures accompanied by declining precipitation indicate that global warming is considerably affecting snow cover in northern Pakistan. This regional snow cover decline reflects global patterns of glacier retreat connected to current climate change phenomena. Additionally, the decrease in glacial accumulation has led to reduced flow in the Astore river basin, posing significant risks to agricultural efficiency in the downstream low-lying areas. Conclusively, this study highlights the critical effects of climatic changes on snow cover and glacier health in the Astore region, resultantly affect water resources and regional agriculture. The glacier in the study regions nourish the Indus River, an essential resource and infrequent hazard for about 220 million low- laying peoples. Decreasing glacier mass has diminish river flow in the Astore sub basin, a potentially negative development for downstream agriculture.

5. CONCLUSIONS

This study assessed the spatiotemporal variations in the snow cover area of the Astore area using Landsat data downloaded from USGS for the period 1998-2023. The study was further extended to evaluate the linkages between SCA and core climatic factors such as temperature and precipitation. Results demonstrate that a clear declining trend in SCA in the study area, primarily driven by increasing temperatures and decreasing precipitation during the study period. The SCA decreased at an average rate of approximately -4.92 km^2 per year between 1998 and 2023. The lowest annual SCA of 2.27% was detected in 2008, whereas the highest value of 6.32% was observed in 1998. These finding highlights the significant influence of temperature and precipitation on annual snow cover changes in the region. The detected decrease in average rainfall combined with the rise in mean temperature appears to be the main factor contributing to the declining trend of SCA in Astore. In conclusion, the decrease in snow cover raises serious concerns for future water availability, which may threaten agricultural production and other water-dependent activities in the region that depend on the Astore river. The continuing decrease in precipitation and increase in mean temperature in Astore contrasts with some global trends, highlighting the need for detailed localized studies. This study provides valuable insights to guide effective water resource management and planning under changing climatic conditions.

6. ETHICAL STATEMENT

This work does not include any studies involving human or animal subjects.

7. ACKNOWLEDGEMENTS

The authors acknowledge the Department of Geography Islamia College Peshawar.

8. CONFLICT OF INTEREST

The authors declare no conflict of interest.

9. FUNDING

No funding was received to conduct this research.

10. AUTHORSHIP CONTRIBUTION STATEMENT

Bahadar Khan: writing methodology, original draft writing, and investigation of data analysis; Abdur Raziq: supervision; writing-review and editing, resources and English correction, proofreading, original draft extensive editing and finalizing; Izhar Ullah: writing, methodology, review of the manuscript, and editing; Yasir Hanif: review and rewriting of the manuscript.

11. REFERENCES

1. S.R. Bajracharya, S.B. Maharjan, F. Shrestha, W. Guo, S. Liu, W. Immerzeel, and B. Shrestha. The glaciers of the Hindu Kush Himalayas: current status and observed changes from the 1980s to 2010. *International Journal of Water Resources Development* 31(2): 161-173 (2015). https://doi.org/10.1080/07900627.2015.1005731
2. J. Gul, S. Muhammad, S.Y. Liu, S. Ullah, S. Ahmad, H. Hayat, and A.A. Tahir. Spatiotemporal changes in the six major glaciers of the Chitral River basin (Hindukush Region of Pakistan) between 2001 and 2018. *Journal of Mountain Science* 17(3): 572-587 (2020). https://doi.org/10.1007/s11629-019-5728-9
3. M. Bousbaa, A. Boudhar, C. Kinnard, H. Elyoussfi, I. Karaoui, Y. Eljabiri, and A. Chehbouni. An accurate snow cover product for the Moroccan Atlas Mountains: optimization of the MODIS NDSI index threshold and development of snow fraction estimation models. *International Journal of Applied Earth Observation and Geoinformation* 129: 103851 (2024). https://doi.org/10.1016/j.jag.2024.103851
4. A. Agrawal, R.J. Thayyen, and A.P. Dimri. Mass-balance modelling of Gangotri glacier. *Geological Society London Special Publications* 462(1): 99-117 (2018). https://doi.org/10.1144/SP462.1
5. R. Gul, S. Khan, R. Ullah, S. Bibi, and M. Ali. Spatial-temporal change in the glaciers of Astore Basin (North-Western Himalaya), between 2016 and 2021 by using Sentinel-2 satellite data. (2023). https://doi.org/10.21203/rs.3.rs-2524501/v1
6. N.M. Kehrwald, L.G. Thompson, Y. Tandong, E. Mosley-Thompson, U. Schotterer, V. Alfimov, J. Beer, J. Eikenberg, and M.E. Davis. Mass loss on Himalayan glacier endangers water resources. *Geophysical Research Letters* 35(22): L22503 (2008). https://doi.org/10.1029/2008GL035556
7. A. Banerjee, R. Chen, M.E. Meadows, D. Sengupta, S. Pathak, Z. Xia, and S. Mal. Tracking 21st century climate dynamics of the Third Pole: an analysis of topo-climate impacts on snow cover in the central Himalaya using Google Earth Engine. *International Journal of Applied Earth Observation and Geoinformation* 103: 102490 (2021). https://doi.org/10.1016/j.jag.2021.102490
8. V. Sharma, V.D. Mishra, and P.K. Joshi. Implications of climate change on stream flow of a snow-fed river system of the Northwest Himalaya. *Journal of Mountain Science* 10: 574-587 (2013). https://doi.org/10.1007/s11629-013-2667-8
9. R. Sahu and R. Gupta. Snow cover area analysis and its relation with climate variability in Chandra basin, Western Himalaya, during 2001-2017 using MODIS and ERA5 data. *Environmental Monitoring and Assessment* 192(8): 1-26 (2020). https://doi.org/10.1007/s10661-020-08442-8
10. S.K. Jain, A. Goswami, and A.K. Saraf. Role of elevation and aspect in snow distribution in western Himalaya. *Water Resources Management* 23: 71-83 (2009). https://doi.org/10.1007/s11269-008-9265-5
11. M.A. Qureshi, C. Yi, X. Xu, and Y. Li. Glacier status during the period 1973-2014 in the Hunza basin, western Karakoram. *Quaternary International* 444: 125-136 (2017). https://doi.org/10.1016/j.quaint.2016.08.029
12. P. Wester, A. Mishra, A. Mukherji, and A.B. Shrestha (Eds.). The Hindu Kush Himalaya assessment—mountains, climate change, sustainability and people. *Springer Nature Switzerland, Cham, Switzerland* (2019). https://doi.org/10.1007/978-3-319-92288-1
13. N.I. Faruqui. Final Report to CIDA: Snow and Ice Hydrology Project (SHIP). *International Development Research Centre Ottawa, Ontario,*

Canada, Report No. IDRC.54 (1997). https://idl-bnc-idrc.dspacedirect.org/server/api/core/bitstreams/ccc3f781-edd0-433a-88ed-b1b8e4e20e30/content

14. B. Bookhagen and D.W. Burbank. Toward a complete Himalayan hydrological budget: spatiotemporal distribution of snowmelt and rainfall and their impact on river discharge. *Journal of Geophysical Research* 115: F03019 (2010). https://doi.org/10.1029/2009JF001426
15. W.W. Immerzeel, L.V. Beek, M. Konz, A. Shrestha, and M.F.P. Bierkens. Hydrological response to climate change in a glacierized catchment in the Himalayas. *Climatic Change* 110: 721-736 (2012). https://doi.org/10.1007/s10584-011-0143-4
16. R. Krishnan, A.B. Shrestha, G. Ren, R. Rajbhandari, S. Saeed, J. Sanjay, *et al*. Unravelling climate change in the Hindu Kush Himalaya: rapid warming in the mountains and increasing extremes. In: The Hindu Kush Himalaya assessment: mountains, climate change, sustainability and people. P. Wester, A. Mishra, A. Mukherji, and A.B. Shrestha (Eds.). *Springer International Publishing*, *Cham, Switzerland* (2019). https://doi.org/10.1007/978-3-319-92288-1_3
17. C. Notarnicola. Hotspots of snow cover changes in global mountain regions over 2000-2018. *Remote Sensing of Environment* 243: 111781 (2020). https://doi.org/10.1016/j.rse.2020.111781
18. Y. Yi, S. Liu, Y. Zhu, K. Wu, F. Xie, and M. Saifullah. Spatiotemporal heterogeneity of snow cover in the central and Western Karakoram Mountains based on a refined MODIS product during 2002-2018. *Atmospheric Research* 250: 105402 (2021). https://doi.org/10.1016/j.atmosres.2020.105402
19. A.A. Tahir, S.A. Hakeem, T. Hu, H. Hayat, and M. Yasir. Simulation of snowmelt-runoff under climate change scenarios in a data scarce mountain environment. *International Journal of Digital Earth* 12: 910-30 (2019). https://doi.org/10.1080/17538947.2017.1371254
20. M. Matiu, A. Crespi, G. Bertoldi, C.M. Carmagnola, C. Marty, S. Morin, *et al*. Observed snow depth trends in the European Alps 1971-2019. *The Cryosphere* 15(3): 1343-1382 (2021). https://doi.org/10.5194/tc-15-1343-2021
21. R. Hock, G. Rasul, C. Adler, B. Cáceres, S. Gruber, Y. Hirabayashi, M. Jackson, A. Kääb, S. Kang, S. Kutuzov, A. Milner, U. Molau, S. Morin, B. Orlove, and H. Steltzer. High Mountain Areas. In: IPCC Special Report on the Ocean and Cryosphere in a Changing Climate. H.-O. Pörtner, D.C. Roberts, V. Masson-Delmotte, P. Zhai, M. Tignor, E. Poloczanska, K. Mintenbeck, A. Alegría, M. Nicolai, A. Okem, J. Petzold, B. Rama, and N.M. Weyer (Eds.). pp. 131-202. *Intergovernmental Panel on Climate Change (IPCC)* (2019). https://www.ipcc.ch/site/assets/uploads/sites/3/2022/03/04_SROCC_Ch02_FINAL.pdf
22. Intergovernmental Panel on Climate Change (IPCC). Climate Change 2022: Impacts, Adaptation and Vulnerability. Contribution of Working Group II to the Sixth Assessment Report of the Intergovernmental Panel on Climate Change. *Cambridge University Press* (2022). https://doi.org/10.1017/9781009325844
23. A.A. Tahir, J.F. Adamowski, P. Chevallier, A.U. Haq, and S. Terzago. Comparative assessment of spatiotemporal snow cover changes and hydrological behavior of the Gilgit, Astore and Hunza River basins (Hindukush–Karakoram–Himalaya region, Pakistan). *Meteorology and Atmospheric Physics* 128: 793-811 (2016). https://doi.org/10.1007/s00703-016-0440-6
24. M.U. Shafiq, P. Ahmed, Z.U. Islam, P.K. Joshi, and W.A. Bhat. Snow cover area change and its relations with climatic variability in Kashmir Himalayas, India. *Geocarto International* 34: 688-702 (2019). https://doi.org/10.1080/10106049.2018.1469675
25. A.H. Azizi and F. Akhtar. Analysis of spatiotemporal variation in the snow cover in Western Hindukush-Himalaya region. *Geocarto International* 37(22): 6602-6624 (2021). https://doi.org/10.1080/10106049.2021.1939442
26. P.K. Panday, J. Thibeault, and K.E. Frey. Changing temperature and precipitation extremes in the Hindu Kush-Himalayan region: an analysis of CMIP3 and CMIP5 simulations and projections. *International Journal of Climatology* 35: 3058-3077 (2015). https://doi.org/10.1002/joc.4192
27. M.F.U. Moazzam, G. Rahman, S. Munawar, A. Tariq, Q. Safdar, and B-G. Lee. Trends of rainfall variability and drought monitoring using standardized precipitation index in a scarcely gauged basin of northern Pakistan. *Water* 14(7): 1132 (2022). https://doi.org/10.3390/w14071132
28. H.S. Negi and N. Kanda. An appraisal of spatio-temporal characteristics of temperature and precipitation using gridded datasets over NW-Himalaya. In: Climate Change and the White World. P.S. Goel, R. Ravindra, and S. Chattopadhyay (Eds.). *Springer International Publishing, Cham, Switzerland* pp. 219-238 (2019). https://doi.org/10.1007/978-3-030-21679-5_14
29. J.S. Yadav, A. Misra, D.P. Dobhal, R.B.S. Yadav, and

R. Upadhyay. Snow cover mapping, topographic controls and integration of meteorological data sets in Din-Gad Basin, Central Himalaya. *Quaternary International* 575-576: 160-177 (2021). https://doi.org/10.1016/j.quaint.2020.05.030

30. F.M. Jacobsen and W.H. Theakstone. Monitoring glacier changes using a global positioning system in differential mode. *Annals of Glaciology* 24: 314-319 (1997). https://doi.org/10.3189/S0260305500012374
31. Z. Abid and S. Zia. Mapping and analysis of Baltoro glacier and Shigar River. *Pakistan Geographical Review* 74: 20-32 (2019). https://pu.edu.pk/images/journal/geography/pdf/3_V74_No1_2019.pdf
32. I. U. Khan, M. Iqbal, Z. Ali, A. B. Arshed, M. Wang, and R. M. Adnan. Evaluation and Mapping of Snow Characteristics Using Remote Sensing Data in Astore River Basin, Pakistan. Atmosphere 16(5): 550 (2025). https://doi.org/10.3390/atmos16050550
33. Z. Ali, M. Iqbal, I. U. Khan, et al. Hydrological response under CMIP6 climate projection in Astore River Basin, Pakistan. *Journal of Mountain Science* 20: 2263–2281 (2023). https://doi.org/10.1007/s11629-022-7872-x
34. S. A. Dar and M. O. Sarif. Status on snow cover area, mass balance, glacial area loss, surface velocities and applications of snowmelt runoff model over Kashmir Himalayas and Upper Indus Basin: A review. *Polar Science* 42: 101075 (2024). https://doi.org/10.1016/j.polar.2024.101075
35. C. D. Almagioni, V. Manara, G. A. Diolaiuti, M. Maugeri, A. Spezza, and D. Fugazza. Snow Cover Variability and Trends over Karakoram, Western Himalaya and Kunlun Mountains During the MODIS Era (2001–2024). *Remote Sensing* 17(5): 914 (2025). https://doi.org/10.3390/rs17050914
36. M.F.U. Moazzam, G. Rahman, B.G. Lee, and N.A. Ansari. Trend of snow cover under the influence of climate change using Google Earth Engine platform: a case study of Astore (Western Himalayas) and Shigar (Karakoram region). *Frontiers in Environmental Science* 10: 1006399 (2022). https://doi.org/10.3389/fenvs.2022.1006399
37. M.P. Bishop, A.B. Bush, L. Copland, U. Kamp, L.A. Owen, Y.B. Seong, and *et al*. Climate change and mountain topographic evolution in the central Karakoram, Pakistan. *Annals of the Association of American Geographers* 100: 772-793 (2010). .https://doi.org/10.1080/00045608.2010.500521
38. S.B. Farhan, Y. Zhang, Y. Ma, Y. Guo, and N. Ma. Hydrological regimes under the conjunction of westerly and monsoon climates: a case investigation in the Astore basin, northwestern Himalaya. *Climate Dynamics* 44: 3015-3032 (2015). https://doi.org/10.1007/s00382-014-2409-9
39. S.B. Farhan, Y. Zhang, A. Aziz, H. Gao, Y. Ma, J. Kazmi, *et al*. Assessing the impacts of climate change on the high-altitude snow- and glacier-fed hydrological regimes of Astore and Hunza, the sub-catchments of Upper Indus Basin. *Journal of Water and Climate Change* 11: 479-490 (2020). https://doi.org/10.2166/wcc.2018.107
40. A.A. Tahir, P. Chevallier, Y. Arnaud, M. Ashraf, and M.T. Bhatti. Snow cover trend and hydrological characteristics of the Astore River basin (Western Himalayas) and its comparison to the Hunza basin (Karakoram region). *Science of the Total Environment* 505: 748-761 (2015). https://doi.org/10.1016/j.scitotenv.2014.10.065
41. N. Afzal, A. Ahmad, S.A. Shirazi, and I. Younes. GIS-based landslide susceptibility mapping using analytical hierarchy process: a case study of Astore region, Pakistan. *EQA – International Journal of Environmental Quality* 48: 27-40 (2022). https://doi.org/10.6092/issn.2281-4485/12600
42. S.U. Baig, M.U. Rehman, and N.N. Janjua. District-level disaster risk and vulnerability in the Northern mountains of Pakistan. *Geomatics, Natural Hazards and Risk* 12(1): 2002–2022 (2021). https://doi.org/10.1080/19475705.2021.1944331
43. M. Bernhardt and K. Schulz. SnowSlide: A simple routine for calculating gravitational snow transport. *Geophysical Research Letters* 37(11): L11502 (2010). https://doi.org/10.1029/2010GL043086
44. A.I. Maher, P.M. Treitz, and M.A. Ferguson. Can Landsat data detect variations in snow cover within habitats of arctic ungulates? *Wildlife Biology* 18(1): 75-87 (2012). https://doi.org/10.2981/11-055
45. M. Warscher, T. Marke, E. Rottler, and U. Strasser. Operational and experimental snow observation systems in the upper Rofental: data from 2017 to 2023. *Earth System Science Data* 16(8): 3579-3599 (2024). https://doi.org/10.5194/essd-16-3579-2024
46. J. Dozier. Spectral signature of alpine snow cover from the Landsat Thematic Mapper. *Remote Sensing of Environment* 28: 9-22 (1989). https://doi.org/10.1016/0034-4257(89)90101-6
47. D.K. Hall, G.A. Riggs, and V. V. Salomonson. Development of methods for mapping global snow cover using moderate resolution imaging spectroradiometer data. *Remote Sensing of Environment* 54(2): 127-140 (1995). https://doi.org/10.1016/0034-4257(95)00137-P
48. X. Xiao, Z. Shen, and X. Qin. Assessing the

potential of vegetation sensor data for mapping snow and ice cover: a Normalized Difference Snow and Ice Index. *International Journal of Remote Sensing* 22(13): 2479-2487 (2001). https://doi.org/10.1080/01431160119766

49. A.V. Kulkarni, S.K. Singh, P. Mathur, and V.D. Mishra. Algorithm to monitor snow cover using AWiFS data of Resourcesat-1 for the Himalayan region. *International Journal of Remote Sensing* 27(12): 2449-2457 (2006). https://doi.org/10.1080/01431160500497820
50. S. Raghubanshi, R. Agrawal, and B.P. Rathore. Enhanced snow cover mapping using object-based classification and normalized difference snow index (NDSI). *Earth Science Informatics* 16(3): 2813-2824 (2023). https://doi.org/10.1007/s12145-023-01077-6
51. A. Patel, R. Prajapati, J.K. Dharpure, S. Mani, and D. Chauhan. Mapping and monitoring of glacier areal changes using multispectral and elevation data: a case study over Chhota-Shigri glacier. *Earth Science Informatics* 12: 489-499 (2019). https://doi.org/10.1007/s12145-019-00388-x
52. P. Rastner, R. Prinz, C. Notarnicola, L. Nicholson, R. Sailer, G. Schwaizer, et al. On the automated mapping of snow cover on glaciers and calculation of snow line altitudes from multi-temporal Landsat data. *Remote Sensing* 11: 1410 (2019). https://doi.org/10.3390/rs11121410
53. S. Khan, M. Ashiq, and H. Gabriel. Assessment of flows in a glaciated region Shigar River Basin, Pakistan. *Technical Journal, University of Engineering and Technology Taxila* 19: 38-50 (2014).
54. S.A. Hakeem, M. Bilal, A. Pervez, and A.A. Tahir. Remote sensing data application to monitor snow cover variation and hydrological regime in a poorly gauged river catchment—Northern Pakistan. *International Journal of Geosciences* 5(1): 27 (2014). https://doi.org/10.4236/ijg.2014.51005
55. P. Burns and A. Nolin. Using atmospherically-corrected Landsat imagery to measure glacier area change in the Cordillera Blanca, Peru from 1987 to 2010. *Remote Sensing of Environment* 140: 165-178 (2014). https://doi.org/10.1016/j.rse.2013.08.026
56. M. Shafique, B. Faiz, A.S. Bacha, and S. Ullah. Evaluating glacier dynamics using temporal remote sensing images: a case study of Hunza Valley, northern Pakistan. *Environmental Earth Sciences* 77: 162 (2018). https://doi.org/10.1007/s12665-018-7365-y
57. R. Tong, J. Parajka, J. Komma, and G. Blöschl. Mapping snow cover from daily Collection 6 MODIS products over Austria. *Journal of Hydrology* 590: 125548 (2020). https://doi.org/10.1016/j.jhydrol.2020.125548
58. S. Ali, D. Li, F. Congbin, and F. Khan. Twenty-first century climatic and hydrological changes over Upper Indus Basin of Himalayan region of Pakistan. *Environmental Research Letters* 10: 014007 (2015). https://doi.org/10.1088/1748-9326/10/1/014007
59. H. Hayat, T.A. Akbar, A.A. Tahir, Q.K. Hassan, A. Dewan, and M. Irshad. Simulating current and future river-flows in the Karakoram and Himalayan regions of Pakistan using snowmelt-runoff model and RCP scenarios. *Water* 11: 761 (2019). https://doi.org/10.3390/w11040761
60. A.A. Tahir, P. Chevallier, Y. Arnaud, and B. Ahmad. Snow cover dynamics and hydrological regime of the Hunza River basin, Karakoram Range, Northern Pakistan. *Hydrology and Earth System Sciences* 15(7): 2275-2290 (2011). https://doi.org/10.5194/hess-15-2275-2011
61. M. Raza and F. Wahab. Spatial and Temporal Analysis of Temperature Time Series over Gilgit-Baltistan (GB), Pakistan. *Journal of Xi'an Shiyou University, Natural Science Edition* 18(9): 548-554 (2022).
62. M. Adnan, G. Nabi, S. Kang, G. Zhang, R.M. Adnan, M.N. Anjum, and A.F. Ali. Snowmelt runoff modelling under projected climate change patterns in the Gilgit river basin of northern Pakistan. *Polish Journal of Environmental Studies* 26(2): 525-542 (2017). https://doi.org/10.15244/pjoes/66719
63. M.S. Shazil, S.A. Mahmood, S. Ahmad, M. Haseeb, A. Masood, J. Qureshi, and S. Batool. Assessing long-term variability and trends in temperature and precipitation in Gilgit and Hunza River basins. *Environmental Earth Sciences* 83(8): 248 (2024). https://doi.org/10.1007/s12665-024-11571-9
64. Z. Zafar, M.S. Mehmood, A. Akbar, and M.A. Khan. Spatiotemporal dynamics analysis of surface water body and snow cover area to climate change in Gilgit Baltistan, Pakistan. *Physical Geography* 44(5): 600-619 (2023). https://doi.org/10.1080/02723646.2023.2188633
65. M. Yahya, U. Noreen, K.A. Attia, F. Jabeen, A. Aslam, N. Anjum, and Q.U. Ain. Assessing climate-driven glacial retreat, snow-cover reduction and GLOF risks: implications for water resource management amid rising global temperatures and CO_2. *Marine and Freshwater Research* 75(18): MF24177 (2024). https://doi.org/10.1071/MF24177
66. Z. Zafar, A.A. Nadeem, Y. Zha, H. Gilani, and A.

Tariq. Snow cover variability assessment and its interplay with hydro-climatic characteristics in data scarce region of Gilgit-Baltistan, Pakistan. *Journal of Environmental Management* 382: 125375 (2025). https://doi.org/10.1016/j.jenvman.2025.125375

67. D. Scherler, B.Bookhagen, and M.R. Strecker. Spatially variable response of Himalayan glaciers to climate change. *Nature Geoscience* 4(3): 156-159 (2011). https://doi.org/10.1038/ngeo1068
68. M. Nüsser and S. Schmidt. Glacier changes on the Nanga Parbat 1856–2020: A multi-source retrospective analysis. *Science of the Total Environment* 785: 147321 (2021). https://doi.org/10.1016/j.scitotenv.2021.147321
69. G. Tauqir, W. Zhao, M. Xu, and D. Fu. Elevation-Dependent Trends in Himalayan Snow Cover (2004–2024) Based on MODIS Terra Observations. *Remote Sensing* 17(18): 3175 (2025). https://doi.org/10.3390/rs17183175

Proceedings of the Pakistan Academy of Sciences: A Physical and Computational Sciences 63(1): 47-59 (2026)

ISSN (Print): 2518-4245; ISSN (Online): 2518-4253
http://doi.org/10.53560/PPASA(63-1)703

Pakistan Academy of Sciences

Research Article

Antibiotics, Vital Signs and Comorbidities as Predictors of COVID-19 Mortality: An Unadjusted and Adjusted Logistic Regression Analysis

Muhammad Islam[1*], Imtiaz Ahmed[2], Hashaam Akhtar[3], Muhammad Amin[4], Samar Akhtar[5], Shahzad Ali Khan[6], and Muhammad Faisal[7,8]

[1]Crop Reporting Service (Director Bahawalpur), Agriculture Department, Punjab, Pakistan

[2]Punjab Land Records Authority (Deputy Director Bahawalpur), Board of Revenue Punjab, Pakistan

[3]Global Health Department, Health Services Academy, Islamabad, 44000, Pakistan

[4]Department of Statistics, University of Sargodha, Sargodha, Pakistan

[5]Department of Clinical Pharmacy, Yusra Institute of Pharmaceutical Sciences, Rawalpindi, 44000, Pakistan

[6]Health Services Academy, Islamabad, 44000, Pakistan

[7]Centre for Digital Innovations in Health and Social Care, Institute of Health and Social Care, University of Bradford, Bradford, UK

[8]Wolfson Centre for Applied Health Research, Bradford Royal Infirmary, Bradford Teaching Hospitals Foundation Trust, Bradford, UK

Abstract: This study explores the association between COVID-19 patients and antibiotic usage (Azithromycin, Ceftriaxone, Tanzo, Tienum) concerning vital signs and comorbidities (diseases) to enhance treatment efficacy, emphasizing mortality risk. Logistic regression is used for unadjusted model (M_0) links antibiotics, while adjusted models (M_1, M_2, M_3) incorporate vital signs and comorbidities, etc. Antibiotics are categorized into low (L_1) and high (L_2) doses. Models are classified as ILRM (insignificant with low risk of mortality), SLRM (significant with low risk of mortality), IHRM (insignificant with high risk of mortality) and SHRM (significant with high risk of mortality). Azithromycin exhibits IHRM at L_1 and SLRM at L_2 for M_0, M_1/M_2 show IHRM at L_1 and ILRM at L_2. M_3 shows IHRM. Ceftriaxone transitions from ILRM at L_1 to IHRM at L_2 (except M_3). Tanzo shows SLRM at L_1 (M_0) and ILRM in other models (except M_3 at L_2). Tienum indicates IHRM at both levels (M_0), while adjusted models associate it with ILRM at L_1 and IHRM at L_2. This research provides crucial insights for healthcare professionals to predict and manage vital signs and comorbidities variations, and to underline the mortality risk in COVID-19 patients.

Keywords: COVID, Antibiotic, Vital Signs, Comorbidities, Unadjusted and Adjusted Models, Mortality Risk.

1. INTRODUCTION

The Coronavirus disease (COVID-19) dramatically reshaped societal structures, impacted human psychology, influenced public policies and redefined interpersonal interactions through isolation and digital reliance [1, 2]. COVID-19 is a highly contagious respiratory illness caused by the severe acute respiratory syndrome [3-5]. The virus was first identified in December 2019 in the city of Wuhan, China. The global situation with COVID-19 has been dynamic, with various waves of infections.

Received: October 2025; Revised: February 2026; Accepted: March 2026
* Corresponding Author: Muhammad Islam <mislam6667@gmail.com>

Vaccination campaigns have played a crucial role in mitigating the impact of the virus, providing immunity to individuals and reducing the severity of illness. Several vaccines have been developed and authorized for emergency use, contributing to a significant decrease in severe cases and mortality rates in many regions [6-7]. However, challenges persist, including the emergence of new variants of the virus, vaccine distribution disparities and ongoing public health measures [8, 9]. Some areas of world have experienced resurgences of COVID-19 cases, leading to fluctuations in containment efforts [10, 11]. Governments and health authorities continue to adapt strategies based on the evolving nature of the pandemic, balancing public health concerns with the need for economic stability and societal well-being. The virus has been responsible for a significant number of deaths worldwide and has presented a critical challenge for Pakistan's healthcare sector [12, 13]. Pakistan managed well to meet the high standards for COVID-19 treatment set by the World Health Organization [14-16].

Islam *et al.* [17], Gul and Yucesan [18] and Spangler *et al.* [19] reported that different vital signs play a vital role in monitoring the individuals, whether it is suspected or confirmed COVID-19 patient, and these vital signs, i.e., (temperature, respiratory rate, oxygen saturation, pulse rate, blood pressure and level of consciousness) are associated with the symptoms of a COVID-19 infection. Fever is a common symptom of COVID-19. Generally, normal body temperature for a healthy adult can range between 97.8 degrees Fahrenheit (36.5 degrees Celsius) and 99 degrees Fahrenheit (37.2 degrees Celsius) and body temperature above 100.4 °F (38 °C), is often observed in infected individuals [20, 21], Generally, normal respiration rates for an adult person at rest typically range from 12 to 16 breaths per minute and increased respiratory rate may be indicative of respiratory distress or pneumonia, which can be associated with severe cases of COVID-19 [22, 23]. COVID-19 can lead to respiratory issues and monitoring oxygen saturation levels is crucial. A decrease in oxygen saturation may indicate respiratory compromise or the development of acute respiratory distress syndrome [24]. American Heart Association (AHA) defined the accepted normal blood pressure as: a systolic blood pressure of less than 120 mm Hg and a diastolic blood pressure of less than 80 mm Hg, and monitoring pulse rate and blood pressure helps assess the cardiovascular impact of the infection [25, 26]. Generally, the normal resting heart rate for healthy adults typically falls within the range of 60 to 100 beats per minute [27, 28]. Monitoring vital signs is a crucial aspect of managing and providing care to individuals with COVID-19, especially in severe cases where prompt medical intervention may be necessary. Regular monitoring helps healthcare professionals assess the progression of the illness and adjust treatment plans accordingly. Different antibiotics, i.e., Azithromycin, Cefatriaxone, Tanzo, and Tienum had been applied in Pakistan for the treatment of COVID-19 [29-31].

In the healthcare domain, the standard practice involves administering various antibiotics, such as Azithromycin, Cefatriaxone, Tanzo, and Tienum, to treat bacterial infections. It is crucial to understand the potential impact of these antibiotics on essential indicators like temperature, respiratory rate, oxygen saturation, pulse rate and blood pressure. It is important to consider their effects on different comorbidities (diseases), i.e., diabetes, high blood pressure, heart, kidney, asthma, tuberculosis, cancer, nervous disorders, allergies, Chronic Obstructive Pulmonary Disease (COPD), etc. This understanding is essential for effective patient management and safety. The primary goal is to examine the dataset of post-COVID-19 patients and develop a robust and accurate logistic regression model that can predict the mortality risk of individuals with COVID-19. This involves developing various unadjusted and adjusted statistical models using different levels of antibiotics, vital measurements and diseases. The goal is to assist healthcare professionals in anticipating and effectively managing potential fluctuations in vital signs following antibiotic treatment. This research aims to contribute to the improvement of patient care by providing healthcare professionals with a reliable tool for managing antibiotic-related effects on vital signs and comorbidities.

2. MATERIALS AND METHODS

2.1. Data Collection and Variables Descriptions

The research gathered secondary data of COVID-19 patients, admitted to four hospitals, both public and private, located in Rawalpindi and Islamabad. These hospitals are Pakistan Air Force Hospital, Pakistan Institute of Medical Sciences Hospital,

Holy Family Hospital and Benazir Bhutto Shaheed Hospital. The study encompassed the timeframe spanning from February to August 2020. The statistical analysis was conducted using SPSS to ensure robust estimation and validation of results. The identification of variables is described as follows:

i. Antibiotics used are classified into two relative categories (levels) as: *"L_1"* = low dose is given, and *"L_2"* = high dose is given. Four antibiotics (Azithromycin, Cefatriaxone, Tanzo, and Tienum) are studied. Patients received Azithromycin as follows: 113 in L_1 and 1485 in L_2. Ceftriaxone was administered to 214 in L_1 and 212 in L_2. Tienum was provided to 39 in L_1 and 124 in L_2. Tanzo was prescribed to 97 in L_1 and 199 in L_2. The classification of antibiotic use into low (L_1) and high (L_2) levels is a relative categorization derived from four hospital records and does not represent standardized or guideline defined dosage thresholds. It is important to note that, in the context of COVID-19 management in Pakistan, antibiotic prescribing practices were heterogeneous and largely physician dependent, with dose variations influenced by clinical severity and institutional protocols rather than fixed benchmarks. Therefore, the L_1 and L_2 classifications represent comparative groupings derived from observed prescribing patterns across hospitals, rather than fixed or universally defined dosing standards.
ii. The presence and absences of various variables recorded, i.e., respiration rate, body temperature, oxygen saturation level, blood pressure, pulse rate, patient age, gender and survival outcome of individuals.
iii. The presence and absences of various comorbidities recorded, i.e., diabetes, blood pressure, heart disease, kidney disease, asthma, tuberculosis, cancer, nervous disorders, allergies, HCV, anemia, Chronic Obstructive Pulmonary Disease (COPD), etc.

2.2. Odds ratio, Un-adjusted and Adjusted Logistics Regression Models

Logistic regression is a statistical model used to forecast the likelihood of a binary outcome by considering one or more predictor variables (categorical or continuous) [32-35]. Logistic regression model (logistic function) is also known as the sigmoid function. The sigmoid function is useful for representing probabilities of any real value numbers to the range of 0 and 1. In logistic regression, the model predicts the probability of an event occurring as a function of one or more predictor variables. The coefficients of logistic regression represent the log-odds or logit transformation of the odds ratio for each predictor variable.

$$\log\left(\frac{p}{1-p}\right) = \beta_0 + \beta_1 y_1 + \beta_2 y_2 + \beta_3 y_3 + \cdots + \beta_m y_m \quad (1)$$

Where "*p*" stands the probability of the event occurring, "*1-p*" stands the probability of the event not occurring and *"p/1-p"* stands the odds of the event occurring. *"β_0"* stands the intercept, and *"β_i"* (I = 1, 2, 3, … m) stands regression coefficients associated with independent variables *"y_i"*.

The odds ratio is a measure of association between an interest and outcome [36, 37]. In logistic regression, the odds ratio for a predictor variable is given by:

$$Odds\ Ratio = e^{\beta_i} \quad (2)$$

The odds ratio represents the multiplicative change in the odds of the event for a one-unit increase in the predictor variable [36, 37]. The logistic regression coefficients represent the change in the log-odds of the event per unit change in the corresponding predictor variable. The odds ratio is the exponential of the coefficient and represents the multiplicative change in the odds of the event for a one-unit change in the predictor variable [38-40]. Logistic regression coefficients are in the log-odds scale, while odds ratios provide a more interpretable measure of the effect of predictor variables on the odds of the event. The odds ratio (OR) measures the strength and direction of the association between two variables. It is calculated as the ratio of the odds of an event occurring in one group to the odds of it occurring in another group.

$$OR = \frac{OG_a/1 - OG_a}{OG_b/1 - OG_b} \quad (3)$$

Where *"OG_a"* stands the odds of the event of interest for group-a, and *"OG_b"* stands the odds of the event of interest for group-b. "*OR = 1"*, suggests that there is no association between the interest and the outcome. *"OR > 1"*, implies a positive association

between the interest and the outcome, and *"OR < 1"*, indicates a negative association between the interest and the outcome. The significance of the OR is often assessed through confidence intervals (CI), and if 95% CI does not include 1, suggests association is statistically significant. In logistic regression, both unadjusted (single predictor variables, without considering the effects of other variables) and adjusted models (multiple predictor variables) are commonly used to analyze the relationship between predictor variables and a binary outcome [41-44]. Various unadjusted and adjusted models are developed to predict the mortality risk (yes/no) of COVID-19 patients (Died/ Alive), incorporating with age, gender, antibiotics, vital signs and different comorbidities. The un-adjusted mode used as:

$$M_i = \log\left(\frac{p}{1-p}\right) = \beta_0 + \beta_i y_i \quad (4)$$

Where *"M_i"* stands the dependent variable, as the mortality risk (yes/no) in COVID-19 patients (Died/Alive), *"β_0"* stands the intercept, and *"β_i"* stands coefficients associated with covariate antibiotics *"y_i"*. Three adjusted models used as:

i. "M_1" as dependent variable, as the mortality risk (yes/no) in COVID-19 patients (Died/ Alive) against with coefficients associated with covariate, antibiotics, age and gender.
ii. "M_2" applied with dependent variable, as the mortality risk (yes/no) in COVID-19 patients (Died/Alive) against with covariate antibiotic, age, gender, respiration rate, temperature, oxygen saturation, blood pressure and pulse rate.
iii. "M_3" used the dependent variable, as the mortality risk (yes/no) in COVID-19 patients (Died/Alive), against with covariate antibiotic, age, gender, respiration rate, temperature, oxygen saturation, blood pressure, pulse rate, diabetes, BP, heart disease, kidney disease, asthma, TB, cancer, nervous disorder, allergies, HCV, Anemia, COPD and others comorbidities.

2.3. Decision Analysis

The decision criteria for both adjusted and unadjusted models are as follows:

i. Statistically insignificant with low risk of mortality (ILRM).
ii. Statistically significant with low risk of mortality (SLRM).
iii. Statistically insignificant with high risk of mortality (IHRM).
iv. Statistically significant with high risk of mortality (SHRM).

2.4. Hypothesis Testing

This study explores the relationship between mortality risk in COVID-19 patients and various predictors. To ensure methodological clarity and reproducibility, the statistical framework of the study is explicitly defined through the following hypotheses.

The statistical hypotheses of this study are:

- **Null Hypothesis (H_0):** The estimated odds ratios are statistically insignificant for the risk of mortality at the 5% level of significance in COVID-19 patients for the predictors, i.e., antibiotics usage, vital signs and existing comorbidities.
- **Alternative Hypothesis (H_1):** There is a statistically significant association between the estimated odds ratios and the risk of mortality at the 5% level of significance in COVID-19 patients for the predictors, i.e., antibiotics usage, vital signs and existing comorbidities.

3. RESULTS

A distinct model is used simultaneously for each antibiotic. The coefficient represents the estimated change in the log-odds of the outcome variable associated with a one-unit change in the predictor variable. Positive coefficients suggest an increase in the odds, while negative coefficients suggest a decrease. The odds ratio (OR) represents the ratio of the odds of the event in one group to the odds of the event in another group. The 95% confidence interval provides a range within which we can be reasonably confident that the true value of the odds ratio lies. P-values and 95% confidence intervals (CI) is used to identified the significance of the results

3.1. Comparisons of Azithromycin Models

Table 1 provides coefficients, p-values, odds ratios (OR), and 95% confidence intervals (CI) for different models (M_0, M_1, M_2 and M_3) of the antibiotic Azithromycin across two levels (L_1 and

L_2). In the unadjusted model (M_0), the odds ratio (OR) for the exposure variable Azithromycin at a low dose (L_1) is determined to be 1.16, indicating an OR greater than 1. The corresponding 95% confidence interval (CI) ranges from 0.71 to 1.90 (inclusive of 1) and coefficient is found as 0.15. An odds ratio greater than 1 suggests a positive association between the exposure variable and the outcome. For the response variable mortality (yes/no), an OR greater than 1 implies that the odds of dying are higher in L_1 compared to the other group, and it could indicate an increasing risk associated with L_1. The odds of mortality risk are greater in the L_1 being compared to the L_2, and this might imply an increased likelihood of being died, but this association is statistically insignificant, as the reported p-value is 0.55. Similarly, in the case of a high dosage (L_2), the exposure variable Azithromycin yields coefficient as -0.35, odds ratio values of 0.71, accompanied by a 95% confidence interval (CI) ranging from 0.52 to 0.97. An odds ratio less than 1 suggests a negative association between the exposure variable Azithromycin at L_2 and the outcome. 1t implies that the odds of dying are lower in L_2 compared to the others group. It could indicate a protective effect (lower risk) of the mortality, and this association is statistically significant, as indicated by a p-value of 0.03.

In the case of model M_1, administering L_1 level of Azithromycin antibiotic yielded an odds ratio of 1.17, with a 95% confidence interval (CI) in the range of 0.69 to 1.99, and coefficient as 0.16. These findings suggest an increasing risk associated with the L_1, and it is statistically insignificant as p-value is found 0.56. For model M_1, employing L_2 level of Azithromycin, resulted in an odds ratio of 0.76, with a 95% CI of 0.54 to 1.08, p-v1lues of 0.13 and slop is -0.26. These results indicate a potential protective effect (lower risk) of the mortality, and this association is observed statistically insignificant.

In the case of M_2, the OR for the L_1 of the Azithromycin antibiotic is found as 1.17, with a 95%CI of 0.69 to 2.00 and slope coefficient as 0.16. These findings indicate a potential risk or high risk of mortality in L_1 compared with L_2 for M_2, and it is statistically insignificant as p-values are found as 0.56. Similarly, for the L_2 level of Azithromycin in M_2, the OR is 0.76, and the 95% CI is from 0.53 to 1.07) with p- value of 0.13, and slope coefficient as -0.27. These results suggest a potential protective effect (low risk of mortality), and this is statistical insignificant. In the case of model M_3, the administration of a L_1 level of Azithromycin antibiotic, yielded an odds ratio of 1.34, with a 95% CI of 0.74 to 2.43, p- values is found greater than 0.05 and coefficient as 0.29. These findings indicate a statistically insignificant risk. For model M_3 with a L_2 level of the Azithromycin, the resulting odds ratio is 1.09, the 95% CI is lies between 0.74 and 1.62, and slope as 0.09. These outcomes suggest a potential risk (high risk) both for L_1 and L_2, and it do not reach statistical significance as p-values > 0.05 in both cases L_1 and L_2.

The current statistical analysis suggests a statistically insignificant high risk of mortality (IHRM) for the unadjusted model (M_0) and all adjusted models (M_1, M_2 and M_3) for low dose. In the case of high dose, there is a potential protective

Table 1. Odd ratio, confidence interval (CI) and slope coefficient for Azithromycin models.

Antibiotics	Model	Levels	Coefficient	P-Value	OR	CI (95%)		Decision
						Lower Bound	Upper Bound	
Azithromycin	M_0	L_1	0.15	0.55	1.16	0.71	1.90	IHRM
		L_2	-0.35	0.03	0.71	0.52	0.97	SLRM
	M_1	L_1	0.16	0.56	1.17	0.69	1.99	IHRM
		L_2	-0.26	0.13	0.76	0.54	1.08	ILRM
	M_2	L_1	0.16	0.56	1.17	0.69	2.00	IHRM
		L_2	-0.27	0.12	0.76	0.53	1.07	ILRM
	M_3	L_1	0.29	0.33	1.34	0.74	2.43	IHRM
		L_2	0.09	0.66	1.09	0.74	1.62	IHRM

effect (low risk of mortality) for all models except M_3, where it falls into the high-risk. The statistically significant p-value for L_2 in the unadjusted model (M_0) indicates a statistically significant low risk of mortality (SLRM). However, for adjusted models M_1 and M_2, it is found to be a statistically insignificant low risk of mortality (ILRM), and for adjusted model M_3, it is an insignificant high risk of mortality (IHRM). The term insignificant implies that the observed effects may be due to random variability rather than a true association.

3.2. Comparisons of Ceftriaxone Models

Table 2 presents the results of the logistic regression analysis for the association between different levels of Ceftriaxone use and the odds of outcome, as indicated by the coefficients, p-values, odds ratios and corresponding confidence intervals (CI). For the antibiotic Ceftriaxone, at M_0, both levels L_1 and L_2 exhibit coefficients, which are not statistically significant with p-values 0.26 and 0.67, respectivrly, suggesting no significant impact of Ceftriaxone. Similar patterns are observed for M_1, M_2 and M_3, indicating no substantial change in the odds of the outcome with use of Ceftriaxone. The 95% confidence intervals (include 1), further supporting the lack of statistical significance and implies uncertainty.

In case of Model M_0 at L_1, OR value is found as 0.82, that suggests a possible protective effect (low risk of mortality). The slope is found negative -0.19. For the L_2, OR is reported as of 1.07, implies a possible risk (high risk of mortality). The positive slope coefficient is found as 0.06. For M_1 at L_1, OR is founds as 0.85, it is suggesting a potential protective effect (low risk of mortality). The slope is found negative with as values of -0.16. In similar case at L_2, OR value is 1.01 indicates a potential risk (high risk of mortality). The slope is found positive with as values of 0.003. M_2 shows the OR value is 0.84 at L_1, suggests a possible protective effect. The negative slope value is found as -0.16, while for L_2, the OR value is 1.06, indicating a possible risk, the coefficient is found as 0.06. The OR of 0.78, and 0.80 are found for M_3 at L_1 and L_2, respectively, suggests a possible protective effect.

In summary, both the unadjusted model (M_0) and all adjusted models (M_1, M_2 and M_3) show statistically insignificant results. The odds ratios and p-values consistently indicate an insignificant low risk of mortality (ILRM) at L_1 for the unadjusted model (M_0) and all adjusted models (M_1, M_2, and M_3). However, at L_2, the odds ratios and p-values reveal a statistically insignificant high risk of mortality (IHRM) for the unadjusted model (M_0) and adjusted models M_1 and M_2. In the case of adjusted model M_3, the results are reported as ILRM. The term insignificant implies that the observed effects may be due to random variability rather than a true association.

3.3. Comparisons of Tanzo Models

Table 3 shows the odd ratio, CI, and slope coefficient for Tanzo antibiotic. For model M_0, L_1 of Tanzo antibiotic yielded an OR of 0.50 with a 95% CI) in the range of 0.28 to 0.87. These findings indicate a protective effect (low risk of mortality) that is statistically significant with p-value is 0.01.

Table 2. Odd ratio, confidence interval (CI) and slope coefficient for Ceftriaxone models.

Antibiotics	Model	Levels	Coefficient	P-Value	OR	CI (95%)		Decision
						Lower Bound	Upper Bound	
Ceftriaxone	M_0	L_1	-0.19	0.26	0.82	0.58	1.16	ILRM
		L_2	0.06	0.67	1.07	0.77	1.48	IHRM
	M_1	L_1	-0.16	0.40	0.85	0.58	1.24	ILRM
		L_2	0.003	0.98	1.01	0.70	1.43	IHRM
	M_2	L_1	-0.16	0.39	0.84	0.58	1.24	ILRM
		L_2	0.06	0.74	1.06	0.74	1.53	IHRM
	M_3	L_1	-0.24	0.27	0.78	0.51	1.21	ILRM
		L_2	-0.22	0.30	0.80	0.52	1.22	ILRM

Table 3. Odd ratio, confidence interval (CI) and slope coefficient for Tanzo models.

Antibiotics	Model	Levels	Coefficient	P-Value	OR	CI (95%)		Decision
						Lower Bound	Upper Bound	
Tanzo	M_0	L_1	-0.70	0.01	0.50	0.28	0.87	SLRM
		L_2	-0.22	0.20	0.79	0.56	1.13	ILRM
	M_1	L_1	-0.57	0.06	0.56	0.31	1.03	ILRM
		L_2	-0.16	0.39	0.84	0.57	1.24	ILRM
	M_2	L_1	-0.52	0.08	0.59	0.32	1.08	ILRM
		L_2	-0.09	0.62	0.91	0.61	1.34	ILRM
	M_3	L_1	-0.38	0.26	0.68	0.35	1.33	ILRM
		L_2	0.25	0.26	1.28	0.82	1.99	IHRM

For model M_0, the L_2 resulted in an OR of 0.79 with a 95% CI of 0.56 to 1.13. These results suggest a potential protective effect (low risk of mortality), and not statistically significant as p-value is 0.20. All coefficients found negative except M_3 for L_2. In the case of model M_1, the L_1 and L_2 of Tanzo antibiotic produced an OR of 0.56, 0.84; 95% CI from 0.31 to 1.03 and 0.57 to 1.24 with p-values of 0.06 and 0.39, respectivrly. Similarly, for M_2, the L_1 and L_2 produced OR values of 0.59 and 0.91, 95% CI from 0.32 to 1.08 and 0.61 to 1.34 with p-values of 0.08 and 0.62, respectively. These results suggest a potential protective effect (low risk of mortality) for M_1 and M_2, and the findings are statistically insignificant. Concerning model M_3, the L_1 of Tanzo antibiotic generated an OR of 0.68 and the 95% CI is from 0.35 to 1.33. These findings suggest a potential protective effect, and it is not statistically significant as p-value is greater the level of significance and 95% CI includes 1. For model M_3, the L_2 of Tanzo antibiotic produced an OR of 1.28 with a 95% CI in the range of 0.82 to 1.99. These results indicate a potential risk (high risk of mortality), and it is statistically insignificant. All coefficients found negative except M_3 for L_2.

In summary, both the unadjusted model (M_0) and all adjusted models (M_1, M_2 and M_3) exhibit statistically insignificant results, except for the low dose (L_1) in the unadjusted model M_0, where a statistically significant low risk of mortality (SLRM) is observed. The odds ratios and p-values consistently indicate an insignificant low risk of mortality (ILRM) at L_1 for all adjusted models (M_1, M_2 and M_3). However, at L_2, the odds ratios and p-values reveal a statistically insignificant low risk of mortality (ILRM) for the unadjusted model (M_0) and adjusted models M_1 and M_2. In the case of adjusted model M_3, the results are reported as IHRM. The term insignificant implies that the observed effects may be due to random variability rather than a true association.

3.4. Comparisons of Tienum Models

Table 4 shows the odds ratio, 95% CI, and slope coefficient for Tienum antibiotic. For each level of Tienum (M_0, M_1, M_2 and M_3), the coefficients represent the change in the log-odds of the outcome variable found negative for L_1 (M_1, M_2 and M_3), and positive for L_2 (M_1, M_2 and M_3). OR values found greater than 1 for L_1 (M_0) and L_2 (M_0) with values of 1.02 and 1.35, respectively, indicating the possible risk, and found statistically insignificant. P-values of all models with 95% CI (includes 1), indicating that the results are statistically insignificant. For each level of Tienum (M_1, M_2 and M_3), the OR for L_1, is found 0.64, 0.66 and 0.51, respectively; while for L_2, it is found 1.22, 1.43 and 1.45, respectively. These results show that there is a possible protection (low risk of mortality) for each level of Tienum (M_1, M_2 and M_3) for L_1, while possible risk (high risk of mortality) for L_2 (M_1, M_2 and M_3).

In summary, both the unadjusted model (M_0) and all adjusted models (M_1, M_2 and M_3) exhibit statistical insignificance for the antibiotic Tienum. The odds ratios and p-values consistently indicate a statistically significant high risk of mortality (IHRM) at L_1 and L_2 for unadjusted model (M_0). For the low dose (L_1), all the adjusted models (M_1, M_2 and M_3) produced ILRM, while for L_2, it is reported

Table 4. Odd ratio, confidence interval (CI) and slope coefficient for Tienum models.

Antibiotics	Model	Levels	Coefficient	P-Value	OR	CI (95%)		Decision
						Lower Bound	Upper Bound	
Tienum	M_0	L_1	0.01	0.96	1.02	0.49	2.10	IHRM
		L_2	0.30	0.13	1.35	0.91	2.00	IHRM
	M_1	L_1	-0.45	0.27	0.64	0.28	1.42	ILRM
		L_2	0.20	0.35	1.22	0.79	1.89	IHRM
	M_2	L_1	-0.40	0.33	0.66	0.29	1.50	ILRM
		L_2	0.36	0.12	1.43	0.90	2.25	IHRM
	M_3	L_1	-0.66	0.17	0.51	0.20	1.32	ILRM
		L_2	0.37	0.16	1.45	0.85	2.46	IHRM

as IHRM. The term insignificant implies that the observed effects may be due to random variability rather than a true association.

4. DISCUSSIONS

The present study provides a comprehensive evaluation of antibiotic usage (Azithromycin, Ceftriaxone, Tanzo, and Tienum) in relation to mortality risk using unadjusted and adjusted logistic regression models. The findings contribute to the ongoing debate regarding the clinical effectiveness and risk implications of empirical antibiotic therapy in COVID-19 management in Pakistan. In line with earlier research, the findings reaffirm the central role of vital signs in determining disease severity and patient characteristics outcomes. Previous studies by Islam *et al*. [17], Gul and Yucesan [18] and Spangler *et al.* [19] have highlighted the importance of indicators such as oxygen saturation, respiratory rate and body temperature in monitoring and predicting COVID-19 progression. By incorporating these variables into the adjusted models, the present analysis provides a more reliable estimation of mortality risk, underscoring the limitations of relying solely on unadjusted associations. The results for Azithromycin reflect the inconsistency widely reported in the literature. While some investigations have suggested that its use may contribute to improved recovery or reduced mortality [45, 46], other studies have found no meaningful clinical benefit [47, 48]. In the present study, associations between Azithromycin and mortality were not statistically significant. Although a slight protective trend appeared in unadjusted models at higher doses, this effect weakened after controlling for confounding variables. This indicates that earlier observed benefits may be attributed more to patient characteristics than to the drug itself, reinforcing concerns about its routine use without clear clinical indication. For Ceftriaxone, the analysis consistently shows no statistically significant relationship with mortality across all model specifications. This observation aligns with broader evidence indicating that the widespread use of antibiotics during the pandemic often as a precaution against secondary infections did not necessarily improve patient survival [30, 31]. These findings emphasize the importance of promoting judicious antibiotic use, particularly in resource constrained settings where antimicrobial resistance is an increasing concern. The analysis of Tanzo presents an interesting pattern, where a significant protective effect is observed only in the unadjusted model at low doses. However, this significance disappears in adjusted models, indicating that the initial association was likely confounded by demographic or clinical factors. This pattern reinforces the methodological importance of multivariate adjustments in epidemiological modeling, as emphasized in logistic regression literature [41-44]. Tienum shows no statistically significant association with mortality risk across models, although a pattern of potential increased risk at higher doses is observed. These findings are important in the context of empirical antibiotic escalation strategies used during severe COVID-19 cases. The absence of significant benefits, combined with potential risks, underscores the need for evidence based prescription practices. Overall, the dominance of statistically insignificant results across antibiotics suggests that antibiotic

therapy alone is not a decisive factor in reducing COVID-19 mortality, particularly when adjusted for vital signs and comorbidities. This is consistent with global findings that COVID-19 is primarily a viral disease and antibiotics should be reserved for cases involving confirmed bacterial co-infections [30]. From a methodological standpoint, the study clearly demonstrates the value of progressive model adjustment. The transition from the unadjusted model to fully adjusted specifications illustrate how the inclusion of demographic characteristics, vital signs and comorbidities conditions refines the interpretation of associations. This approach is consistent with established statistical practices, which advocate for adjusted models to obtain more accurate and unbiased estimates [32-35]. The findings suggest that the prescription of antibiotics during COVID-19 should be undertaken with heightened caution, prioritizing decisions grounded in clinical evidence rather than routine or empirical use, especially during pandemic scenarios. The study further underscores the importance of integrating patients' vital signs and pre-existing health conditions into clinical risk assessments, as these factors have a significant influence on patient outcomes. From a healthcare policy standpoint, it is essential for authorities to strengthen formal antimicrobial stewardship programs, aiming to limit unnecessary antibiotic use and curb the potential development of antimicrobial resistance over time.

5. LIMITATIONS AND FUTURE RECOMMENDATIONS

This study provides insights into the role of antibiotics, vital signs and comorbidities as predictors of COVID-19 mortality using both unadjusted and adjusted logistic regression analyses, but it has some limitations. It relies on secondary data from the early pandemic period (February to August 2020), which may limit generalizability to later waves or different healthcare settings. The observational design prevents definitive conclusions about causality, as residual confounding and treatment selection bias may remain. Categorization of antibiotic doses use only in two steps as low and high groups, which may be extends in more dosing, standardized threshold and time span etc. Some models yielded non-significant results, possibly due to small sample sizes, measurement errors or unobserved patient heterogeneity. Key clinical factors, such as drug timing, infection severity and hospital level variations, were not considered. Future studies using larger, prospective datasets with more detailed clinical information are recommended.

6. CONCLUSIONS

This research studying the COVID-19 patients in association with antibiotics, i.e., Azithromycin, Cefatriaxone, Tanzo, and Tienum, in association with vital measurements and underlying comorbidities effects to layout the comprehensive patient management and better treatment efficacies for the mortality risk (yes/no). The logistic regression model for one unadjusted model (M_0) associated with antibiotics and three adjusted models as: M_1 associated with antibiotics, gender and age, M_2 associated with antibiotics, gender, age and vital measurements, and M_3 associated with antibiotics gender, age, vital measurement and comorbidities are applied. Odds ratios (OR), 95% confidence interval (CI) and p-value is used to examine determine the results using the secondary data of COVID-19 patients spanning from February to August 2020. Antibiotics are classified into two relative categories as: low dose (L_1) and high dose (L_2). The decision criteria for both adjusted and unadjusted models hinge on statistical significance and mortality risk. Insignificant models with low risk of mortality are categorized as ILRM, while significant models with low risk fall under SLRM. Insignificant models with high risk of mortality are termed IHRM and significant models with high risk are classified as SHRM.

For Azithromycin, the findings indicate IHRM for unadjusted model (M_0) and adjusted models (M_1, M_2 and M_3) for L_1. The unadjusted model (M_0) at L_2 has SLRM, but adjusted models M_1 and M_2 show ILRM, and M_3 shows IHRM. For ceftriaxone, at L_1, indicating ILRM for all models. However, at L_2, unadjusted model (M_0) and adjusted models M_1 and M_2 suggest an IHRM, while adjusted model M_3 shows ILRM. In Tanzo, all models show statistically insignificant results, except for the unadjusted model (M_0) at low dose (L_1), which indicate SLRM. However, at L_2, all models exhibit ILRM, except for adjusted model M_3, where results are IHRM. The unadjusted model (M_0) and adjusted models (M_1, M_2 and M_3) show statistically insignificance for the antibiotic Tienum. The unadjusted model (M_0) indicates a statistically insignificant high risk

of mortality (IHRM) at L_1 and L_2. The adjusted models (M_1, M_2 and M_3) consistently reporting statistically insignificant high risk of mortality (IHRM) at L_2, while at L_1, they show statistically insignificant low risk of mortality (ILRM). This study can be extended to include others antibiotics and its various levels of doses. The research is supporting to healthcare professionals in predicting and managing vital signs and comorbidities variations for COVID-19 patient.

7. CONFLICTS OF INTEREST

The authors declare no conflict of interest.

8. ETHICAL STATEMENT

The research utilized secondary data of COVID-19 patients admitted to four hospitals, i.e., Pakistan Air Force Hospital, Pakistan Institute of Medical Sciences (PIMS), Holy Family Hospital and Benazir Bhutto Shaheed Hospital, located in Rawalpindi and Islamabad, covering the period from February to August 2020. The data were used in National College of Business Administration and Economics (NCBA&E), Multan, as part of the M.Phil. Thesis of Imtiaz Ahmed in Statistics, titled as: "Validation of early warning scores for detecting deteriorating patients in Pakistani hospitals during pandemic: A multicenter study" in 2023. As this study involved anonymized secondary data without any direct interaction with patients or human subjects, therefore no ethical approval was required.

9. ACKNOWLEDGMENT

All the authors appreciate the support and data provided by Pakistan Air Force Hospital, Pakistan Institute of Medical Sciences Hospital, Holy Family Hospital, and Benazir Bhutto Shaheed Hospital of Pakistan.

10. FUNDING

No funding was received to conduct this research.

11. AUTHORSHIP CONTRIBUTION STATEMENT

All authors have equal contributions.

12. REFERENCES

1. O. Delardas, K.S. Kechagias, P.N. Pontikos, and P. Giannos. Socio-Economic impacts and challenges of the coronavirus pandemic (COVID-19): an updated review. *Sustainability* 14(15): 9699 (2022). https://doi.org/10.3390/su14159699
2. J.J. Baugh, B.A. White, D. McEvoy, B.J. Yun, D.F. Brown, A.S. Raja, and S. Dutta. The cases not seen: patterns of emergency department visits and procedures in the era of COVID-19. *The American Journal of Emergency Medicine* 46: 476-481 (2021). https://doi.org/10.1016/j.ajem.2020.10.081
3. S.J. Pleasure, A.J. Green, and S.A. Josephson. The spectrum of neurologic disease in the severe acute respiratory syndrome coronavirus 2 pandemic infection: neurologists move to the frontlines. *JAMA Neurology* 77(6): 679-680 (2020). https://jamanetwork.com/journals/jamaneurology/fullarticle/2764548
4. W. Tan and J. Aboulhosn. The cardiovascular burden of coronavirus disease 2019 (COVID-19) with a focus on congenital heart disease. *International Journal of Cardiology* 309: 70-77 (2020). https://doi.org/10.1016/j.ijcard.2020.03.063
5. S. Khan, M. Mujaddad, M.N. Uddin, S. Ullah, A. Rasheed, N.A. Jatoi, W.A. Bhatti, A. Khan, M. Islam, and A. Iqbal. Strategies adopted by government of Pakistan to cope with the pandemic and comparative cases of COVID-19 in all provinces of Pakistan. *Advances in Bioresearch* 11(4): 41-48 (2020). https://soeagra.com/abr/abrjuly2020/7.pdf
6. S. Kashte, A. Gulbake, and S.F. El-Amin, A. Gupta. COVID-19 vaccines: rapid development, implications, challenges and future prospects. *Human Cell* 34: 711-733 (2021). https://doi.org/10.1007/s13577-021-00512-4
7. L. Forchette, W. Sebastian, and T. Liu. A comprehensive review of COVID-19 virology, vaccines, variants, and therapeutics. *Current Medical Science* 41: 1037-1051 (2021). https://doi.org/10.1007/s11596-021-2395-1
8. J.A. Plante, B.M. Mitchell, K.S. Plante, K. Debbink, S.C. Weaver, and M. Vineet. The variant gambit: COVID-19's next move. *Cell Host & Microbe* 29(4): 508-515 (2021). https://www.cell.com/cell-host-microbe/fulltext/S1931-3128(21)00099-8
9. K.Y Loo and V. Letchumanan. COVID-19: Understanding the new variants of concern. *Progress in Microbes & Molecular Biology* 5(1): a0000282 (2022). https://distantreader.org/stacks/journals/pmmb/pmmb-673.pdf
10. Y. Wei, J. Guan, X. Ning, Y. Li, L. Wei, S. Shen, R. Zhang, Y. Zhao, H. Shen, and F. Chen. Global COVID-19 pandemic waves: Limited lessons

learned worldwide over the past year. *Engineering* 13: 91-98 (2022). https://doi.org/10.1016/j.eng.2021.07.015

11. L. Lopez and X. Rodo. The end of social confinement and COVID-19 re-emergence risk. *Nature Human Behaviour* 4: 746-755 (2020). https://doi.org/10.1038/s41562-020-0908-8
12. A. Khalid and S. Ali. COVID-19 and its challenges for the healthcare system in Pakistan. *Asian Bioethics Review* 12: 551-564 (2020). https://doi.org/10.1007/s41649-020-00139-x
13. R. Rasheed, A. Rizwan, H. Javed, F. Sharif, and A. Zaidi. Socio-economic and environmental impacts of COVID-19 pandemic in Pakistan: an integrated analysis. *Environmental Science and Pollution Research* 28: 19926-19943 (2021). https://doi.org/10.1007/s11356-020-12070-7
14. M. Habib and M. Abbas. Facing the threat of COVID-19 in Pakistan: a nation's dilemma. *Value in Health Regional Issues* 24: 90-95 (2021). https://doi.org/10.1016/j.vhri.2020.10.005
15. F. Emmanuel, A. Hassan, A. Ahmad, and T.E. Reza. Pakistan's COVID-19 prevention and control response using the world health organization's guidelines for epidemic response interventions. *Cureus* 15(1): e34480 (2023). https://assets.cureus.com/uploads/review_article/pdf/122922/20230303-26060-lxntcu.pdf
16. B.T. Shaikh. Strengthening health system building blocks: configuring post-COVID-19 scenario in Pakistan. *Primary Health Care Research & Development* 22: e9 (2021). https://www.cambridge.org/core/services/aop-cambridge-core/content/view/S1463423621000128
17. M. Islam, I. Ahmed, M. Shehzad, and K. Nadeem. Resilience of antibiotic usage and vital signs in COVID-19 patients: A post-pandemic analysis in Pakistan. *Proceedings of the Pakistan Academy of Sciences: A. Physical and Computational Sciences*, 61(4): 373–379 (2024). https://doi.org/10.53560/PPASA(61-4)683
18. M. Gul and M. Yucesan. Hospital preparedness assessment against COVID-19 pandemic: a case study in Turkish tertiary healthcare services. *Mathematical Problems in Engineering* 2021: Article ID 2931219 (2021). https://doi.org/10.1155/2021/2931219
19. D. Spangler, H. Blomberg, and D. Smekal. Prehospital identification of Covid-19: an observational study. *Scandinavian Journal of Trauma, Resuscitation and Emergency Medicine* 29: s13049 (2021). https://doi.org/10.1186/s13049-020-00826-6
20. S.N. Facente, L.A. Hunter, L.J. Packel, Y. Li, A. Harte, G. Nicolette, S. McDevitt, M. Petersen, and A.L. Reingold. Feasibility and effectiveness of daily temperature screening to detect COVID-19 in a prospective cohort at a large public university. *BMC Public Health* 21: s12889 (2021). https://doi.org/10.1186/s12889-021-11697-6
21. C. Harding, F. Pompei, S.F. Bordonaro, D.C. McGillicuddy, D. Burmistrov, and L.D Sanchez. The daily, weekly, and seasonal cycles of body temperature analyzed at large scale. *Chronobiology International* 36(12): 1646-1657 (2019). https://doi.org/10.1080/07420528.2019.1663863
22. P.G. Gibson, L. Qin, and S.H. Puah. COVID-19 acute respiratory distress syndrome (ARDS): clinical features and differences from typical pre-COVID-19 ARDS. *Medical Journal of Australia* 213(2): 54-56. (2020). https://www.mja.com.au/system/files/issues/213_02/mja250674.pdf
23. B. Hill and S.H. Annesley. Monitoring respiratory rate in adults. *British Journal of Nursing* 29(1): 12-16 (2020). https://doi.org/10.12968/bjon.2020.29.1.12
24. Y. Xiao, C. Shuhan, L. Yun, Z. Fangfang, H. Ming, Z. Yan, Z. Ruiqiang, L. Xuyan, H. Bo, and P. Zhiyong. Extracorporeal membrane oxygenation for coronavirus disease 2019-induced acute respiratory distress syndrome: a multicenter descriptive study. *Critical Care Medicine* 48(9): 1289-1295 (2020). https://journals.lww.com/ccmjournal/fulltext/2020/09000/Extracorporeal_Membrane_Oxygenation_for.6.aspx
25. E.A. Amaratunga, D.S. Corwin, L. Moran, and R. Snyder. Bradycardia in patients with COVID-19: a calm before the storm? *Cureus* 12(6): e8599 (2020). https://www.cureus.com/articles/34085#!/
26. J.W. McEvoy, N. Daya, F. Rahman, R.C. Hoogeveen, R.S. Blumenthal, A.M. Shah, C.M Ballantyne, J. Coresh, and E. Selvin. Association of isolated diastolic hypertension as defined by the 2017 ACC/AHA blood pressure guideline with incident cardiovascular outcomes. *Journal of the American Medical Association* 323(4): 329-338 (2020). https://jamanetwork.com/journals/jama/fullarticle/2759472
27. K. Fox, J.S. Borer, A.J. Camm, N. Danchin, R. Ferrari, L. Jose, L. Sendon, P.G. Steg, J.C. Tardif, L. Tavazzi, and M. Tendera. Resting heart rate in cardiovascular disease. *Journal of the American College of Cardiology* 50(9): 823-830 (2007). https://doi.org/10.1016/j.jacc.2007.04.079
28. J.G. Logan and S.S. Kim. Resting heart rate and aortic stiffness in normotensive adults. *Korean*

Circulation Journal 46(6): 834-840 (2016). https://doi.org/10.4070/kcj.2016.46.6.834

29. H. Akhtar, S. Akhtar, F.U. Rahman, M. Afridi, S. Khalid, S. Ali, N. Akhtar, Y.S. Khader, H. Ahmad, and M.M. Khan. An overview of the treatment options used for the management of COVID-19 in Pakistan: Retrospective observational study. *JMIR Public Health and Surveillance* 79(5): e28594 (2021). https://publichealth.jmir.org/2021/5/e28594
30. S.H. Al-Hadidi, H. Alhussain, H.A. Hadi, A. Johar, H.M. Yassine, A.A. Al-Thani, and N.O. Eltai. The spectrum of antibiotic prescribing during COVID-19 pandemic: a systematic literature review. *Microbial Drug Resistance* 27(12): 1705-1725 (2021). https://doi.org/10.1089/mdr.2020.0619
31. Z.U. Mustafa, A.H. Khan, S.N. Harun, M. Salman, and B. Godman. Antibiotic overprescribing among neonates and children hospitalized with COVID-19 in Pakistan and the implications. *Antibiotics* 12(4): 12040646 (2023). https://doi.org/10.3390/antibiotics12040646
32. H.A. Park. An introduction to logistic regression: from basic concepts to interpretation with particular attention to nursing domain. *Journal of Korean Academy of Nursing* 43(2): 154-164 (2013). https://doi.org/10.4040/jkan.2013.43.2.154
33. D.W. Hosmer Jr, S. Lemeshow, and R.X. Sturdivant (Eds.). Applied Logistic Regression. *John Wiley & Sons. Hoboken, New Jersey, U.S* (2013).
34. A. Agresti. Categorical Data Analysis: *John Wiley & Sons. Hoboken, New Jersey, U.S* (2012).
35. D.A. Grimes and K.F. Schulz. Making sense of odds and odds ratios. *Obstetrics & Gynecology* 111(2): 423-426 (2008). https://journals.lww.com/greenjournal/abstract/2008/02000/making_sense_of_odds_and_odds_ratios.24.aspx
36. P. Ospina, D.V. Nydam, and T.J. DiCiccio. The risk ratio, an alternative to the odds ratio for estimating the association between multiple risk factors and a dichotomous outcome. *Journal of Dairy Science* 95(5): 2576-2584 (2012). https://doi.org/10.3168/jds.2011-4515
37. M.A. Halvorson, C.J. McCabe, D.S. Kim, X. Cao, and K.M. King. Making sense of some odd ratios: A tutorial and improvements to present practices in reporting and visualizing quantities of interest for binary and count outcome. *Psychology of Addictive Behaviors* 36(3): 284-295 (2022). https://psycnet.apa.org/buy/2021-40400-001
38. J.P. Bentley, S. Ramachandran, and T.M. Salgado. Moderation analysis with binary outcomes: Interactions on additive and multiplicative scales. Contemporary Research Methods in Pharmacy and Health Services. S.P. Desselle, V.G Cardenas, C. Anderson, P. Aslani, A.M.H. Chen, and T.F. Chen. *Academic Press* pp. 313-328 (2022). https://doi.org/10.1016/B978-0-323-91888-6.00039-9
39. G. Tucker, A. Metcalfe, C. Pearce, A.G. Need, I.M. Dick, R.L. Prince, and B.E.C Nordin. The importance of calculating absolute rather than relative fracture risk. *Bone* 41(6): 937-941 (2007). https://doi.org/10.1016/j.bone.2007.07.015
40. J.P. Bentley, S. Ramachandran, and T.M. Salgado. Considerations when conducting moderation analysis with a binary outcome: Applications to clinical and social pharmacy research. *Research in Social and Administrative Pharmacy* 18(2): 2276-2282 (2022). https://doi.org/10.1016/j.sapharm.2021.04.020
41. M.P. LaValley. Logistic regression. *Circulation* 117(18): 2395-2399. (2008). https://doi.org/10.1161/CIRCULATIONAHA.106.682658
42. A.F Schmidt, O.H. Klungel, R.H. Groenwold, and G. Consortium. Adjusting for confounding in early postlaunch settings: going beyond logistic regression models. *Epidemiology* 27(1): 133-142 (2016). https://journals.lww.com/epidem/abstract/2016/01000/adjusting_for_confounding_in_early_postlaunch.19.aspx
43. S. Menard. Coefficients of determination for multiple logistic regression analysis. *The American Statistician* 54(1): 17-24. (2000). https://doi.org/10.1080/00031305.2000.10474502
44. G.A. Nichols and J.B. Brown. Unadjusted and adjusted prevalence of diagnosed depression in type 2 diabetes. *Diabetes Care* 26(3): 744-749 (2003). https://doi.org/10.2337/diacare.26.3.744
45. D. Echeverria-Esnal, C. Martin-Ontiyuelo, M.E. Navarrete-Rouco, C.M. De-Antonio, O. Ferrandez, J.P. Horcajada, and S. Grau. Azithromycin in the treatment of COVID-19: a review. *Expert Review of Anti-Infective Therapy* 19(2): 147-163 (2020). https://doi.org/10.1080/14787210.2020.1813024
46. E. Sekhavati, F. Jafari, S. SeyedAlinaghi, S. Jamalimoghadamsiahkali, S. Sadr, M. Tabarestani, M. Pirhayati, A. Zendehdel, N. Manafic, M. Hajiabdolbaghi, Z. Ahmadinejad, H.E. Kouchak, S. Jafari, H. Khalili, M. Salehi, A. Seifi, F.S. Golestan, and F. Ghiasvand. Safety and effectiveness of azithromycin in patients with COVID-19: an open-label randomised trial. International Journal of Antimicrobial Agents 56(4): 106143 (2020). https://doi.org/10.1016/j.ijantimicag.2020.106143
47. A. Rodriguez-Molinero, C. Perez-Lopez, C. Galvez-

Barron, A. Minarro, O. Macho, G.F. Lopez, M.T. Robles, M.D. Dapena, S. Martınez, E. Rodrıguez, and I. Collado. Observational study of azithromycin in hospitalized patients with COVID-19. *PLOS One* 15(9): e0238681 (2020). https://doi.org/10.1371/journal.pone.0238681

48. A.M. Kamel, M.S.A. Monem, N.A. Sharaf, N. Magdy, S.F. Farid. Efficacy and safety of azithromycin in Covid-19 patients: A systematic review and meta-analysis of randomized clinical trials. *Reviews in Medical Virology* 32(1): e2258 (2022). https://doi.org/10.1002/rmv.2258

Proceedings of the Pakistan Academy of Sciences: A Physical and Computational Sciences 63(1): 61-70 (2026)

ISSN (Print): 2518-4245; ISSN (Online): 2518-4253
http://doi.org/10.53560/PPASA(63-1)706

Pakistan Academy of Sciences

Research Article

Density Estimation and Efficiency Analysis of a New Beta Polynomial Family

Edith Akpevwe Siloko[1]*, Rita Nneka Nwaka[2], Israel Uzuazor Siloko[3], Esosa Enoyoze[3], Oyaimare Osemengbe Uddin[4], Simon Ejokema Imoisi[5], Cyril Chukwuka Ishiekwene[6], and Osayomore Ikpotokin[7]

[1]Department of Mathematics, Delta State College of Education, Mosogar, Nigeria
[2]Department of Mathematics and Statistics, University of Delta, Agbor, Nigeria
[3]Department of Mathematics and Statistics, Edo State University, Iyamho, Nigeria
[4]Department of Computer Science, Edo State University, Iyamho, Nigeria
[5]Department of Public Law, Edo State University, Iyamho, Nigeria
[6]Department of Statistics, University of Benin, Benin City, Nigeria
[7]Department of Statistics, Ambrose Alli University, Ekpoma, Nigeria

Abstract: A popular non-parametric approach constantly employed in the estimation of probability density function (PDF) of data is kernel density estimation (KDE) and the technique is vital in several statistical methodologies because of its functionality in data analysis. This study assesses the efficacy and efficiency of new kernel family known as the new beta polynomial family (NBPF) kernels which is generated by additional power to the polynomial functional form. The numerical efficiency of the newly introduced kernel family improves substantially due to the integration of the functional modification. The efficiencies of the classical polynomial family decreases with increase in the polynomial power while the reverse is the case with the new family which demonstrates an exceptional improvement with increase in its power and also sustaining computational flexibility. A comparative assessment of the efficiencies of NBPF shows that it exhibits superiority over the existing beta kernel family (BKF), demonstrating their adaptability to modern techniques in probability density functions without rigid parametric assumptions. Again, a real data application of the NBPF reveals that the family possesses retention capacity of intrinsic characteristics of the dataset. The numerical improvement of the efficiencies of NBPF as well as the ability of NBPF to retain essentials statistical characteristics emphasise the importance of the NBPF in data analysis and data visualization.

Keywords: Bandwidth, Beta, Density, Estimation, Efficiency, Kernel.

1. INTRODUCTION

Kernel density estimation (KDE) is one of the vital non-parametric methods in statistics primarily for the estimation of probability density functions (PDFs) of random variables [1-3]. The classical parametric methods usually assume that data been evaluated belong to distributional group, whereas, KDE is void of distributional assumption but allow the observations to speak for themselves. The lack of distributional assumptions in KDE enhances more flexibility in the detection of complex features, particularly in real-life observations. Kernel estimation is greatly important in the analysis of data with no prior knowledge on the fundamental distribution by generating a smooth continuous density estimate over the entire datasets [4]. KDE usually generate a smooth curve that provides the information embedded in the data and also display statistical features such as peaks known as the

Received: December 2025; Revised: February 2026; Accepted: March 2026
* Corresponding Author: Edith Akpevwe Siloko <siloko.akpevwe@descoem.edu.ng>

modes of the data and troughs of the distributions. The analysis of data using the KDE strategy is vital in most data analytic techniques and of wide applications as well as a strong foundation in different fields. One of the importance of the KDE approach is that the knowledge derived is generic and can be extended to other smoothing setting. Again, the effectiveness of the KDE approach in several disciplines is due to the simplicity of extending the technique to other complex estimation methodologies.

The KDE methodology is a prominent tool in exploratory data analysis (EDA) and data visualization (DV) especially amid investigation of the statistical composition of dataset in reference to the underlying probability distribution. One of the essential benefits of KDE is the idea of non-imposition of distributional assumptions on the observations which has resulted in widespread use of the approach on different datasets [5-7]. The occurrence of vehicular road accidents between 2010 and 2020 which accounted for 30% of road traffic crashes as published by the European Union was analysed by Baranyai and Sipos [8] using kernel method by implementing the black-spot technique. Additionally, owing to the extensive applicability of KDE, the technique is of great utilization in identification of region having elevated data density in clustering analysis as well as bump hunting with significant uses in pattern identification and image editing [9]. More so, KDE has gained popularity in anomalies detection or outliers especially in estimation of underlying data distribution, affirming KDE as a veritable tool in the detection of fraud as well as network security [10, 11]. The kernel approach is of great significance in estimation of income distribution, analysis of income inequality, and suitable policies formulation with recommendations [12]. The volatility of the stock market can be determined using the kernel technique in examining the frequent changes usually associated with the trading volumes in order to acknowledge the behaviour of the stock market. Fan and Cheng [13] investigated stock trading volumes with respect to market share and their probability distribution using KDE with the aid of long-term and short-term integration memory network strategies in modelling the dynamics of trading volume. The prevention of traffic accidents is critical to effective road management systems particularly, the identification of hotspots. In the study of Srikanth and Srikanth [14], hotspots in the city of Des Moines, United States, were identified with KDE for five consecutive years' data from 2008 to 2012. The identified hotspots were provided by a visual display of traffic crashes locations based on the statistical significance of their density estimates.

Heavy rainfall that is characterized by massive destructive winds and accompanied by snow is frequently experienced in Bangladesh which is located in Southern Asia due to the climatic irregularity and distinctive geographical position. The analysis of cyclone data was investigated by Tuya *et al.* [15] from 1960 to 2023 in Bangladesh using the KDE method by identifying areas that are prone to cyclones. The study furnished the government with invaluable knowledge to improve effective planning that mitigates the consequence of cyclones in the country. Lasocki [16] examined the application of KDE in seismology in which the magnitude was estimated as seismic variables with continuous distributions. Similarly, Pollard *et al.* [17] applied KDE in archaeological investigation of spatial analysis and the findings provided valuable insights into spatial archaeological results especially in Geographic Information Systems (GIS). Additionally, in clustering analysis, KDE approach is of great importance especially in the identification of areas having high density of data points. The KDE methodology has gain popularity in several fields of studies, such as road network, image editing, and pattern identification [18-20].

The extensive applications of the kernel approach are accompanied with numerous difficulties for effective implementation. The main problem associated with the KDE approach is the accurate selection of the bandwidth as well as the kernel function. The kernel estimator (KE) and kernel function (KF) are impacted by the choice of the bandwidth greatly however, with minimal impact on KF since most KFs are probability density function [21]. Despite the difficulties connected with accurate bandwidth selection, researchers are regularly introducing novel bandwidth selectors to improve KDE's performance [22, 23]. Moreover, there is a decrease of the applicability of kernel technique in multivariate environment due to the phenomenon known as "curse of dimensionality effect" usually connected with non-parametric statistical estimation [24, 25]. This condition has given rise to the application of sophisticated

techniques capable of successfully addressing these challenges.

The introduction of modern methodologies into kernel approaches have largely contributed effectively to performance improvement especially in bandwidth selection, new kernel estimators, and extension of the kernel method in numerous disciplines [26]. Again, the introduction of modern computational techniques has addressed the problem of scalability in large datasets [27, 28]. The performance and efficiency of a newly introduced beta polynomial kernel is examined in this study. The justification for the introduction of new kernel family is hinge on the need for improvement in kernel performance as well as efficient estimation techniques. The new kernel family promises improved performance, that is reduction of estimation error using the asymptotic mean integrated squared error (AMISE) as criterion function, and better efficiency in density estimation. The improvement of performance and efficiency of the novel beta kernel family is ascertained in comparison with the classical beta family.

2. MATERIALS AND METHODS

This study employed strategy geared towards the exploration of the efficacy and effectiveness of a novel kernel family in statistical density estimation. The kernel techniques are versatile and widely recognized especially in modelling probability density functions that do not require stringent parametric assumptions. This study assesses the efficacy and efficiency of NBPF in KDE, demonstrating their adaptability to modern methodologies in probability density functions without the rigid parametric assumptions. The proposed kernel family demonstrate a propitious behaviour and adaptability feature when evaluated within the interval support of [−1, 1]. Typically, the KDE technique is of widespread uses in non-parametric estimation methods in modelling several events. Rosenblatt [29] proposed the kernel estimator, while Parzen [30] popularized its applications across multiple disciplines, particularly in exploratory data analysis and data visualization [2, 31]. Generally, the kernel's closed form is:

$$\hat{f}(\mathrm{y}) = \frac{1}{nh_{\mathrm{y}}}\sum_{i=1}^{n} K\left(\frac{\mathrm{y}-\mathrm{Y}_i}{h_{\mathrm{y}}}\right) \quad (1)$$

In this context, $K(\cdot)$ represent a kernel function, h_{y} denotes the bandwidth that controls the estimates' smoothness, n is the total observations, y refers to data variations and Y_i denotes variables to be estimated [12]. Certain conditions are usually satisfied by this estimator, which are:

$$\int K(\mathrm{y})d\mathrm{y} = 1, \quad \int \mathrm{y}K(\mathrm{y})d\mathrm{y} = 0 \quad \text{and} \quad \int \mathrm{y}^2K(\mathrm{y})d\mathrm{y} = \mu_2(K) \neq 0 \quad (2)$$

A kernel function is typically symmetric, integrates to one with zero mean, non-zero moment, and is a PDF (probability density function). The two fundamental components in KDE are the selection of bandwidth and the choice of the kernel function. In terms of bandwidth selection, numerous researchers have introduced innovative selectors, whereas there has been limited investigation into the kernel function [1, 32]. The selection of bandwidth significantly influences the efficacy of the KDE, and a globally utilized evaluation performance metric in KDE is the mean integrated squared error, which is:

$$MISE\left(\hat{f}(\mathrm{y})\right) = \frac{R(K)}{nh_{\mathrm{y}}} + \frac{1}{4}\mu_2(K)^2h_{\mathrm{y}}^4R(f'') + O\left(\frac{1}{nh_{\mathrm{y}}} + h_{\mathrm{y}}^4\right) \quad (3)$$

where $R(K)$ denotes kernel roughness, $\mu_2(K)^2$ depicts the kernel moment and $R(f'') = \int f''(\mathrm{y})^2d\mathrm{y}$ represents unknown function roughness [33]. The MISE has an asymptotic version, which is:

$$AMISE\left(\hat{f}(\mathrm{y})\right) = \frac{R(K)}{nh_{\mathrm{y}}} + \frac{1}{4}\mu_2(K)^2h_{\mathrm{y}}^4R(f'') \quad (4)$$

The bandwidth with the minimum AMISE, as presented in Equation (4), is referred to as the optimal bandwidth and is given by:

$$h_{\mathrm{AMISE}} = \left[\frac{R(K)}{\mu_2(K)^2R(f'')}\right]^{1/5} \times n^{-1/5} \quad (5)$$

The bandwidth value derived from Equation (5) yields the minimum AMISE. Accurate selection of the bandwidth is of great significance in KDE methodologies due to its smoothing role. Innovative techniques have been recently introduced to address the difficulties linked with accurate bandwidth selection [21, 34].

2.1. The Existing Beta Polynomial Kernel Functions

There are different kernel families in density estimation but the beta kernel family is frequently

used due to its unique mathematical tractability. The compact form of the beta kernel is:

$$K_{[p,r]}(t) = \frac{(2r+1)!}{2^{2r+1}(r!)^2}(1-t^2)^r \quad (6)$$

Here $r = 0, 1, 2, \ldots, \infty$ is the input of the kernels, and p is the kernel order, which is two in this study [35]. The kernel orders typically refer to kernel moments, which are non-zero values, while the odd moments of kernels are equal to zero. Kernels that display negativity within their interval of support are typically not classified as second-order. The beta kernels are probability density functions that are assessed within the closed interval $-1 \leq t \leq 1$. Certain kernel functions, including Uniform, Epanechnikov, Biweight, and Triweight kernels, have corresponding values of r ranging from 0 to 3. As r approaches infinity, the resulting kernel converges to that of the Gaussian kernel [36]. The Epanechnikov kernel, characterized by $r = 1$, is considered optimal for the AMISE because it produced the least value which is:

$$K_{[2,1]}(t) = \frac{3}{4}(1-t^2) \quad (7)$$

Other members corresponding to $r = 2, 3, 4$ called Biweight, Triweight, and Quadriweight kernels, are:

$$K_{[2,2]}(t) = \frac{15}{16}(1-t^2)^2 \quad (8)$$

$$K_{[2,3]}(t) = \frac{35}{32}(1-t^2)^3 \quad (9)$$

$$K_{[2,4]}(t) = \frac{315}{256}(1-t^2)^4 \quad (10)$$

However; as r approaches infinity, the resultant is the normal kernel function that is not exactly a member of this family, and it is expressed as:

$$K_{[2,\mathrm{Normal}]}(t) = \frac{1}{\sqrt{2\pi}}\, exp\left(-\frac{t^2}{2}\right) \quad (11)$$

The commonly used kernels from the beta family in KDE include Equations (7) to (9), along with the normal distribution function, classified not firmly belonging this group. Other members derived from this family are rarely used because those with higher powers tend to be less efficient. The efficiency of these kernels is evaluated using the Epanechnikov kernel (EK), the first member of this family, which is regarded as optimal in reference to AMISE. Generally, the efficiency of kernel functions besides Equations (7) to (9) decline as the index of the generated function increases. The optimum efficiency for the function is typically equal to one, whereas other functions usually exhibit efficiencies that are less than one, with numerical values progressively decreasing.

2.2. The New Beta Polynomial Family

The technique for the derivation of the new beta polynomial family (NBPF) is based on the modification of the additive construction approach. The modified additive construction rule is:

$$K_{[p,r]}(t) = \frac{3}{2}K_{[p,r]}(t) + \frac{1}{2}tK'_{[p,r+1]}(t) \quad (12)$$

where p is the kernel order and r denotes the argument of the kernel. On letting $r = r+1$ in Equation (6), we have Equation (13) given as:

$$K_{[p,r+1]}(t) = \frac{(2r+3)!}{2^{2r+3}[(r+1)!]^2}(1-t^2)^{r+1} \quad (13)$$

Again, taking the derivative of Equation (13) with respect to t, yields Equation (14), which is:

$$K'_{[p,r+1]}(t) = \frac{(2r+3)!}{2^{2r+3}[(r+1)!]^2}(r+1)(1-t^2)^r(-2t) \quad (14)$$

Furthermore, substituting Equation (6) and Equation (14) into Equation (12), we have:

$$K_{[p,r]}(t) = \frac{3}{2}\left[\frac{(2r+1)!}{2^{2r+1}(r!)^2}(1-t^2)^r\right] + \frac{1}{2}t\left[\frac{(2r+3)!}{2^{2r+3}[(r+1)!]^2}(r+1)(1-t^2)^r(-2t)\right] \quad (15)$$

Further simplification of Equation (15) results in the new second-order kernel, which is:

$$K_{[2,r]}(t) = \frac{1}{2}\left\{\left(\frac{(2r+1)!}{2^{2r+1}(r!)^2}(1-t^2)^r\right)\{3-(3+2r)t^2\}\right\} \quad (16)$$

The initial members of the newly proposed second-order kernels are:

$$K_{[2,1]}(t) = \frac{3}{8}(3-5t^2)(1-t^2) \quad (17)$$

$$K_{[2,2]}(t) = \frac{15}{32}(3-7t^2)(1-t^2)^2 \quad (18)$$

$$K_{[2,3]}(t) = \frac{35}{64}(3-9t^2)(1-t^2)^3 \quad (19)$$

$$K_{[2,4]}(t) = \frac{315}{512}(3 - 11t^2)(1 - t^2)^4 \quad (20)$$

Similarly, when r tends to infinity, the resulting normal kernel is:

$$K_{[2,\text{Normal}]}(t) = \frac{1}{2\sqrt{2\pi}}(1 - t^2)(3 - t^2)exp\left(-\frac{t^2}{2}\right) \quad (21)$$

The bandwidth of both the traditional and proposed kernels, as well as the AMISE, demonstrates comparable orders. However, the proposed kernels exhibit remarkable qualities that distinguish them in performance. The proposed kernels meet the criteria for second-order kernels in Equation (2). Again, the advantage of the proposed method over its classical counterpart is the possession of additional powers that resulted in a high degree of differentiability, which significantly enhances their performance in terms of AMISE and efficiency. Polynomial kernels are of broader uses due to their ability of handling data with nonlinearity characteristics in data analysis [37]. In classification and regression methodologies, the kernel approached has been widely applied as noted by Liu and Xie [38], while Ngu *et al*. [39] presented a detailed assessment of the applications of kernel functions particularly with emphasis on regression and classification in the framework of sensors.

2.3. The Efficiency of Kernel Function

Generally, kernel efficiency is often assessed in comparison with the Epanechnikov function. The kernel efficiency is derived from the established relationship defined as follows:

$$Eff(K) = \left(\frac{C(K_e)}{C(K)}\right)^{1/4} = \left(\frac{R(K_e)^4\mu_2(K_e)^2}{R(K)^4\mu_2(K)^2}\right)^{1/4} \quad (22)$$

Here $C(K) = R(K)^4\mu_2(K)^2$ denotes other kernel constants while $C(K_e) = R(K_e)^4\mu_2(K_e)^2$ is Epanechnikov kernel constant [36]. Equation (22) shows that determining the efficiency of a kernel function requires two key statistics: kernel roughness and kernel moment. The kernel roughness is defined by:

$$R(K) = \int K(t)^2 dt \quad (23)$$

Again, the kernel moment, commonly known as variance, is:

$$\mu_2(K) = \int t^2 K(t) dt \quad (24)$$

Typically, the AMISE optimum kernel of the proposed family is also Epanechnikov kernel (EK), as it yields a minimal value as the conventional kernels.

3. RESULTS AND DISCUSSION

To evaluate the effectiveness of the new beta kernel family, the study employed both simulated and real-world data. Application of the NBPF to real-world data of the old faithful geyser is done for practical implementation [2]. The achievement of NBPF was compared to that of BKF using AMISE as a performance metric. This metric provides a quantitative basis for measuring the accuracy and efficiency of the new kernel function. The numerical computations and the graphical analysis were performed using Mathematica version 12.3 software. This study examines the statistical properties of Epanechnikov, Biweight, Triweight, and Quadriweight kernels because they serve as foundational kernel members for a comprehensive discussion, particularly the optimum kernel function, in the evaluation of efficiencies of other functions within this family of kernels. The efficiency of kernels can be used as an assessment of their performance.

The efficiency values were calculated for both the NBPF and BKF kernels. The efficiencies of the NBPF and BKF kernels are presented in Table 1 with the results obtained being compared with EK as the optimum kernel. NBPF displayed superior efficiencies over BKF kernel family comparatively, demonstrating their dominance and effectiveness over the traditional BKF family. The noticeable improvement in efficiencies of the proposed NBPF kernels is ascribed to the degree of the constant of normalization as well as the functional modification incorporated into the NBPF family. The coefficient of any beta kernel is typically the normalization constant which contributes significantly to the performance and numerical values of the efficiency. The optimum kernel is the Epanechnikov function, hence its efficiency value is always one while other members of the traditional BKF kernels exhibited numerical values that are less than one as their efficiencies. Table 1 illustrates that as the power of the kernel increases, the efficiency of the proposed NBPF kernels also rises, in contrast to the decreasing efficiency observed in conventional BKF kernels. The enhanced efficiency of the NBPF

functions is linked to their larger normalization constants and the functional modifications, hence more effective than traditional BKF functions. Figures 1 and 2 are the graphical representations of the conventional BKF and newly introduced NBPF kernels, respectively. The plots of both NBPF and BKF were evaluated in a specified interval of $-1 \leq t \leq 1$. All beta polynomial kernels are typically analyzed within this interval, and statistical components such as kernel roughness and moment are numerically computed within this interval in the determination of bandwidths and kernel efficiency. The efficiency of the existing BKF is denoted by $Eff\,(K_{BKF})$ while the efficiency of NBPF is denoted by $Eff\,(K_{NBPK})$ in Table 1 respectively.

The AMISE of the simulated data of 6000 as the sample size for both BKF and NBPF is presented in Table 2. The results in Table 2, in terms of AMISE as a metric of performance, suggested that the NBPF kernels are more effective than BKF. An increase in kernels' power leads to graphs with narrower peaks, as shown in Figures 1 and 2, and both plots illustrate the characteristics of the conventional BKF and proposed NBPF kernel functions regarding peakedness. The estimates derived from the traditional BKF Epanechnikov function and Biweight kernel are classified as platykurtic, as they exhibit a wider peak. In contrast, the newly introduced NBPF exhibit leptokurtic behaviour, especially at higher powers with more acute peaks. The level of differentiability of the kernel serves as the primary factor in determining the peakedness of the kernel, as illustrated in graphs featuring higher-degree polynomials in Figure 2 of the NBPF. Kernel functions characterized by higher degrees possess more derivatives and substantial normalization constants, which typically result in graphs that exhibit acute peaks with enhanced quality kernel estimates.

One of the main applications of kernel density estimation is the exploration of obscured or hidden features in a dataset [40]. Statistical properties such as skewness and modes in a dataset are easily revealed by KDE while in some cases, KDE do provide invaluable insights that would give essential information for additional investigation. The identification of the underlying statistical properties of a dataset through a smooth curve of the data is a fundamental role of KDE, and this is vital in understanding the intrinsic nature of the observations, thereby providing information for making decisions. This study investigated the Old Faithful Geyser data which comprises 107 observations with emphasis on the durations of

Table 1. Traditional BKF efficiencies and proposed NBPF efficiencies.

Kernel Functions $K(t)$	**Traditional BKF**			**Proposed NBPK**		
	$R(K)$	$\mu_2(K)$	$Eff(K_{BKF})$	$R(K)$	$\mu_2(K)$	$Eff(K_{NBPK})$
Epanechnikov	$\frac{3}{5}$	$\frac{1}{5}$	1.000	$\frac{31}{35}$	$\frac{3}{35}$	1.000
Biweight	$\frac{5}{7}$	$\frac{1}{7}$	0.994	$\frac{1110}{1001}$	$\frac{1}{21}$	1.072
Triweight	$\frac{350}{429}$	$\frac{1}{9}$	0.987	$\frac{3150}{2450}$	$\frac{1}{33}$	1.159
Quadriweight	$\frac{2205}{2431}$	$\frac{1}{11}$	0.981	$\frac{67410}{46189}$	$\frac{3}{143}$	1.227

Table 2. AMISE and efficiencies of BKF with NBPF using a sample size of 6000.

Kernel Functions	**AMISE of BKF**	$Eff(K_{BKF})$	**AMISE of NBPF**	$Eff(K_{NBPK})$
Epanechnikov	0.000559711	1.000	0.000264222	1.000
Biweight	0.000776042	0.994	0.000294581	1.072
Triweight	0.000852696	0.987	0.000323289	1.159
Quadriweight	0.000952354	0.981	0.000353209	1.227

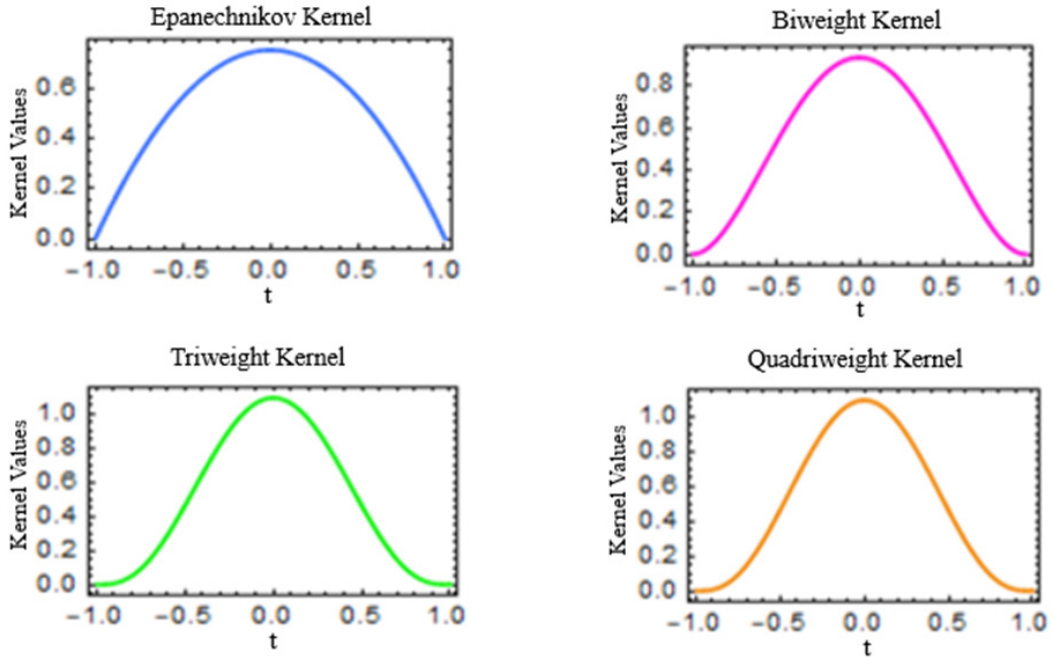

Fig. 1. The plots of traditional (BKF) second order beta kernel family.

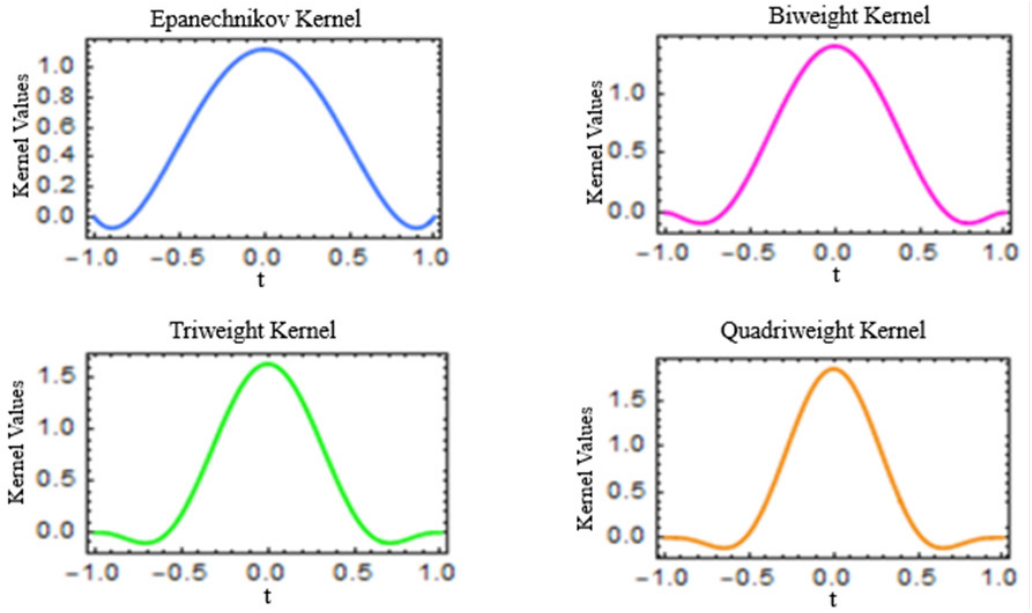

Fig. 2. The plots of proposed (NBPF) second order beta kernel family.

eruption in minutes [2]. The kernel estimates of the real data as seen in both the BKF and NBPF demonstrate bimodality as presented in Figures 3 and 4 by Epanechnikov kernel (EK) and Biweight kernel (BK), respectively. The results reveal that there are two unique clusters in times of eruption with focus at 1.9 minutes and 4.5 minutes, respectively. This bimodal characteristic implies that the duration of the eruption can be influenced by several indispensable factors.

The visualization of the data using the KDE approach has established its usefulness in capturing features in the data with the bimodality being evidenced. The bandwidth employed in constructing the kernel estimates of the BKF and NBPF in Figures 3 and 4 is obtained by standardization of the data, and the bandwidth is 0.437. The bimodality of the real data as evidenced in Figures 3 and 4 which are estimates of BKF and NBPF is a validation of the proposed NBPF functions in preservation of

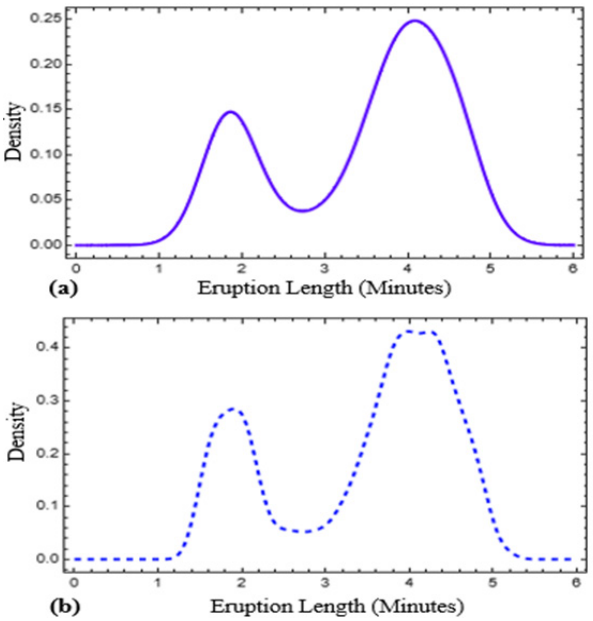

Fig. 3. The plots of real data of EK **(a)** BKF and **(b)** NBPF.

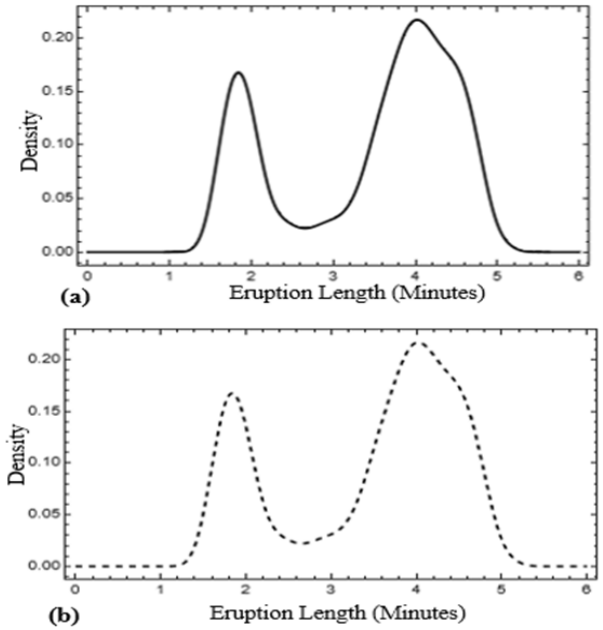

Fig. 4. The plots of real data of BK **(a)** and BKF **(b)** NBPF.

vital statistical characteristics. The estimates of the proposed NBPF of Epanechnikov and Biweight kernels exhibit similarity but the traditional BKF Biweight estimate display a sharp presentation of the modes. The retention of inherent features of a dataset is essentially based on the appropriate selection of the bandwidth as well as the kernel function. The vital responsibility of revealing inherent statistical features in a dataset has been corroborated by the proposed NBPF functions.

4. CONCLUSIONS

The proposed kernel family are versatile in density estimation, effective in data analysis as authenticated by the AMISE, and superior efficiency values. The versatility of the proposed kernels is particularly noticeable in the AMISE as well as the efficiencies. The incorporation of the functional form gives high level of smoothness that guaranteed their wide applicability across the spectrum of many statistical fields. Selection of kernel function typically depends on level of smoothness of its estimates, and the degree of differentiability of the function. Kernel functions with higher degree usually generate smoother estimates because they can be differentiated continuously, while noisier estimates are often produced by kernels with lower degrees of differentiability. The outcomes of the research show that NBPFs outplay BKFs with reference to AMISE and efficiency. The improvement in performance of both AMISE and efficiency of the new kernel family is attributed to the magnitude of the coefficients of the kernel functions and the structural modification of the functional form.

5. CONFLICTS OF INTEREST

The authors declare no conflict of interest.

6. ETHICAL STATEMENT

This work does not include any studies involving human or animal subjects.

7. FUNDING

No funding was received for this work.

8. AUTHORSHIP CONTRIBUTION

All authors equally contributed in this study.

9. DECLARATION

All authors declare the originality of results and copyright are assigned to the Pakistan Academy of Sciences.

10. REFERENCES

1. S.J. Sheather. Density estimation. *Statistical Science* 19(4): 588-597 (2004). https://www.jstor.org/stable/4144429

2. B.W. Silverman (Ed.). Density estimation for statistics and data analysis. *Routledge, NY, USA* (2018). https://doi.org/10.1201/9781315140919
3. I.U. Siloko, K.E. Ukhurebor, E.A. Siloko, E. Enoyoze, A.O. Bobadoye, C.C. Ishiekwene, O.O. Uddin, and W. Nwankwo. Effects of some meteorological variables on cassava production in Edo State, Nigeria via density estimation. *Scientific Africa* 13: e00852 (2019). doi:10.1016/j.sciaf.2021.e00852
4. P. Janssen, J. Swanepoel, and N. Veraverbeke. A note on the behaviour of a kernel-smoothed kernel density estimator. *Statistics and Probability Letters* 158: 108663 (2019). doi:10.1016/j.spl.2019.108663
5. B. Bèranger, T. Duong, S.E. Perkins-Kirkpatrick, and S.A. Sisson. Tail density estimation for exploratory data analysis using kernel methods. *Journal of Nonparametric Statistics* 31(1): 144-174 (2018). doi:10.1080/10485252.2018.1537442
6. I.U. Siloko and O.O. Uddin. A statistical study of wind speed and its connectivity with relative humidity and temperature in Ughelli, Delta State, Nigeria. *Science World Journal* 18(3): 404-413 (2023). https://dx.doi.org/10.4314/swj.v18i3.13
7. J.C.Y. Ngu, W.S. Yeo, T.F. Thien, and J. Nandong. A comprehensive overview of the applications of kernel functions and data-driven models in regression and classification tasks in the context of software sensors. *Applied Soft Computing Journal* 164: 111975 (2024). doi:10.1016/j.asoc.2024.111975
8. D. Baranyai and T. Sipos. Black-spot analysis in Hungary based on kernel density estimation. *Sustainability* 14(14): 8335 (2022). doi:10.3390/su14148335
9. J.E. Chacón and T. Duong. Data-driven density derivative estimation, with applications to nonparametric clustering and bump hunting. *Electronic Journal of Statistics* 7: 499-532 (2013). doi:10.1214/13-EJS781
10. J. Rosenberger, J. Müller, A. Selig, M. Bühren, and D. Schramm. Extended kernel density estimation for anomaly detection in streaming data. *15th CIRP Conference on Intelligent Computation in Manufacturing Engineering, Gulf of Naples, Italy, Procedia CIRP* 112: 156-161 (2022). doi:10.1016/j.procir.2022.09.065
11. G. Aarthi, S. Sharon-Priya, and A.W. Banu. KRF-AD: Innovating anomaly detection with KDE-KL and random forest fusion. *Intelligent Decision Technologies* 18(3): 2275-2287 (2024). doi:10.3233/IDT-240628
12. S. Wang, A. Li, K. Wen, and X. Wu. Robust kernels for kernel density estimation. *Economics Letters* 191: 109138 (2020). doi:10.1016/j.econlet.2020.109138
13. Y. Fan and X. Cheng. Application of kernel density estimation in stock trading volume distribution. *Proceedings of Artificial Intelligence of Things and Computing, Hangzhou Jiangsu, China* pp. 173-180 (2024). doi:10.1145/3708282.3708314
14. L. Srikanth and I. Srikanth. A case study on kernel density estimation and hotspot analysis methods in traffic safety management. 2020 International Conference on Communication Systems & Networks (COMSNETS). *Bengaluru, India* pp. 99-104 (2020). doi:10.1109/COMSNETS48256.2020.9027448
15. J.H. Tuya, U.M. Coalee, and R. Ahmed. Potentiality of kernel density estimation tool for tropical cyclone frequency analysis in Bangladesh. *The Jahangirnagar Review: Part II: Social Science* 48(1): 87-105 (2024).
16. S. Lasocki. Kernel density estimation in seismology. In: Statistical Methods and Modeling of Seismogenesis. 1st Edition. N. Limnios, E. Papadimitriou, and G. Tsaklidis (Eds.). *Wiley Online Library, New Jersey, United States* pp. 1-25 (2021). doi:10.1002/9781119825050.ch1
17. A.M. Pollard, Q. Ma, A.I. Bidegaray, and R. Liu. The use of kernel density estimates on chemical and isotopic data in Archaeology. In: Handbook of Archaeological Sciences. 2nd Edition. A.M. Pollard, R.A. Armitage, and C.A. Makarewicz (Eds.). *John Wiley & Sons, New Jersey, United States* pp. 1227 (2023). doi:10.1002/9781119592112.ch61
18. S. Hashimoto, S. Yoshiki, R. Saeki, Y. Mimura, R. Ando, and S. Nanba. Development and application of traffic accident density estimation models using kernel density estimation. *Journal of Traffic and Transportation Engineering* 3(3): 262-270 (2016). https://doi.org/10.1016/j.jtte.2016.01.005
19. M. Govorov, G. Beconyte, and G. Gienko. Trivariate kernel density estimation of spatiotemporal crime events with case study for Lithuania. *Sustainability* 15(11): 8524 (2023). doi:10.3390/su15118524
20. A.C. Neto, A.L.M. Levada, and M.F.C. Haddad. A new kernel density estimation-based entropic isometric feature mapping for unsupervised metric learning. *Annals of Data Science* 12(3): 929-945 (2024). doi:10.1007/s40745-024-00548-x
21. Y. Tsuruta and M. Sagae. Theoretical properties of bandwidth selectors for kernel density estimation

on the circle. *Annals of the Institute of Statistical Mathematics* 72: 511-530 (2020). doi:10.1007/s10463-018-0701-x

22. I.U. Siloko, O. Ikpotokin, F.O. Oyegue, C.C. Ishiekwene, B.A.E. Afere. A note on application of kernel derivatives in density estimation with the univariate case. *Journal of Statistics and Management Systems* 22(3): 415-423 (2019). doi.org/10.1080/09720510.2018.1524956
23. I.U. Siloko, E.A. Siloko, S.A. Ojobor, S.A. Wasan, E. Enoyoze, C.C. Ishiekwene, O. Ikpotokin, and E.M. Ogbeide. A new multivariate product kernel function of the beta polynomial family. *Journal of Statistics Applications and Probability* 12(3): 1385-1398 (2023). http://dx.doi.org/10.18576/jsap/120340
24. M.P. Wand and M.C. Jones (Eds.). Kernel Smoothing. *Chapman and Hall, London, UK* (1995). http://dx.doi.org/10.1007/978-1-4899-4493-1
25. D.W. Scott (Ed.). Multivariate density estimation. Theory, practice, and visualization. 2nd Edition. *Wiley, New Jersey*, *USA* (2015). https://doi.org/10.1002/9781118575574
26. S.M. Somé and C.C. Kokonendji. Bayesian selector of adaptive bandwidth for multivariate gamma kernel estimator on $[0,\infty)^d$. *Journal of Applied Statistics* 49(7): 1692-1713 (2022). doi:10.1080/02664763.2021.1881456
27. S. Zámečník, I. Horová, S. Katina, and K. Hasilová. An adaptive method for bandwidth selection in circular kernel density estimation. *Computational Statistics* 39: 1709-1728 (2023). https://doi.org/10.1007/s00180-023-01401-0
28. I. Fuentes-Santos, W. González-Manteiga, and J. Mateu. Bootstrap bandwidth selection for the pair correlation function of inhomogeneous spatial point processes. *Journal of Statistical Computation and Simulation* 93(18): 3329-3361 (2023). https://doi.org/10.1080/00949655.2023.2220860
29. M. Rosenblatt. Remarks on some nonparametric estimates of a density function. *Annals of Mathematical Statistics* 27: 832-837 (1956). http://dx.doi.org/10.1214/aoms/1177728190
30. E. Parzen. On the estimation of a probability density function and the mode. *Annals of Mathematical Statistics* 33: 1065-1076 (1962). http://dx.doi.org/10.1214/aoms/1177704472
31. I.U. Siloko and E.A. Siloko. An investigation on interdependence between rainfall and temperature in Ekpoma, Edo State, Nigeria. *Iranian (Iranica) Journal of Energy and Environment* 14 (3): 197-204 (2023). https://doi.org/10.5829/ijee.2023.14.03.01
32. I.U. Siloko, C.C. Ishiekwene, and F.O. Oyegue. New gradient methods for bandwidth selection in bivariate kernel density estimation. *Journal of Mathematics and Statistics* 6(1): 1-8 (2018). http://dx.doi.org/10.13189/ms.2018.060101
33. I.U. Siloko, O. Ikpotokin, and E.A. Siloko. On hybridizations of fourth-order kernel of the beta polynomial family. *Pakistan Journal of Statistics and Operations Research* 15(3): 819-829 (2019). doi:10.18187/pjsor.v15i3.2625
34. N. Gündüz and S. Karakoç. Optimal bandwidth selection methods with application to wind speed distribution. *Mathematics* 11(21): 4478 (2023). doi:10.3390/math11214478
35. T. Duong. Spherically symmetric multivariate beta family kernels. *Statistics and Probability Letters* 104: 141-145 (2015). http://dx.doi.org/10.1016/j.spl.2015.05.012
36. I.U. Siloko, O. Ikpotokin, F.O. Oyegue, E.A. Siloko, and C.C. Ishiekwene. Numerical computation of efficiency of beta polynomial kernels using product method. *Journal of Applied Science and Technology* 23 (1&2): 32-38 (2019). https://www.ajol.info/index.php/jast/article/view/192584
37. K. Haddad and A. Rahman. Regional flood frequency analysis: evaluation of regions in cluster space using support vector regression. *Natural Hazards* 102: 489-517 (2020). https://doi.org/10.1007/s11069-020-03935-8
38. Y. Liu and M. Xie. Rebooting data-driven soft-sensors in process industries: a review of kernel methods. *Journal of Process Control* 89: 58-73 (2020). https://doi.org/10.1016/j.jprocont.2020.03.012
39. J.C.Y. Ngu, W.S. Yeo, T.F. Thien, and J. Nandong. A comprehensive overview of the applications of kernel functions and data-driven models in regression and classification tasks in the context of software sensors. *Applied Soft Computing Journal* 164: 111975 (2024). https://doi.org/10.1016/j.asoc.2024.111975
40. I.U. Siloko, K.E. Ukhurebor, and A.I. Otsupius. Non-parametric statistical approach for assessing the environmental impacts of petroleum spillages in the Niger Delta region of Nigeria. *Discover Environment* 3: 173 (2025). doi.org/10.1007/s44274-025-00273-z

Proceedings of the Pakistan Academy of Sciences: A Physical and Computational Sciences 63(1): 71-81 (2026)

ISSN (Print): 2518-4245; ISSN (Online): 2518-4253
http://doi.org/10.53560/PPASA(63-1)711

Pakistan Academy of Sciences

Research Article

A Small-Scale Comparative Evaluation of ChatGPT-3.5 and Google Translate for English-Urdu and Urdu-English Translation

Aatka Faryal Riaz[1*], Rafay Azmat[2], and Rubeka Sehar[3]

[1]Department of Computer Science, International University of Applied Science, Bad Honnef, Germany

[2]Department of Electronics Engineering, Mehran University of Engineering & Technology, Jamshoro, Pakistan

[3]ICT Department, University of Sindh, Jamshoro, Pakistan

Abstract: Today, technologies like ChatGPT and Google Translate are utilized for translating text and enabling smooth exchange of information. Urdu is the national language of Pakistan, while English serves as the official language and the primary medium of communication in schools and workplaces. Since people commonly speak Urdu, they often use machine translators for English to Urdu and Urdu to English translation. These machine translators can produce translations with a diverse vocabulary but sometimes their translations are not contextually correct or fully reliable. Therefore, it is essential to evaluate the translation outputs of the machine translators. The prime objective of this paper is to compare the performance of machine translation systems at the paragraph level, enabling users to identify the most effective one. In this research, Google Translate and ChatGPT-3.5 were used as translation tools to translate text between English and Urdu in both directions. The texts were selected from different categories, such as historical texts, poetry, literary works, novels, and legal documents. The machine translation systems translated English text into Urdu, and the generated outputs were compared and assessed by authors. Similarly, Urdu text was translated into English, and the resulting translations were compared and assessed by authors. We assessed and compared the translated outputs based on phrasing style, linguistic accuracy, and contextual meaning. To ensure a reliable comparison, we calculated the BiLingual Evaluation Understudy (BLEU) and Metric for Evaluation of Translation with Explicit ORdering (METEOR) scores of the translations generated by these translation tools. Based on our analysis and BLEU and METEOR scores, we concluded that the performance of ChatGPT-3.5 is better than Google Translate.

Keywords: Machine Translators, Chat GPT, Google Translate, English-Urdu Language, Urdu-English Language, Evaluation Metrics, BLEU, METEOR.

1. INTRODUCTION

Pakistan is a multilingual country where numerous languages are spoken as native tongues. Urdu is the national language of Pakistan, and the official language of Pakistan is English. According to Ethnologue [1], Urdu ranks as the eleventh most extensively spoken language globally, with a total of 246 million speakers including those who use it as a secondary language and approximately 1.5 billion people around the world speak English. According to international center for language studies [2], even though English is the most widely spoken language globally, only 25% are native speakers, while the rest have acquired it as a second language. Almost all online media is in English, with over half of all websites (52.1%) using it for their content.

As English is the official language, and school textbooks are written in English. However, since students primarily speak Urdu, they often rely on machine translators to write essays or assignments in English language. They also frequently use these tools to comprehend English-language content.

Received: December 2025; Revised: February 2026; Accepted: March 2026
* Corresponding Author: Aatka Faryal Riaz <aatkafaryal@gmail.com >

To gain a deeper understanding, they translate entire paragraphs rather than isolated sentences. This research evaluates the accuracy of machine translators at the paragraph level, as opposed to single-sentence translations, to better reflect the above requirement. Moreover, nowadays people from Pakistan are relocating and migrating to other countries for their jobs and business. Students are travelling to other countries for their studies. They are required to understand and communicate in different languages, so they have to use translators. Owing to the need for instant translations, they use machine translators for effective exchange of information. The translation generated by these machine translators is of high quality and employs diverse synonyms; however, it is not always correct and dependable. There is a need to assess the accuracy of their generated translations. Once users are aware of the accuracy levels, it will be easy for them to choose the most reliable translator.

This research aims to conduct a comparative evaluation of the translation outputs produced by ChatGPT-3.5 and Google Translate to help people to select the best one. The ChatGPT-3.5 model and Google Translate were used in this research. We opted for ChatGPT due to the significant attention it has recently received, while Google Translate was chosen because of its widespread popularity. To evaluate we gave a set of English paragraphs as input to these translators and compare the quality of their outputs (i.e., Urdu translations) using evaluation metric BiLingual Evaluation Understudy (BLEU) and Metric for Evaluation of Translation with Explicit Ordering (METEOR). Similarly, we checked their performance for Urdu to English translation. In literature, most of the research to evaluate the performance of machine translators has focused on using sentences rather than paragraphs. For example, Malik and Habib [3] used seven different sentences, not paragraphs, to assess machine translators in their study. Similarly, Ghassemiazghandi [4] evaluated ChatGPT's performance for Persian-to-English translation using sentence-level assessment. In this study, we mainly focused on using paragraphs instead of individual sentences. We conducted a comparative evaluation of translations produced by ChatGPT-3.5 and Google Translate with respect to contextual relevance, phrasing style, and word choice using expert human translations as a benchmark. To validate our analysis, we also calculated the BLEU and METEOR scores of each generated translation to determine which system performed better. To the best of our knowledge, this work is unique in evaluating and comparing the translation quality of paragraphs rather than individual sentences for English to Urdu and Urdu to English translations.

2. MATERIALS AND METHODS

We used ChatGPT and Google Translate in this research. These state-of-the-art technologies are described in this section.

2.1. ChatGPT

According to Biswas [5], due to the fast progress in the field of Artificial Intelligence (AI) and Natural Language Processing (NLP), highly sophisticated language models have been developed, such as ChatGPT, which is a large language model developed by OpenAI. This model employs deep learning techniques to interpret and generate text that is very similar to the human communication. ChatGPT is built using transformer architecture, which enables it to produce responses in a conversational manner. As it can produce text in a human style, it holds significant potential to impact areas such as healthcare, research, and language translation, as explained by Biswas [6].

2.1.1. A transformer-based architecture

ChatGPT (Generative Pretrained Transformer) was created to overcome the constraints of previous language processing techniques, such as Recurrent Neural Networks (RNNs) and Convolutional Neural Networks (CNNs), as discussed by Ray [7]. ChatGPT utilizes transformer models, which allow it to recognize patterns and grammatical structures of languages. The transformer is a neural network framework that employs a self-attention mechanism. This architecture has two principal advantages. First, it is highly effective at applying context in language processing tasks. For example, when a sentence is processed, the meaning of a word or phrase may vary considerably depending on its context, which can be difficult to capture by using only conventional grammatical rules because it also relies on the functional relationships between the words. The self-attention mechanism in the transformer, however, enables the model to incorporate contextual information in a data-

driven manner. Second, the transformers permit substantial parallelization and can attain cutting-edge translation accuracy after just 3.5 days of training on eight GPUs, as investigated by Vaswani *et al.* [8].

2.1.2. How ChatGPT is trained

ChatGPT is trained on massive volumes of text data, including web content, articles, and books, enabling it to generate grammatically correct and contextually appropriate output. A brief overview of ChatGPT's training process is presented here. According to Memon [9], the model's training occurs in the following three stages.

1. Generative Pre-Training
2. Supervised Fine-Tuning (SFT)
3. Reinforcement Learning through Human Feedback (RLHF)

Stage 1: Generative Pre-Training

At the first stage, the model is trained on a vast collection of textual data gathered from across the internet, including content from books, magazines, articles, and other sources. The dataset covers a wide range of genres and subjects, enabling the model to produce text in diverse linguistic forms and contextual backgrounds. Stage 1 equips the model with general language capabilities such as summarizing text, completing sentences, translating content, and analyzing sentiment, but it is not specialized in doing a particular task. For instance, the model performs well in summarizing lengthy articles into concise versions. However, at this stage, it cannot engage in topic-specific conversations with humans, even though it excels in general language processing.

Stage 2: Supervised Fine-Tuning

Supervised Fine-Tuning (SFT) represents the 2nd stage of ChatGPT's training. In this phase, the model is trained to perform specific tasks, such as engaging in conversational dialogue. Until this point, ChatGPT's knowledge is only limited to the data on which it has been trained. You can think of it as having a small snapshot of the world in its "brain." So, if you ask it something outside of what it has learned, it may give a wrong or any unpredictable answer.

Stage 3: Reinforcement Learning through Human Feedback (RLHF)

This is the third stage of training. In this stage, the model undergoes additional training to respond to queries it was not explicitly taught. This stage uses reinforcement learning, where the model is guided by a reward system and receives feedback from humans to improve its responses. During the third stage of training, a human agent was also involved to guide the process of reinforcement learning. This is why it is referred to as Reinforcement Learning with Human Feedback (RLHF).

2.1.3. How ChatGPT performs language translation

ChatGPT is not intended solely for translation, but its ability to follow complicated instructions makes it a valuable tool for translation, as noted by Siu [10]. ChatGPT can facilitate seamless interaction between people communicating in different languages. For example, if a user's primary language is Urdu, he can enter text in Urdu, and ChatGPT will generate an immediate translation in the target language. Below is a concise description of ChatGPT's translation process.

As described earlier, the training of ChatGPT consists of three stages. The pre-training and fine-tuning phases equip the model with language translation abilities. In the pre-training phase, the model learns from a large collection of multilingual data, which helps it to understand general linguistic patterns. Then, in the fine-tuning stage, ChatGPT is trained using aligned sentence pairs in different languages, such as English and Urdu, to perform specific translation tasks. The model then learns to generates translations by predicting the most appropriate output sentence based on the input. While its translations are generally accurate, it occasionally struggles with complex texts, such as literary content.

2.2. Google Translate

Google Translate is a machine translation service which is developed by Google to provide translations between different languages. It enables direct translation of text from one language to another, as discussed by Boitet *et al.* [11]. As of 2022, Google Translate provided a free automated

translation service for 133 languages [12], including Urdu. The translation service uses Neural Machine Translation (NMT) framework. Furthermore, it is widely used, with over 500 million daily users and approximately 100 billion words translated each day [13]. The widespread use of Google Translate has led to a decline in the use of traditional digital dictionaries, the researchers who study English as a Foreign Language (EFL) course at a Chilean high school suggested to employ Google Translate to assist students in enhancing their syntax and grammar, as discussed by Chang *et al.* [14]. Similarly, Tsai's study [15] also emphasized the effectiveness of Google Translate in reducing typing errors and producing longer texts.

2.2.1. Google translate architecture

As explained by King [16], Google Translate's translation system processes information in a manner similar to the human brain: it ingests data, encodes it, situates it within a context, and then re-encodes it to produce an output. The Google's Neural Machine Translation (GNMT) system architecture includes an encoder, a decoder, and an attention mechanism. In the encoder, the bottom layer operates bidirectionally, with the green nodes processing words from right to left and the pink nodes processing words from left to right. To accelerate training, the model is distributed across multiple GPUs. The system has eight Long Short-Term Memory (LSTM) layers each in the encoder and decoder, as illustrated in Figure 1 by Wu *et al.* [17].

2.2.2. Working principle of Google Neural Machine Translation

The Google's Neural Machine Translation (GNMT) system uses its encoder, decoder, and attention module to perform language translation. For example, translating a sentence from English to Urdu involves the following steps, as illustrated in Figure 2.

1. The English sentence is fed into the encoder, where it is converted into a fixed-length vector that can only be understood by a computer.
2. Then the attention mechanism then determines which English words should be assigned greater weight to produce the corresponding Urdu words.
3. Finally, the decoder generates the Urdu translation one word at a time, by focusing its attention on the words determined by the attention mechanism.

2.3. Research Methodology

For the present study, we selected 14 different paragraphs and 2 idiomatic sentences to assess and compare the accuracy of translation of ChatGPT and Google Translate. In order to generalize the results, we selected paragraphs from different genres, for instance, historical texts, poetry, literary and religious writings, and legal texts. Each paragraph consists of approximately 3 to 4 sentences. We took texts from history, poetry, novels, and literature because English in these genres is often complex.

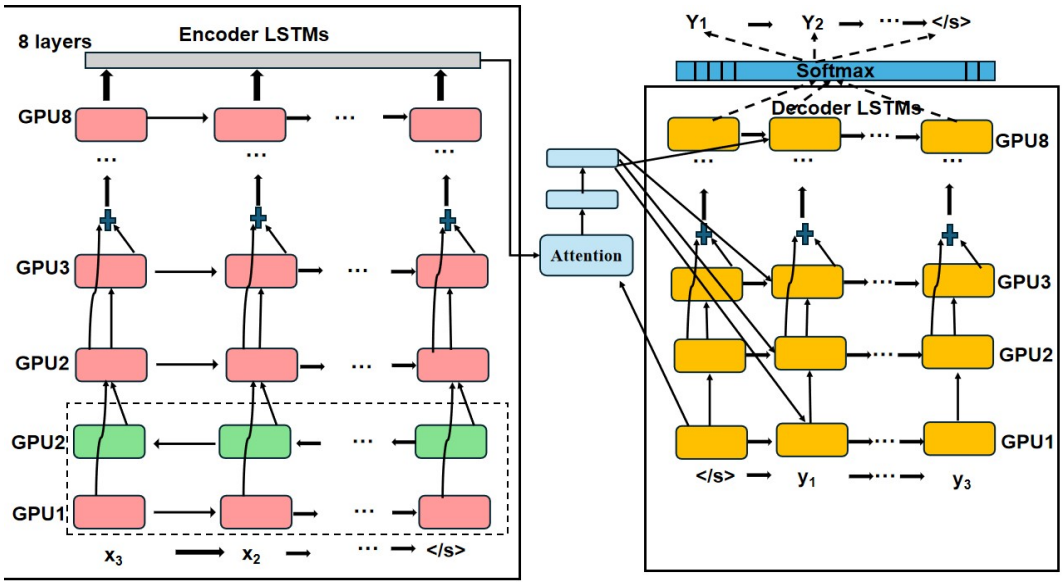

Fig. 1. Model architecture of Google Translate.

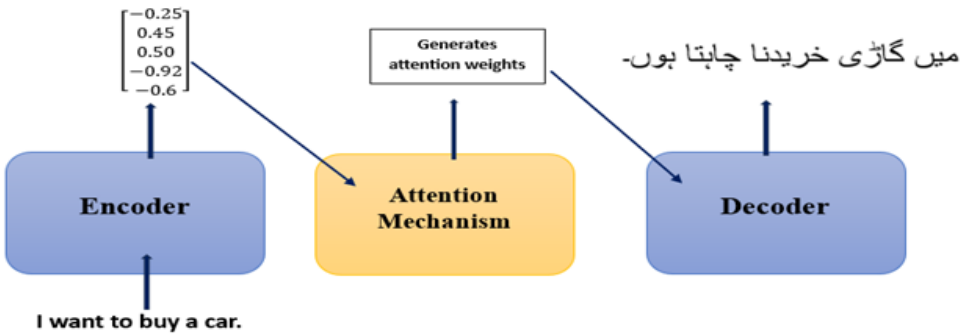

Fig. 2. The language translation process of the Google Translate.

In contrast, we selected texts from articles, textbooks, and newspapers because they usually contain simpler language. All texts have been collected from reliable sources such as textbooks (e.g., Punjab Textbook Board), published novels, and newspaper articles. Although these machine translators can translate English language into several other languages, but we mainly focused on English and Urdu languages because of the large number of English language users in Pakistan who rely on these tools for various purposes.

The methodology used in this research is illustrated in Figure 3. English text was input into ChatGPT-3.5 and Google Translate to obtain Urdu translations. The BLEU and METEOR scores were calculated for each translation. The authors then assessed the accuracy of generated translations with respect to context, selection of words, and phrasing style, in comparison with professional human translations and compared the BLEU and METEOR scores to determine which system performed better. The same approach was applied to assess the accuracy of Urdu-to-English translations. We translated each paragraph multiple times with both ChatGPT-3.5 and Google Translate and used the more accurate translation for analysis.

2.4. Dataset

The dataset consists of 14 different paragraphs and 2 idiomatic sentences. These paragraphs were selected from various genres, such as history, poetry, etc. We also included human translations for each paragraph to use as reference texts for evaluating the translation quality of machine translation outputs and for calculating BLEU and METEOR scores. These human translations were carefully prepared by professional translators who are proficient in the target language.

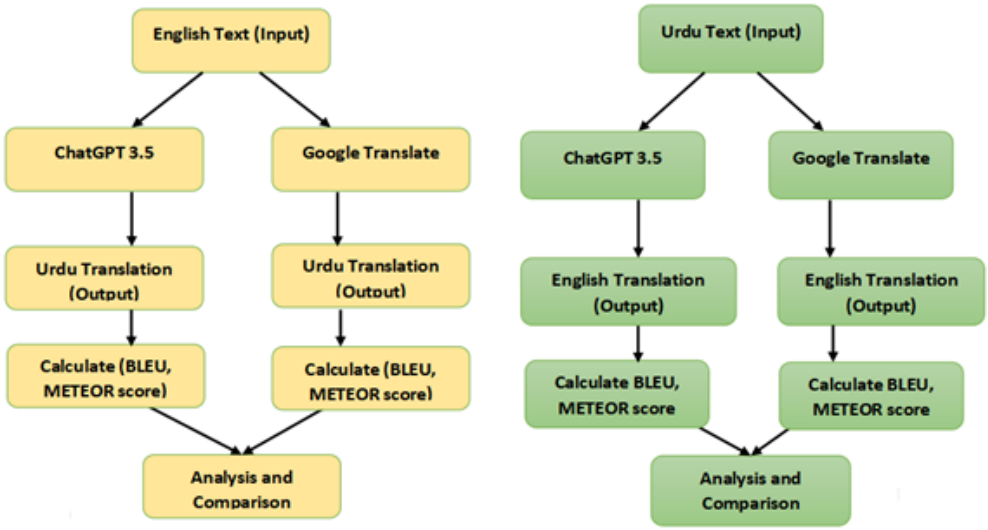

Fig. 3. Layout of the research methodology.

2.5. Performance Metric

As we are assessing the translations of paragraphs which consist of several lines. In addition to human observation, we incorporated an automatic evaluation method to enhance the credibility and reliability of machine translation assessment. Specifically, we used BLEU and METEOR as an evaluation metric to compare the accuracy of machine translators for English to Urdu translation and vice versa. According to the rule, the machine translator that achieved higher METEOR and BLEU score will be considered more accurate. This is the essence of the evaluation of machine translators.

2.5.1. BLEU

BLEU stands for BiLingual Evaluation Understudy. The BLEU is an algorithm to assess the quality of translated text that is translated from one natural language to another. According to Papineni *et al.* [18], the core idea behind BLEU is the quality of the translation increases when it looks more similar to the professional human translation. The output value of BLEU always lies between 0 and 1. This value indicates the degree of similarity between the reference translation (i.e., human translation) and candidate sentences (i.e., machine translator output). The machine translation that exhibits a higher resemblance to the reference translation got value closer to 1. A higher BLEU score shows better quality of machine translation system as described by Ayesha *et al.* [19].

2.5.1.1. N-grams in bleu score:

To calculate the BLEU score we used NLTK (Natural Language Toolkit), a popular open-source library for Natural Language Processing (NLP) in Python, which allows to set the value of n-grams in the calculation of the BLEU score. Here 'n' is the set of consecutive words in a sentence. We can have n-grams as unigram (1-gram), bigram (2-gram), and trigram (3-gram) depending on the length of sentence. For example, for a sentence **"The water is colorless"**, we can have n-grams as:

- **1-gram (unigram):** The unigram approach focuses only on individual word matches during comparison between the machine translation and human translation, e.g., "The", "water", "is", "colorless".
- **2-gram (bigram):** The bigram approach considers matches of two consecutive words during comparison between the machine translation and human translation, for example, "The water", "water is", "is colorless".
- **3-gram (trigram):** The trigram approach considers matches of three consecutive words during comparison between the machine translation and human translation, for example, "The water is", "water is colorless".
- **4-gram:** The 4-gram approach considers matches of four consecutive words, for example, "The water is colorless".

2.5.1.2. How bleu score is calculated:

BLEU uses a modified form of precision to measure how closely the predicted text matches the reference text. The BLEU precision score can be determined using the following formula,

$P = m_{max}/W_t$

Where P is precision value of BLEU, m_{max} is the number of words found similar in reference sentence and predicted text and W_t is total number of words in predicted sentence.

To explain how BLEU score is calculated assume two sentences. A predicted text generated by a machine translator and a reference text which is a human translated text.

- **Reference Text**: Our guest arrived late because it was raining
- **Predicted Text**: Our guest arrived late because of the rain

The unigram calculation focuses on individual word match. In the following example, out of 8 words in the predicted text 5 words are correctly matched with the reference text. So, the total similar words (m_{max}) between predicted sentence and reference sentences are 5, and the number of words in predicted sentence (W_t) is 8. Thus, using the BLUE formula gives us the precision value of 0.625 for this predicted sentence.

Example:

Here in our code, we used a unigram and bigram approach with smoothing function to get a more reliable BLEU score when the predicted text of a machine translator is short or has missing n-grams.

2.5.2. Meteor

METEOR stands for Metric for Evaluation of Translation with Explicit ORdering, is a metric used to measure the quality of translation generated by machine translators. The METEOR was developed at the Carnegie Mellon University, Pittsburgh, USA as described by Banerjee and Lavie [20]. Unlike BLEU, which primarily focuses on Precision, the METEOR is the more balanced approach as it considers both PRECISION AND RECALL. Recall evaluates how effectively the candidate translation includes all the words or information from the reference translation. This comprehensive approach enables METEOR to offer a more well-rounded assessment of translation quality.

One of the key strengths of the METEOR score is its ability to look beyond exact word matches. It includes stemming, which simplifies words to their base forms (e.g., "clapping" becomes "clap"), and synonym recognition (e.g., "quick" and "fast"), which treats similar words as valid matches. This helps METEOR better handle differences in language, such as varying word forms or different ways of saying the same thing. Assume the following reference translation **Our guest arrived late because it was raining** and candidate translation **Our guest came late because of the rain**.

- **Exact Match: "**Our", "guest", "late", "because"
- **Stemming: "**raining" and "rain"
- **Synonym:** "arrived" and "came"

The METEOR aligns these matches and then calculates the score that reflects the quality of translation. We calculated the METEOR score by using Natural Language Toolkit (NLTK), a popular open-source library for Natural Language Processing (NLP) in Python.

3. RESULTS AND DISCUSSION

As we discussed, we used different types of paragraphs in this research to assess the translation quality of machine translation systems. In this section, we included one example of Urdu to English translation and one example of English to Urdu translation in tabular form (other examples are given in supplementary file, Tables S1-S14). Each table presents the selected text in its original form, the translation generated by ChatGPT, the translation produced by Google Translate, BLEU and METEOR scores of both machines, and the translation by a professional human. In this section we presented our analysis and comparison about the accuracy of translations generated by ChatGPT-3.5 and Google Translate. We also validate our analysis with the help of the BLEU and METEOR score of both translators.

The text presented in Table 1 is an example of Urdu to English translation taken from the Pakistan studies book of Punjab textbook board [21]. According to our analysis the translation generated by ChatGPT is correct, however, the translation of the last sentence produced by Google Translate "Humans are obligated to enter Islam and perform the duties that Allah has imposed on them" is incorrect. This translation shows that humans are forced to enter Islam and perform religious duties, whereas the correct meaning should be humans are bound to pay duties of Allah after they have entered Islam. This intended meaning is also reflected in the human translation provided by professional translator. The Google Translate's version appears to force humans to enter Islam which is not true. Moreover, if we compare the BLEU and METEOR scores of ChatGPT and Google Translate presented in Table 1, we noticed that ChatGPT got more score than Google Translate. Therefore, based on our analysis and the BLEU and METEOR scores it is concluded that ChatGPT performed better than Google Translate.

The text in Table 2 is an example of English to Urdu translation taken from the book *Genghis Khan: The Emperor of All Men* by Lamb [22]. We observed that neither translation is fully accurate, as both contain errors. They fail to fully convey the intended meaning of certain lines in this text. For instance, the translation of the sentence, "Children of this corner of the northern Gobi were not hardened to suffering; they were born to it," is incorrect. The correct version is provided in the human translation provided by professional translator. Additionally, Google Translate was unable to translate some words into Urdu instead generated them as it is. For example, the meaning of the word Reed-bordered is present in Urdu language as سرکنڈوں سے گھری but Google Translate rendered the English word in Urdu script as ریڈ بارڈر instead of translating it. However, ChatGPT accurately translated Reed-bordered as سرکنڈوں سے گھری and correctly captured the meaning of winged creatures as پرندے.

Table 1. Islamic text (Urdu to English translation).

Original Text		اسلام میں حقوق پر بڑا زور دیا گیا ہے۔ اور اسلامی ریاست شہریوں کے حقوق کی ذمہ دار قرار دی گئ ہے۔ اللہ تعالی نے قرآن مجید میں اور حضرت محمّد نے اپنی احادیث مبارکہ میں شہریوں کے حقوق کے حوالے سے بڑی واضح ہدایات فرمائی ہیں۔ انسانوں کو پابند کیا گیا ہے کہ وہ اسلام میں داخل ہوکر فرائض ادا کریں جو اللہ نے ان پر عائد کئے ہیں۔
ChatGPT Translation		In Islam, great emphasis has been placed on rights. The Islamic state is held responsible for ensuring the rights of its citizens. Allah Almighty has given clear guidelines in the Holy Quran, and Prophet Muhammad (peace be upon him) has provided explicit instructions in his noble hadiths regarding the rights of citizens. Humans have been bound to fulfill the duties imposed upon them by Allah after entering Islam.
ChatGPT Score	**BLEU**	0.5
	METEOR	0.216
Google Translation		Islam places great emphasis on rights. And the Islamic state is responsible for the rights of its citizens. Allah Almighty has given clear instructions regarding the rights of citizens in the Holy Quran and Hazrat Muhammad in his blessed hadiths. Humans are obligated to enter Islam and perform the duties that Allah has imposed on them.
Google Translate Score	**BLEU**	0.48
	METEOR	0.173
Human Translation		Rights have been greatly emphasized in Islam and Islamic state has been declared responsible for the protection of citizen's rights. Allah Almighty in the Holy Quran and Hazrat Muhammad (peace be upon him) in Ahadees have instructed much clearly regarding the rights of citizens. Men have been bound to pay duties bestowed by Almighty Allah after embracing Islam.

If we compare the BLEU and METEOR scores of ChatGPT and Google Translate presented in Table 2, we noticed that ChatGPT achieved higher scores than Google Translate. Therefore, based on our analysis and the BLEU and METEOR scores it is concluded that ChatGPT performed better than Google Translate.

3.1. Summary of Discussion

The results of the analysis can be summarized as follows:

1. Overall, ChatGPT performed better than Google Translate.
2. Out of 16 paragraphs (Annexure A), ChatGPT had higher BLEU and METEOR scores for 8 translations, Google Translate performed better for 5, and both had the same scores for the remaining 3. Therefore, ChatGPT generally outperformed Google Translate.
3. ChatGPT's average BLEU score is 0.370, while Google Translate's is 0.353, as shown in Figure 4. Similarly, ChatGPT's average METEOR score is 0.322 and Google Translate's average METEOR score is 0.313, as presented in Figure 5.
4. It was observed that ChatGPT sometimes introduces extra content in its translations that are not present in the original text.
5. We noticed that ChatGPT improves its translation quality by learning from users' feedback; whereas Google Translate produces the same translation every time. We observed that AI-powered translators perform well when translating simple paragraphs, such as news articles. However, they struggle with complex texts, such as idioms.

Table 2. Text from novel (English to Urdu translation).

Original Text		**"Life did not matter very much in the Gobi. Lofty plateaus, wind-swept, lying close to the clouds. Reed bordered lakes, visited by migratory winged creatures on their way to the northern tundras. Children of this corner of the northern Gobi were not hardened to suffering; they were born to it."**
ChatGPT Translation		گوبي میں زندگی کی زیادہ اہمیت نہیں تھی۔ بلند و بالا سطح مرتفع، ہوا سے جھلسے ہوئے، بادلوں کے قریب واقع۔ سرکنڈوں سے گھری جھیلیں، جہاں ہجرت کرنے والے پرندے شمالی ٹنڈرا کی جانب جاتے ہوئے قیام کرتے تھے۔ شمالی گوبي کے اس گوشے کے بچے تکلیف کے عادی نہیں تھے؛ وہ تو اسی میں پیدا ہوتے تھے۔
ChatGPT Score	**BLEU**	**0.288**
	METEOR	**0.272**
Google Translation		گوبی میں زندگی بہت زیادہ اہمیت نہیں رکھتی تھی۔ اونچی سطح مرتفع، ہوا سے بھری ہوئی، بادلوں کے قریب پڑی ہے۔ ریڈ بارڈر والی جھیلیں، جن کا دورہ شمالی ٹنڈراس کے راستے میں نقل مکانی کرنے والے پروں والے جانور کرتے ہیں۔ شمالی گوبی کے اس کونے کے بچوں کو تکالیف سے دوچار نہیں کیا گیا تھا۔ وہ اس سے پیدا ہوئے تھے۔
Google Translate Score	**BLEU**	**0.270**
	METEOR	**0.177**
Human Translation		گوبی میں زندگی کی کوئی اہمیت نہیں تھی۔ اونچے بلند ہموار ٹیلے، جن پر تیز ہواؤں کے جھکڑ چلتے، اور جن کی بلندی بادلوں کے قریب قریب پہنچتی۔ جھیلیں جن کے اطراف اونچی اونچی گھاس تھی۔ جن میں ہجرت کرنے والے پرندے شمالی ٹنڈراؤں کی طرف اڑتے ہوئے آن کر بسیرا لیتے۔ شمالی گوبی کے اس گوشے کی اولاد جو انسان تھے۔ انہیں تکلیفوں نے سخت جان نہیں بنایا تھا بلکہ سخت جانی ان کو ورثے میں ملی تھی۔

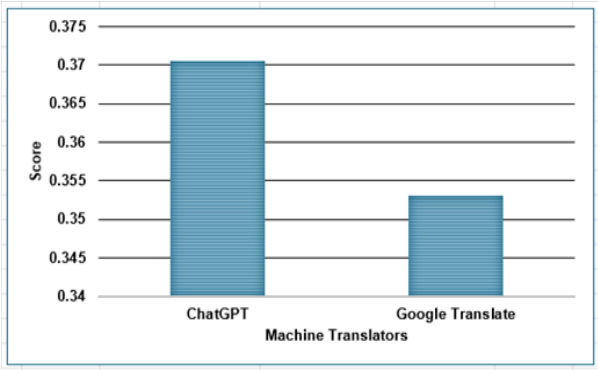

Fig. 4. The average BLEU score of ChatGPT and Google Translate.

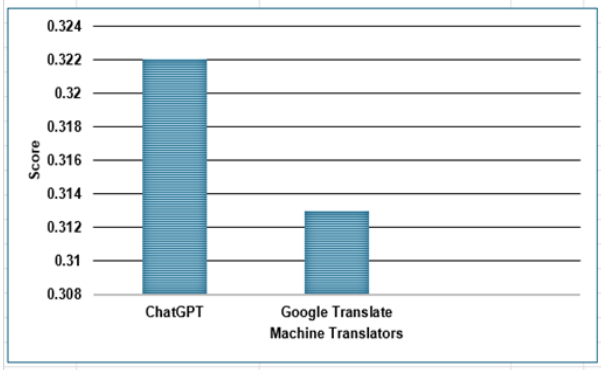

Fig. 5. The average METEOR score of ChatGPT and Google Translate.

4. CONCLUSIONS

Several online translation tools are available that offer reasonable accuracy, are free to use, and support a wide range of languages. Out of these, Google Translate remains the most widely utilized, while OpenAI's ChatGPT has recently gained significant attention. These translation systems are capable of processing complex languages such as Urdu, Chinese, and Arabic. Machine translation tools can be particularly beneficial for multinational organizations, facilitating communication with

partners from diverse linguistic backgrounds. Additionally, they can also help students in translating and understanding content. We evaluated and compared the translations of 16 paragraphs, from English to Urdu and Urdu to English, generated by ChatGPT and Google Translate. Based on the evaluations in the preceding section, ChatGPT outperformed Google Translate, achieving higher METEOR and BLEU scores. ChatGPT's average BLEU score was 0.370, while Google Translate's was 0.353. Similarly, ChatGPT's average METEOR score was 0.322, compared to 0.313 for Google Translate. This study provides valuable insights for users seeking reliable online machine translation between English and Urdu and vice versa. To compare these translations, we used reference translations carefully crafted by experts in this domain. Mostly the machine-generated and human-generated translations convey a similar meaning to some extent, but they differ in terms of phrasing style and word selection, for example, in the translation of "Poetry" (Annexure A), the human translator chose the words "decree" and "ascertain", which preserve the depth and nuance of the original text. In contrast, the machine-generated translations use simple sentences to ensure general accuracy, but they often lack the depth and essence which we can feel in human translation. We observed that Google Translate was unable to translate some English words into Urdu and retained them as it is in Urdu script. For example, in the English to Urdu paragraph, the meaning of the word Reed-bordered in Urdu language is سرکنڈوں سے گھری but Google Translate rendered the English word in Urdu script as ریڈ بارڈر instead of translating it. In contrast, ChatGPT successfully translated most of the text. Overall, ChatGPT demonstrated higher translation accuracy compared to Google Translate for paragraph translation. However, there is always room for improvement, as some lines translated by ChatGPT were inaccurate and not giving the actual sense, as discussed in the previous section. Similarly, the translating idioms is a major challenge for these machine translators because they do not understand the cultural background or context in which they were expressed. One key feature of the ChatGPT is its ability to learn from user feedback and adjust its responses accordingly, which helps improve its translation accuracy. For example, for the translation of some text, we prompted ChatGPT with commands like "Translate again" or "Revise the translations" to enhance accuracy. After a few attempts, it began generating correct translations. In the future, we plan to explore prompt engineering techniques to further improve translation accuracy.

5. ETHICAL STATEMENT

This study did not involve human participants or animals; therefore, ethical approval was not required.

6. FUNDING

No funding was received to conduct this research.

7. AUTHORSHIP CONTRIBUTION

All authors contributed equally to this research. They equally contributed to conceptualization, research methodology, data collection, implementation of translation experiments using Google Translate and ChatGPT-3.5, and the assessment of translation quality. The manuscript was primarily written by Aatka Faryal Riaz. The literature review was conducted by Rubeka Sehar. Validation of results, guidance, and final manuscript review were carried out by Rafay Azmat.

8. DECLARATION STATEMENT

We confirm that the results presented in this manuscript are original; these results are based on the study of Aatka Faryal Riaz, as part of M.Sc. Research Report, submitted to the International University of Applied Science, Bad Honnef, Germany; and it has not been published elsewhere nor is it under consideration for publication by another journal. All authors have approved the manuscript and agree that in case the article is accepted for publication, its copyright will be assigned to the *Pakistan Academy of Sciences*. Authors have obtained permission to reproduce, where needed, copyrighted material from other sources and ensured that no copyrights have been infringed upon.

9. REFERENCES

1. Ethnologue. *The Ethnologue 200* (2025). https://www.ethnologue.com/insights/ethnologue200/
2. International Center for Language Studies. *Most Spoken Languages in the World* (2024). https://www.icls.edu/blog/most-spoken-languages-in-the-world/
3. A.A. Malik and A. Habib. Urdu to English machine translation using bilingual evaluation understudy. *International Journal of Computer Applications*

82(7): 5-12 (2013). https://research.ijcaonline.org/volume82/number7/pxc3891040.pdf

4. M. Ghassemiazghandi. An evaluation of ChatGPT's translation accuracy using BLEU score. *Theory and Practice in Language Studies* 14(4): 985-994 (2024). https://tpls.academypublication.com/index.php/tpls/article/view/7867/6371
5. S.S. Biswas. Potential use of ChatGPT in global warming. *Annals of Biomedical Engineering* 51(6): 1126-1127 (2023). https://doi.org/10.1007/s10439-023-03171-8
6. S.S. Biswas. Role of ChatGPT in public health. *Annals of Biomedical Engineering* 51(5): 868-869 (2023). https://link.springer.com/article/10.1007/s10439-023-03172-7
7. P.P. Ray. ChatGPT: A comprehensive review on background, applications, key challenges, bias, ethics, limitations and future scope. *Internet of Things and Cyber-Physical Systems* 3: 121-154 (2023). https://doi.org/10.1016/j.iotcps.2023.04.003
8. A. Vaswani, N. Shazeer, N. Parmar, J. Uszkoreit, L. Jones, A.N. Gomez, L. Kaiser, and I. Polosukhin. Attention is all you need. *Advances in Neural Information Processing Systems* 30: (2017). https://doi.org/10.48550/arXiv.1706.03762
9. P. Memon. Discover how ChatGPT is trained! (2023). https://www.linkedin.com/pulse/discover-how-chatgpt-istrained-pradeep-menon
10. S.C. Siu. ChatGPT and GPT-4 for professional translators: Exploring the potential of large language models in translation. *SSRN* (2023). https://dx.doi.org/10.2139/ssrn.4448091
11. C. Boitet, H. Blanchon, M. Seligman, and V. Bellynck. Evolution of MT with the Web. *Proceedings of the International Conference "Machine Translation 25 Years On", 21-22 November 2009, Cranfield, England* (2009). https://lig-membres.imag.fr/blanchon/Pdfs/MT25YO-Evolution-MT-web.pdf?utm_source=chatgpt.com
12. I. Caswell. Google Translate learns 24 new languages. *Online google blog* (2022). https://blog.google/products/translate/24-new-languages/
13. Google Translate. *Google Translate Wikipedia* (2025). https://en.wikipedia.org/wiki/Google_Translate
14. P. Chang, P.J. Chen, and L.L. Lai. Recursive editing with Google Translate: the impact on writing and error correction. *Computer Assisted Language Learning* 37(7): 2116-2141 (2024). https://doi.org/10.1080/09588221.2022.2147192
15. S.C. Tsai. Using Google Translate in EFL drafts: A preliminary investigation. *Computer Assisted Language Learning* 32(5-6): 510-526 (2019). https://doi.org/10.1080/09588221.2018.1527361
16. K.M. King. Can Google Translate be taught to translate literature? A case for humanists to collaborate in the future of machine translation. *Translation Review* 105(1): 76-92 (2019). https://doi.org/10.1080/07374836.2019.1673268
17. Y. Wu, M. Schuster, Z. Chen, Q.V. Le, M.N. Yonghui, W. Macherey, M. Krikun, Y. Cao, Q. Gao, K. Macherey, J. Klingner, A. Shah, M. Johnson, X. Liu, L. Kaiser, S. Gouws, Y. Kato, T. Kudo, H. Kazawa, K. Stevens, G. Kurian, N. Patil, W. Wang, C. Young, J. Smith, J. Riesa, A. Rudnick, O. Vinyals, G. Corrado, M. Hughes, and J. Dean. Google's neural machine translation system: Bridging the gap between human and machine translation. *arXiv preprint arXiv*: 1609.08144 (2016). https://doi.org/10.48550/arXiv.1609.08144
18. K. Papineni, S. Roukos, T. Ward, and W.J. Zhu. BLEU: A method for automatic evaluation of machine translation. *Proceedings of the 40th Annual Meeting of the Association for Computational Linguistics, Philadelphia, USA* (2002). https://aclanthology.org/P02-1040.pdf
19. M.A. Ayesha, S. Noor, M. Ramzan, H.U. Khan, and M. Shoaib. Evaluating Urdu to Arabic machine translation tools. *International Journal of Advanced Computer Science and Applications* 8(10): 90-96 (2017). https://thesai.org/Downloads/Volume8No10/Paper_12-Evaluating_Urdu_to_Arabic_Machine_Translation_Tools.pdf
20. S. Banerjee and A. Lavie. METEOR: An automatic metric for MT evaluation with improved correlation with human judgments. *Proceedings of the ACL Workshop on Intrinsic and Extrinsic Evaluation Measures for Machine Translation and/or Summarization, Ann Arbor, Michigan, USA* (2005). https://aclanthology.org/W05-0909.pdf?utm_source=chatgpt.com
21. S. Khan, N. Aftab, A. Ali, and R. Mohammad. Mutalia Pakistan, Class 12. *Punjab Textbook Board, Lahore, Pakistan* (2005). https://www.taleem360.com/12th-class-pak-study-new-punjab-text-book-2022-zqx
22. H. Lamb (Ed.). Genghis Khan, the Emperor of All Men. *Doubleday, New York, USA* (1927). https://archive.org/details/genghiskhanemper0000lamb_f6b1/page/n13/mode/2up

Proceedings of the Pakistan Academy of Sciences: A Physical and Computational Sciences 63(1): S1-S12 (2026)

ISSN (Print): 2518-4245; ISSN (Online): 2518-4253

Pakistan Academy of Sciences

Supplementary Data

A Small-Scale Comparative Evaluation of ChatGPT-3.5 and Google Translate for English-Urdu and Urdu-English Translation

Aatka Faryal Riaz[1*], Rafay Azmat[2], and Rubeka Sehar[3]

[1]Department of Computer Science, International University of Applied Science, Bad Honnef, Germany

[2]Department of Electronics Engineering, Mehran University of Engineering & Technology, Jamshoro, Pakistan

[3]ICT Department, University of Sindh, Jamshoro, Pakistan

Table S1. Poetry (Urdu to English Translation).

Original Text		خودی کو کر بلند اتنا کہ ہر تقدیر سے پہلے خدا بندے سے خود پوچھے بتا تیری رضا کیا ہے
ChatGPT Translation		"Elevate yourself so high that before every destiny, God Himself asks the person, 'Tell me, what is your will?"
ChatGPT Score	**BLEU**	0.421
	METEOR	0.460
Google Translation		Elevate yourself so much that before every destiny Ask the servant of God himself and tell him what is your pleasure
Google Translate Score	**BLEU**	0.381
	METEOR	0.374
Human Translation		Develop the self so that before every decree, God will ascertain from you: "What is your wish?"

* Corresponding Author: Aatka Faryal Riaz <aatkafaryal@gmail.com >

Table S2. Historical Text (Urdu to English Translation).

Original Text		دو قومی نظریہ دوقومی نظریہ پاکستان کی بنیاد ہے۔ برصغیر پاک و ہند میں دو قومیں یعنی ہندو اور مسلمان آباد تھیں جن کی سیاسی، مذہبی، معاشرتی اور معاشی اقدار مختلف تھیں۔ ان دو اقوام کے نظریات بلکل مختلف تھے جن کی بنیاد اسلام اور ہندوازم پر تھی۔ تحریک پاکستان کی بنیاد بھی دو قومی نظریہ تھا بر صغیر پاک و ہند میں ہندو اور مسلمان دو مختلف قومیں جو ہندوازم اور اسلام پر ایمان رکھتی تھیں۔ ان دونوں اقوام کے طرز زندگی اور بودوباش بلکل مختلف تھے۔ اسی دو قومی نظریہ کی بنیاد پر مسلمانان ہند نے اپنے لئے الگ ریاست کا مطالبہ کیا اور آخرکار پاکستان معرض وجود میں آیا۔
ChatGPT Translation		Two Nation Theory The Two Nation Theory is the foundation of Pakistan. In British India, there were two major communities, Hindus and Muslims, with distinct political, religious, social, and economic destinies. These two communities had completely different ideologies based on Islam and Hinduism. The foundation of the Pakistan Movement was also based on the Two Nation Theory, as Hindus and Muslims in British India were two distinct communities with beliefs in Hinduism and Islam, respectively. The lifestyles and cultures of these two communities were entirely different. Based on this Two Nation Theory, Muslims in India demanded a separate state for themselves, and ultimately, Pakistan came into existence.
ChatGPT Score	**BLEU**	0.596
	METEOR	0.529
Google Translation		Two nation theory Binational ideology is the foundation of Pakistan. The Indian subcontinent was inhabited by two nations, namely Hindus and Muslims, whose political, religious, social and economic values were different. The ideologies of these two nations were completely different which were based on Islam and Hinduism. The foundation of the Pakistan Movement was also the two-nation theory, Hindus and Muslims in the Indian subcontinent, two different nations who believed in Hinduism and Islam. The lifestyles and lifestyles of these two nations were completely different. On the basis of this two-nation theory, the Muslims of India demanded a separate state for themselves and eventually Pakistan came into existence.

Google Translate Score	**BLEU**	0.403
	METEOR	0.488
Human Translation		Two Nation Theory Two Nation Theory is the base of Pakistan. Two nations, the Hindus and the Muslims were living in the subcontinent who had different political, religious, social and economic values. They had ideologies which were based on Islam and Hinduism. Pakistan Movement was also based on Two Nation Theory i.e. the Hindus and the Muslims were two different nations in Indo-Pak Subcontinent who believed in Hinduism and Islam. These two nations were quite different in lifestyle and living conditions. On the basis of this "Two Nation Theory", the Muslims of India demanded for a separate state for themselves and finally Pakistan came into being.

Table S3. Article (Urdu to English Translation).

Original Text		کامیاب اور موثر معلم کی خصوصیات: موثر اور کامیاب مدرس و معلم بننے کے لئے ضروری ہے کہ استاد اپنی انتظامیہ سے اور زیادہ تجربہ کار لوگوں سے خصوصی رہنمائ اور عمل کے طریقے سیکھتا رہے۔ کمرہ جماعت میں محض جذبات سے بھرپور اسباق اور سرگرمیاں آپ کی تدریس کو موثر اور کامیاب نہیں بناسکتیں۔ معلمی ایک طویل تعلیمی عمل سے حاصل ہونے والی ہنرمندی ہوتی ہے۔
ChatGPT Translation		Characteristics of a Successful and Effective Teacher: To become an effective and successful educator, it is essential for a teacher to continuously learn from their administration and seek guidance from experienced individuals. Classroom lessons filled with enthusiasm alone cannot make your teaching effective and successful. Teaching excellence is achieved through a lengthy process of educational practice.
ChatGPT Score	**BLEU**	0.320
	METEOR	0.344
Google Translation		Characteristics of a successful and effective teacher: In order to become an effective and successful teacher, it is important that the teacher learns specific guidelines and practices from his administration and from more experienced people. Mere emotional lessons and activities in the

	classroom cannot make your teaching effective and successful. Education is a skill acquired through a long educational process.	
Google Translate Score	**BLEU**	0.320
	METEOR	0.419
Human Translation	Characteristics of Effective Teacher Becoming an effective and successful teacher takes practice and special guidance from mentors and administrators. Effective teaching does not involve presenting your exciting lessons or activities to the class, it is a craft learned over time.	

Table S4. News (Urdu to English Translation).

Original Text		بابر اعظم نے سوشل میڈیا پر اپنے بیان میں لکھا کہ ’مجھے وہ لمحہ ٹھیک سے یاد ہے جب مجھےسنہ 2019 میں پاکستان کرکٹ بورڈ کی جانب سے کپتانی کرنے کی آفر کے لیے کال موصول ہوئی تھی۔ گذشتہ چار سالوں کے دوران میں نے گراؤنڈ میں اور اس سے باہر متعدد مرتبہ اتار چڑھاؤ دیکھا ہے لیکن میں نے مستعدی اور پورے دل کے ساتھ دنیا میں پاکستان کی عزت اور عظمت برقرار رکھنے کی کوشش کی ہے۔
ChatGPT Translation		Babar Azam wrote on his social media, "I remember that moment vividly when I received the call in June 2019 from the Pakistan Cricket Board offering me the captaincy. Over the past four years, I have witnessed numerous ups and downs both on and off the field, but I have tried my best with dedication and wholeheartedly to maintain Pakistan's dignity and respect worldwide."
ChatGPT Score	**BLEU**	0.507
	METEOR	0.532
Google Translation		Babar Azam wrote in his statement on social media that "I remember the moment well when I received a call from the Pakistan Cricket Board for the captaincy offer in the year 2019. During the last four years I have seen many ups and downs on and off the ground, but I have tried diligently and wholeheartedly to uphold the honor and greatness of Pakistan in the world.
Google Translate Score	**BLEU**	0.514
	METEOR	0.564

Human Translation	"I vividly remember the moment when I received the call from the Pakistan Cricket Board to lead Pakistan in 2019. Over the last four years, I've experienced many highs and lows on and off the field, but I wholeheartedly and passionately aimed to maintain Pakistan's pride and respect in the cricket world," Babar wrote in a statement.

Table S5. Legal Text (Urdu to English Translation).

Original Text		اقرارنامہ کرایہ داری: یہ کہ فریق اول نے فریق دوم سے اسکا ملکیتی گھر درجذیل شراط کے تحت حاصل کیا ہے۔ 1- یہ کہ مذکورہ مکان کا ماہانہ کرایہ مبلغ 40000 ماہوار مقرر ہوا ہے۔ 2- یہ کہ دوران کرایہ داری، اگر فریق دوم مکان مذکورہ کو خالی کروانا چاہے تو وہ فریق اول کوایک ماہ کا پیشگی تحریری نوٹس دینے کا پابند ہوگا۔ نوٹس ملنے پر فریق اول مکان مذکورہ کو خالی کرنے کا پابند ہوگا۔ اسی طرح اگر فریق اول مکان مذکورہ کو خالی کرنا چاہے تو وہ فریق دوم کو ایک ماہ کا پیشگی تحریری نوٹس دینے کا پابند ہوگا۔
ChatGPT Translation		Rental Agreement: This agreement states that Party One has acquired ownership of the property from Party Two under the following conditions. 1. The monthly rent for the mentioned property is fixed at the amount of 40,000 per month. 2. During the tenancy, if Party Two wishes to vacate the mentioned premises, they are obligated to provide Party One with a written notice at least one month in advance. Upon receiving the notice, Party One is bound to vacate the premises as per the specified terms. Similarly, if Party One intends to vacate the mentioned premises, they must provide Party Two with a written notice at least one month in advance.
ChatGPT Score	**BLEU**	0.370
	METEOR	0.281
Google Translation		Affidavit Tenancy: That the first party has acquired his proprietary house from the second party under the following conditions. 1. That the monthly rent of the said house has been fixed at 40000 per month

		2. That during the tenancy, if the second party wants to vacate the said premises, he shall be obliged to give one month's prior written notice to the first party. Upon receiving the notice, the first party will be bound to vacate the said house. Similarly, if the first party wants to vacate the said house, he will be obliged to give one month's prior written notice to the second party.
Google Translate Score	**BLEU**	0.481
	METEOR	0.422
Human Translation		**WHEREAS** the said 2nd party is the absolute owner in the possession of house and has agreed to let out the said house on monthly rent basis to the Tenant and Tenant has agreed on the same, with the following terms and conditions. 1. That the rent of the above-stated house has been fixed as Rs. 40000 per month. 2. That one month's notice from either party for the vacation of the said House is mandatory, e.g. if Second party wishes to vacate the said House and hand over to the First party or the First party wishes to get that said house vacated from the 2nd party-

Table S6. Idiom (Urdu to English Translation).

Original Text		جو گرجتے ہیں وہ برستے نہیں۔
ChatGPT Translation		Those who thunder do not shower.
ChatGPT Score	**BLEU**	0
	METEOR	0.09
Google Translation		Those who thunder do not rain.
Google Translate Score	**BLEU**	0
	METEOR	0.09
Human Translation		Barking dogs seldom bite.

Table S7. Text from Novel (English to Urdu Translation).

Original Text	Harry Potter was a highly unusual boy in many ways. For one thing, he hated the summer holidays more than any other time of year. For another,

		he really wanted to do his homework but was forced to do it in secret, in the dead of night.
ChatGPT Translation		ہیری پوٹر بہت سے طریقوں میں ایک بہت غیر معمولی لڑکا تھا۔ ایک بات کا تو یہ کہ وہ دوسرے تمام موسموں کی طرح گرمیوں سے نفرت کرتا تھا۔ دوسری بات یہ تھی کہ اُسے واقعی میں اپنا ہوم ورک کرنا بہت شوق تھا لیکن اُسے اسے رات کے چھپ کر کرنا پڑتا تھا۔
ChatGPT Score	**BLEU**	0.569
	METEOR	0.497
Google Translation		ہیری پوٹر بہت سے طریقوں سے ایک انتہائی غیر معمولی لڑکا تھا۔ ایک چیز کے لیے، وہ گرمیوں کی چھٹیوں سے سال کے کسی بھی دوسرے وقت سے زیادہ نفرت کرتا تھا۔ دوسرے کے لیے، وہ واقعی اپنا ہوم ورک کرنا چاہتا تھا لیکن اسے رات کے آخری پہر میں چھپ چھپ کر کرنے پر مجبور کیا گیا۔
Google Translate Score	**BLEU**	0.540
	METEOR	0.451
Human Translation		ہیری پوٹر کئ لحاظ سے ایک غیر معمولی بچہ تھا۔ ایک بات تو یہ تھی کہ اسے گرمیوں کی تعطیلات سال کے کسی بھی دوسرے وقت سے زیادہ بری لگتی تھیں۔ دوسری بات یہ تھی کہ وہ سچ مچ اپنا چھٹیوں کا کام کرنا چاہتا تھا، لیکن اسے رات میں سب سے چھپ کرچوری سے اپنا ہوم ورک کرنا پڑنا تھا۔

Table S8. Text from Novel (English to Urdu Translation).

Original Text	It took Harry several days to get used to his strange new freedom. Never before had he been able to get up whenever he wanted or eat whatever he fancied. He could even go wherever he pleased, as long as it was in Diagon Alley, and as this long cobbled street was packed with the most fascinating wizarding shops in the world, Harry felt no desire to break his word to Fudge and stray back into the Muggle world.
ChatGPT Translation	ہیری کو اپنی عجیب نئی آزادی کا عادی ہونے میں کئی دن لگ گئے۔ اس سے پہلے وہ کبھی بھی اپنی مرضی سے اٹھ نہیں سکتا تھا اور نہ ہی جو چاہے کھا سکتا تھا۔ وہ جہاں چاہے جا بھی سکتا تھا، بشرطیکہ وہ ڈائیگون ایلی کے اندر رہے۔ اور چونکہ یہ لمبی، پتھریلی گلی دنیا کی سب سے دلکش جادوئی دکانوں سے بھری ہوئی تھی، ہیری کو اپنا وعدہ توڑ کر فج سے بے وفائی کرنے اور مگل دنیا میں واپس بھٹکنے کی کوئی خواہش محسوس نہ ہوئی۔

ChatGPT Score	**BLEU**	0.493
	METEOR	0.371
Google Translation		ہیری کو اپنی عجیب نئی آزادی کے عادی ہونے میں کئی دن لگے۔ اس سے پہلے وہ کبھی اس قابل نہیں تھا کہ جب چاہے اٹھ سکے یا جو چاہے کھا لے۔ یہاں تک کہ وہ جہاں چاہے جا سکتا تھا، جب تک کہ وہ ڈائیگن ایلی میں تھا، اور چونکہ یہ لمبی گلی دنیا کی سب سے دلکش جادوگروں کی دکانوں سے بھری ہوئی تھی، ہیری کو کوئی خواہش محسوس نہیں ہوئی کہ وہ فج سے اپنی بات کو توڑ دے اور واپس بھٹک جائے مگلی دنیا۔
Google Translate Score	**BLEU**	0.483
	METEOR	0.371
Human Translation		ہیری کو اس نئی آزادی کی عادت پڑنے میں کئی دن لگ گئے۔ اس سے پہلے ایسا کبھی نہیں ہوا تھا کہ وہ اپنی مرضی سے جب چاہے، سو کر اٹھ سکتا اور کھا سکتا تھا۔ یہاں تک کہ وہ اپنی من پسند جگہ پر آزادانہ آ جا سکتا تھا۔ بشرطیکہ وہ جگہ جادوئ بازار میں ہو۔ چونکہ یہ طویل بل دار سڑک دنیائے جادوگری کی سب سے زیادہ پرکشش دکانوں سے بھری پڑی تھی، اس لئے ہیری کے دل میں یہ خواہش پیدا ہی نہیں ہوئی کہ وہ فج سے کیا ہوا وعدہ توڑے اور ماگلوؤں کی دنیا میں آوارہ گردی کرتا پھرے۔

Table S9. Idiom (English to Urdu Translation).

Original Text		1. Barking dogs seldom bite.
ChatGPT Translation		بھونکتے ہوئے کتے کم کاٹتے ہیں۔
ChatGPT Score	**BLEU**	0
	METEOR	0
Google Translation		بھونکنے والے کتے شاذ و نادر ہی کاٹتے ہیں۔
Google Translate Score	**BLEU**	0
	METEOR	0
Human Translation		جو گرجتے ہیں وہ برستے نہیں۔

Table S10. Idiom (English to Urdu Translation).

Original Text	1. It takes two to quarrel.
ChatGPT Translation	جھگڑے میں دونوں کا ہاتھ ہوتا ہے۔

ChatGPT Score	**BLEU**	0.14
	METEOR	0.08
Google Translation		جھگڑنے میں دو لگتے ہیں۔
Google Translate Score	**BLEU**	0
	METEOR	0
Human Translation		تالی ایک ہاتھ سے نہیں بجتی۔

Table S11. Historical Text (English to Urdu Translation).

Original Text		I was born on June 27, 1880, in Tuscumbia, a little town of northern Alabama. The family on my father's side is descended from Caspar Keler, a native of Switzerland, who settled in Maryland. One of my Swiss ancestors was the first teacher of the deaf in Zurich and wrote a book on the subject of their education—rather a singular coincidence; though it is true that there is no king who has not had a slave among his ancestors, and no slave who has not had a king among his.
ChatGPT Translation		میں 27 جون 1880 کو ٹسکومبیا میں پیدا ہوا، جو شمالی الاباما کا ایک چھوٹا سا قصبہ ہے۔ میرے والد کی جانب سے میرے خاندان کا تعلق کیسپار کیلر سے ہے، جو سوئٹزرلینڈ کے رہنے والے تھے اور میری لینڈ میں آباد ہوئے۔ میرے ایک سوئس آباؤ اجداد زیورخ میں بہروں کے پہلے استاد تھے اور انہوں نے ان کی تعلیم کے موضوع پر ایک کتاب لکھی تھی—یہ ایک غیر معمولی اتفاق ہے۔ اگرچہ یہ بھی سچ ہے کہ کوئی ایسا بادشاہ نہیں جس کے آباؤ اجداد میں کوئی غلام نہ رہا ہو، اور کوئی ایسا غلام نہیں جس کے آباؤ اجداد میں کوئی بادشاہ نہ رہا ہو۔
ChatGPT Score	**BLEU**	0.562
	METEOR	0.421
Google Translation		میں 27 جون 1880 کو شمالی الاباما کے ایک چھوٹے سے قصبے ٹسکومبیا میں پیدا ہوا۔ میرے والد کی طرف کا خاندان کاسپر کیلر سے تعلق رکھتا ہے، جو سوئٹزرلینڈ کے رہنے والے ہیں، جو میری لینڈ میں آباد ہیں۔ میرے سوئس آباؤ اجداد میں سے ایک زیورخ میں بہروں کے پہلے استاد تھے اور انہوں نے ان کی تعلیم کے موضوع پر ایک کتاب لکھی — بلکہ ایک واحد اتفاق؛ حالانکہ یہ سچ ہے کہ کوئی بادشاہ ایسا نہیں ہے جس کے آباؤ اجداد میں کوئی غلام نہ رہا ہو اور کوئی غلام ایسا نہیں جس کا بادشاہ نہ ہو۔
	BLEU	0.551

Google Translate Score	**METEOR**	0.393
Human Translation		میں 27 جون 1880 کو شمالی الابامہ کے ایک چھوٹے سے قصبے ٹسکومبیا میں پیدا ہوئی۔ والد کی جانب سے میرا کنبہ سوئزرلینڈ کے ایک باشندہ کیسپر کیلر کی نسل سے تعلق رکھتا ہے۔ جو "میری لینڈ" میں آکر آباد ہوا۔ سوئزرلینڈ کے میرے آباؤاجداد میں سے ایک شخص زیورچ میں بہروں کو پڑھانے والا پہلا استاد تھا۔ اور اس نے بہروں کی تعلیم کے موضوع پر ایک کتاب بھی لکھی تھی۔ یہ محض ایک اتفاقی مطابقت ہے۔ ویسے یہ ایک سچی بات ہے کہ کوئی بادشاہ ایسا نہیں گزرا جس کے آباؤاجداد میں کوئی غلام نہیں تھا اور کوئی ایسا غلام نہیں ہوا جس کے آباؤاجداد میں کوئی بادشاہ نہیں تھا۔

Table S12. Text from Novel (English to Urdu Translation).

Original Text		Mr. SHERLOCK HOLMES, who was usually very late in the mornings, save upon those not infrequent occasions when he stayed up all night, was seated at the breakfast table. I stood upon the hearth-rug and picked up the stick which our visitor had left behind him the night before.
ChatGPT Translation		مسٹر شرلاک ہومز، جو عام طور پر صبح کے وقت بہت دیر سے جاگتے تھے، سوائے ان مواقع کے جب وہ پوری رات جاگتے رہتے، ناشتہ کی میز پر بیٹھے ہوئے تھے۔ میں قالین پر کھڑا تھا اور وہ چھڑی اٹھائی جو ہمارے مہمان گزشتہ رات چھوڑ گئے تھے۔
ChatGPT Score	**BLEU**	0.319
	METEOR	0.384
Google Translation		مسٹر شرلاک ہومز، جو عموماً صبح بہت دیر سے آتے تھے، ان غیر معمولی مواقع کو چھوڑ کر جب وہ رات بھر جاگتا تھا، ناشتے کی میز پر بیٹھا تھا۔ میں چولہا کے قالین پر کھڑا ہوا اور وہ چھڑی اٹھائی جو ہمارے مہمان نے ایک رات اس کے پیچھے چھوڑ دی تھی۔
Google Translate Score	**BLEU**	0.297
	METEOR	0.420

Human Translation	مسٹر شرلاک ہومز ناشتے کی میز پر بیٹھے ہوئے تھے، وہ عام طور پر صبح تاخیر سے اٹھتے تھے سوائے ان مواقعوں کے جب وہ رات کو سوتے ہی نہیں تھے، اور ایسے مواقع کثیر تعداد میں تھے۔ میں آتشدان کے سامنے پڑے غالیچے پر کھڑا ہوا اور وہ چھڑی اٹھالی جو پچھلی رات ہمارا ایک ملاقاتی چھوڑ گیا تھا۔

Table S13. Text from Novel (English to Urdu Translation).

Original Text		I think it unlikely that he waited at the moor-gate every evening. On the contrary, the evidence Is that he avoided the moor. That night he waited there. It was the night before he was to take his departure for London. The thing takes shape, Watson. It becomes coherent.
ChatGPT Translation		مجھے نہیں لگتا کہ وہ ہر شام مور گیٹ پر انتظار کرتا تھا۔ اس کے برعکس، شواہد یہ ہیں کہ وہ مور سے دور رہتا تھا۔ لیکن اس رات وہ وہاں انتظار کر رہا تھا۔ یہ وہ رات تھی جب وہ لندن روانہ ہونے والا تھا۔ بات اب واضح ہو رہی ہے، واٹسن۔ یہ مربوط ہو رہی ہے۔
ChatGPT Score	**BLEU**	0.392
	METEOR	0.308
Google Translation		میرے خیال میں اس بات کا کوئی امکان نہیں کہ وہ ہر شام مور گیٹ پر انتظار کرتا۔ اس کے برعکس، ثبوت یہ ہے کہ اس نے مور سے گریز کیا۔ اس رات وہ وہاں انتظار کرتا رہا۔ یہ رات تھی اس سے پہلے کہ اسے لندن روانہ ہونا تھا۔ بات شکل اختیار کر لیتی ہے واٹسن۔ یہ مربوط ہو جاتا ہے۔
Google Translate Score	**BLEU**	0.438
	METEOR	0.329
Human Translation		میرے خیال میں تو یہ بیعدازقیاس ہی ہے کہ وہ ہر شام مور دروازے پر کسی کا انتظار کرتے تھے۔ نہیں بلکہ شواہد تو یہ کہتے ہیں کہ وہ مور کی طرف جاتے سے گریز کیا کرتے تھے۔ اس رات وہ وہاں انتظار کررہے تھےجب کہ اسی رات کی آنے والی صبح وہ لندن کے لئے روانہ ہونے والے تھے۔ معاملات کچھ کچھ شکل اختیار کرتے جارہے ہیں واٹسن۔ اب کیس سہل ہوگیا ہے۔

Table S14. Historical text (English to Urdu Translation).

Original Text	Seven hundred years ago a man almost conquered the earth. He made himself master of half the known world, and inspired humankind with a fear that lasted for generations. In the course of his life he was given many names — the

		Mighty Manslayer, the Scourge of God, the Perfect Warrior, and the Master of Thrones and Crowns. He is better known to us as Genghis Khan.
ChatGPT Translation		سات سو سال پہلے ایک شخص نے تقریباً پوری دنیا کو فتح کر لیا تھا۔ اس نے اپنے آپ کو آدھی معلوم دنیا کا حکمران بنا لیا اور انسانیت میں ایسا خوف پیدا کیا جو نسلوں تک قائم رہا۔ اپنی زندگی کے دوران اسے کئ نام دیے گئے — زبردست قاتل، خدا کا عذاب، کامل جنگجو، اور تختوں اور تاجوں کا مالک۔ وہ ہمیں زیادہ تر چنگیز خان کے نام سے جانا جاتا ہے۔
ChatGPT Score	**BLEU**	0.445
	METEOR	0.376
Google Translation		سات سو سال پہلے ایک آدمی نے زمین کو تقریباً فتح کر لیا تھا۔ اس نے اپنے آپ کو آدھی معلوم دنیا کا مالک بنایا، اور انسانوں کو ایک خوف سے متاثر کیا جو نسلوں تک جاری رہا۔ اس کی زندگی کے دوران اسے بہت سے نام دیئے گئے — غالب آدمی، خدا کا عذاب، کامل جنگجو، اور تخت اور تاج کا مالک۔ وہ ہمارے نزدیک چنگیز خان کے نام سے مشہور ہیں۔
Google Translate Score	**BLEU**	0.410
	METEOR	0.340
Human Translation		سات سو سال پہلے ایک آدمی نے دنیا کو قریب قریب بالکل ہی فتح کر لیا تھا۔ اس زمانے کے ربع مسکون کے نصف حصہ پر اس نے اپنا تصرف قائم کیا اور نوع انسان پر ایسی دھاک بٹھائ جس کا اثر کئ نسلوں تک باقی رہا۔ اپنی زندگی میں اس نے کئ نام پائے — قتال اعظم، قہرخدا، جنگجوئےکامل، باج گیرتاج وتخت۔ عام طور پر وہ چنگیزخان کے نام سے معروف ہے۔

Instructions For Authors

Manuscript Writing

The manuscript may contain a Title, Abstract, Keywords, INTRODUCTION, MATERIALS AND METHODS, RESULTS, DISCUSSION (or RESULTS AND DISCUSSION), CONCLUSIONS, ETHICAL STATEMENT (if applicable), ACKNOWLEDGEMENTS, CONFLICT OF INTEREST and REFERENCES, *and any other information that the author(s) may consider necessary*.

Title (Bold and font size 16): The title should be expressive, concise, and informative to the entire readership of the journal. It may include common terms, to make it more identifiable when people search online. Please avoid the use of long pervasive terms and non-standard or obscure abbreviations, acronyms, or symbols.

Abstract (font size 10, max 250 words)**:** Must be self-explanatory**,** stating the rationale, objective(s), methodology, main results, and conclusions of the study. Abbreviations, if used, must be defined on the first mention in the Abstract as well as in the main text. Abstracts of review articles may have a variable format.

Keywords (font size 10)**:** Provide five to eight keywords consisting of words and phrases that are closely associated with the topic depicting the article.

INTRODUCTION (font size 11)**:** Provide a clear and concise statement of the problem, citing relevant recent literature, and objectives of the investigation. Cite references in the text by number in square brackets**,** the reference must be cited in a proper English sentence [1]. or "... as previously described [3, 6–8]". For a single author: Bednorz [2] investigated the environmental pollution ... When there are only two authors: Bednorz and Allan [2] investigated the environmental pollution ... and for three or more authors: Bednorz *et al.* [2] investigated the environmental pollution ..; and list them in the REFERENCES section, in the order of citation in the text.

MATERIALS AND METHODS (font size 11)**:** Provide an adequate account of the procedures or experimental details, including statistical tests (if any), concisely but sufficiently enough to replicate the study. Relevant references to methodology must be cited.

RESULTS (font size 11)**:** Be clear and concise with the help of appropriate Tables, Figures, and other illustrations. Data should not be repeated in Tables and Figures but must be supported with statistics. The data presented in Tables and Figures must be elaborated in the main text.

DISCUSSION (font size 11)**:** Provide interpretation of the RESULTS in the light of previous relevant studies, citing published references.

CONCLUSIONS (font size 11)**:** Briefly state the implication of your study findings, and carefully address the study questions. Confine your conclusions according to the objectives of your study and the aspects covered in the abstract. Discuss both positive and negative findings.

ETHICAL STATEMENT (font size 10)**:** The statement of ethical approval by an appropriate ethics committee or review board must be included in the manuscript (if applicable), as per the Journal's policy.

ACKNOWLEDGEMENTS: (font size 10)**:** In a brief statement, acknowledge the financial support and other assistance.

CONFLICT OF INTEREST (font size 10)**:** State if there is any conflict of interest.

REFERENCES (font size 10)**:** References must be listed in numerical order as listed in the main text. Only published (and accepted for publication) journal articles, books and book chapters, conference proceedings, online reports, a degree thesis, and materials available on the website qualify for REFERENCES. Give online link/doi for published articles.

Declaration: Provide a declaration that: (i) the results are original, (ii) the same material is neither published nor under consideration for publication elsewhere, (iii) approval of all authors has been obtained, and (iv)

in case the article is accepted for publication, its copyright will be assigned to the *Pakistan Academy of Sciences*. Authors must obtain permission to reproduce, where needed, copyrighted material from other sources and ensure that no copyrights are infringed upon.

Manuscript Formatting

Manuscripts must be submitted in Microsoft Word (Latest Version .doc or .docx format); pdf files are not acceptable. Figures can be submitted separately in TIFF, GIF, JPEG, EPS, or PPT. Manuscripts, in *Times New Roman*, 1.15 spaced (but use single-space for Tables, long headings, and long captions of tables and figures). The Manuscript sections must be numbered, i.e., **1. INTRODUCTION, 2. MATERIALS AND METHODS,** and so on… (a) **Title** of the article **(**Capitalize the initial letter of each main word, font-size 16, **bold**), max 160 characters (no abbreviations or acronyms), depicting article's contents; (b) Author's complete name (font size 12, **bold**), and professional affiliation (i.e., each author's Department, Institution, Mailing address, and Email and Contact number, but no position titles) (font size 12); (c) Indicate the corresponding author with *; and (d) **Short running title**, max 50 characters (font size 10).

Headings and Subheadings (font size 11): All flush left

LEVEL-1: **ALL CAPITAL LETTERS; Bold**

Level-2: **Capitalize Each First Letter (**Except prepositions**); Bold**

Level-3: Capitalize the first letter only (Sentence case)***; Bold, Italic***

Level-4: *Run-in head*; *Italics*, *in the normal paragraph position. Capitalize the first letter only and end in a colon (i.e., **:**)*

A list of REFERENCES must be prepared as under:

a. Journal Articles *(Name of journals must be stated in full)*

1. J. Rashid, A. Ahsan, M. Xu, I. Savina, and F. Rehman. Synthesis of cerium oxide embedded perovskite type bismuth ferrite nanocomposites for sonophotocatalysis of aqueous micropollutant ibuprofen. *RSC Advances* 13(4): 2574-2586 (2023). DOI: 10.1039/d2ra07509a

2. A. Fayyaz, N. Ali, Z.A. Umar, H. Asghar, M. Waqas, R. Ahmed, R. Ali, and M.A. Baig. CF-LIBS based elemental analysis of Saussurea simpsoniana medicinal plant: a study on roots, seeds, and leaves. *Analytical Sciences* 40(3): 413-427 (2024). DOI: 10.1007/s44211-023-00480-9

3. W. Bialek and S. Setayeshgar. Cooperative sensitivity and noise in biochemical signaling. *Physical Review Letters* 100: 258-263 (2008). https://doi.org/10.1103/PhysRevLett.100.258101

b. Books

4. W.R. Luellen (Ed.). Fine-Tuning Your Writing. *Wise Owl Publishing Company, Madison, WI, USA* (2001).

5. U. Alon and D.N. Wegner (Eds.). An Introduction to Systems Biology: Design Principles of Biological Circuits. *Chapman & Hall/CRC, Boca Raton, FL, USA* (2006).

c. Book Chapters

6. M.S. Sarnthein, J.E. Smolen, and J.D. Stanford. Basal sauropodomorpha: historical and recent phylogenetic developments. In: The Northern North Atlantic: A Changing Environment. P.R. Schafer and W. Schluter (Eds.). *Springer, Berlin, Germany* pp. 365-410 (2000).

7. S. Brown and L.A. Boxer. Functions of Europhiles. In: Hematology, (4^{th} ed). W.J. Williams, E. Butler, and M.A. Litchman (Eds.). *McGraw Hill, New York, USA* pp. 103-110 (1991).

d. Reports

8. M.D. Sobsey and F.K. Pfaender. Evaluation of the H_2S method for Detection of Fecal Contamination of

Drinking Water. Report No.-WHO/SDE/WSH/02.08. *Water Sanitation and Health Programme, WHO, Geneva, Switzerland* (2002).

e. Online References

These should specify the full URL for reference, please check again to confirm that the work you are citing is still accessible:

9. UNESCO. Global Education Monitoring Report 2024/5: Leadership in education−Lead for learning. *United Nations Educational, Scientific and Cultural Organization, Paris, France* (2024). https://digitallibrary.un.org/record/4066661?ln=en&v=pdf

10. L.M. Highland and P. Bobrowsky. The landslide handbook−A guide to understanding landslides. Circular 1325. *US Geological Survey, Reston, Virginia* (2008).

    https://pubs.usgs.gov/circ/1325/pdf/C1325_508.pdf

f. Conference Proceedings

11. M. Khalid, A.B. Majid, F. Mansour, and C.R. Smith. Word Representations with Recursive Neural Networks for Morphology. *27th European Conference on Signal Processing, (2nd - 6th September 2021), Madrid, Spain* (2021).

g. A Degree Thesis

12. M. Afzal. Investigation of structural and magnetic properties of nanometallic Fe-Mn Alloys. Ph.D. Thesis. *Quaid-i-Azam University, Islamabad, Pakistan* (2023).

Tables: Insert all tables as editable text, not as images. Number tables consecutively following their appearance in the text. A concise but self-explanatory heading must be given. Tables should be numbered according to the order of citation (like **Table 1.**, **Table 2.** (font size 10)). *Do not* abbreviate the word "Table" to "Tab.". Round off data to the nearest three significant digits. Provide essential explanatory footnotes, with superscript letters or symbols keyed to the data. Do not use vertical or horizontal lines, except for separating column heads from the data and at the end of the Table.

Figures: In the main text write Figure, not Fig. Figures may be printed in two sizes: column width of 8.0 cm or page width of 16.5 cm; In the Figure caption, number them as **Fig. 1.**, **Fig. 2.** Captions to Figures must be concise but self-explanatory (font size 10). Laser-printed line drawings are acceptable. Do not use lettering smaller than 9 points or unnecessarily large. Photographs must be of high quality. A scale bar should be provided on all photomicrographs. All Figures should have sufficiently high resolution (minimum 300 dpi) to enhance the readability. Figures as separate files in JPG or TIFF format may be provided.

SUBMISSION CHECKLIST

The following list will be useful during the final checking of an article before submission to the journal.

1. Manuscript in MS Word format
2. Cover Letter
3. Novelty Statement
4. Copyright Form
5. Figures in JPG or TIFF format

In case of any difficulty while submitting your manuscript, please get in touch with:

Editor-in-Chief

Pakistan Academy of Sciences
3-Constitution Avenue,
G-5/2, Islamabad, Pakistan
Email: editor@paspk.org
Tel: +92-51-920 7140
Websites: http://www.paspk.org/proceedings/; http://ppaspk.org/

PROCEEDINGS OF THE
PAKISTAN ACADEMY OF SCIENCES: PART A
Physical and Computational Sciences

CONTENTS

Volume 63, No. 1, March 2026 **Page**

Research Articles

PAKISTAN ACADEMY OF SCIENCES, ISLAMABAD, PAKISTAN

HEC Recognized; Scopus Indexed

Websites: http://www.paspk.org/proceedings/; http://ppaspk.org